ADVANCED ELECTROCHEMICAL METHODS FOR

CHARACTERIZING THE PERFORMANCE OF ORGANIC COATINGS

A Dissertation
Submitted to the Graduate Faculty
of the
North Dakota State University
of Agriculture and Applied Science

By

Vinod Upadhyay

In Partial Fulfillment of the Requirements
for the Degree of
DOCTOR OF PHILOSOPHY

Major Department:
Coatings and Polymeric Materials

February 2012

Fargo, North Dakota

North Dakota State University

Graduate School

Title

Advanced Electrochemical Methods for Characterizing

The Performance of Organic Coatings

By

Vinod Upadhyay

The Supervisory Committee certifies that this *disquisition* complies with North Dakota State University's regulations and meets the accepted standards for the degree of

DOCTOR OF PHILOSOPHY

SUPERVISORY COMMITTEE:

Dr. Gordon Bierwagen

Chair

Dr. Victoria Johnston Gelling

Dr. Dante Battocchi

Dr. Kerry Allahar

Dr. Achintya Bezbaruah

Approved by Department Chair:

06-March-2012	Dr. Dean C. Webster
Date	Signature

ABSTRACT

Advanced electrochemical techniques such as electrochemical impedance spectroscopy (EIS), electrochemical noise method (ENM) and coulometry as tools to study and extract information about the coating system is the focus of this dissertation. This dissertation explored three areas of research. In all the three research areas, advanced electrochemical techniques were used to extract information and understand the coating system. The first area was to use EIS and coulometric technique for extracting information using AC-DC-AC method. It was examined whether the total charge passing through the coating during the DC polarization step of AC-DC-AC determines coating failure. An almost constant total amount of charge transfer was required by the coating before it failed and was independent of the applied DC polarization.

The second area focused in this dissertation was to investigate if embedded sensors in coatings are sensitive enough to monitor changes in environmental conditions and to locate defects in coatings by electrochemical means. Influence of topcoat on embedded sensor performance was also studied. It was observed that the embedded sensors can distinguish varying environmental conditions and locate defects in coatings. Topcoat could influence measurements made using embedded sensors and the choice of topcoat could be very important in the successful use of embedded sensors.

The third area of research of this dissertation work was to examine systematically polymer-structure coating property relationships using electrochemical impedance spectroscopy. It was observed that the polymer modifications could alter the electrochemical properties of the coating films. Moreover, it was also observed that by cyclic wet-dry capacitance measurement using aqueous electrolyte and ionic liquid, ranking of the stability of organic polymer films could be performed.

TABLE OF CONTENTS

LIST OF TABLES

LIST OF FIGURES

CHAPTER 1. GENERAL INTRODUCTION TO CORROSION, CORROSION CONTROL AND ELECTROCHEMICAL MEASUREMENT METHODS

1.1. Corrosion

Most of the metals and alloys that are in use today do not exist in nature in their metallic state. They are processed from their stable oxidation states into metals that are thermodynamically unstable in the environment. Given the first available opportunity for interaction with the environment these metals tend to revert back to their original stable oxidation state. It is this tendency of the metal to oxidize back to their original state that is termed as 'corrosion'. More generally, corrosion can be defined as the deterioration of a material due to its interaction with the environment. Deterioration could be due to weakening of the material due to loss of cross sectional area, shattering of metal due to hydrogen embrittlement, or degradation of polymer due to exposure to UV light. Materials can be metals, polymers, ceramic or composites.[1, 2]

The cost of corrosion in USA is estimated to be around $2.76 billion per year which is approximately 3.1% of the gross domestic product (GDP) according to the study "Corrosion Costs and Preventive Strategies in the US" conducted by CC technologies in 2002.[3] Corrosion, therefore, is a major problem. Most of the metals and alloys that are in use today such as steel, aluminum and their alloys are all prone to corrosion. Structures made up of these metals or alloys such as pipelines, bridges, tanks, aircrafts, vehicles and rebars all corrode unless protective strategies are implemented to avoid severe damage. A major accident attributed to corrosion is the Aloha incident of April 28,1998 in which the Aloha Boeing 737 aircraft lost a major portion of the its upper fuselage during flight at 24,000 feet above the ground. It was reported that the corrosion processes along with the

buildup of voluminous corrosion products inside the lap joint resulted in pillowing and separation of the joints.[4, 5] Many other catastrophic corrosion incidents have also been reported.[6]

1.2. Corrosion process

Corrosion mainly is an electrochemical process and is the result of an electrochemical reaction at the surface of a metal/alloy. For corrosion to occur, four requirements must be met. There must be an anodic reaction, a cathodic reaction, and ionic and electronic conductive pathways between the anode and the cathode.[7]
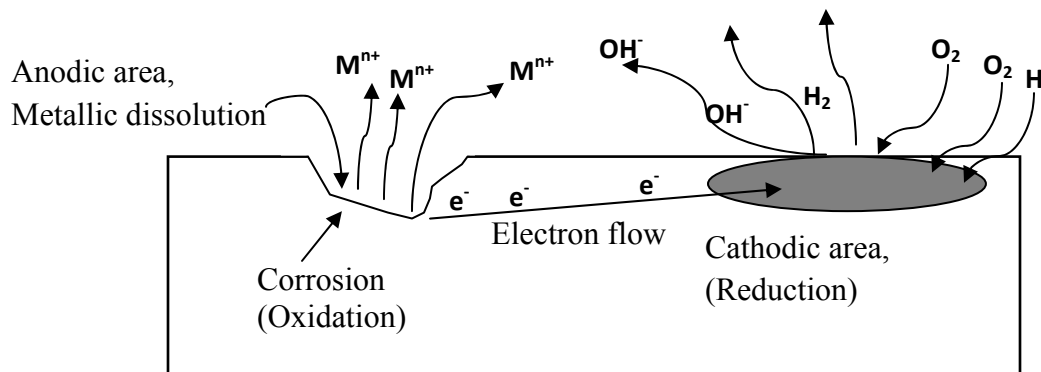
Figure 1.1: Schematic of a typical corrosion event.

During corrosion, the metal undergoes oxidation as the anode and losses electrons to form a more stable compound.

$$M \rightarrow M^{n+} + ne^- \tag{1.1}$$
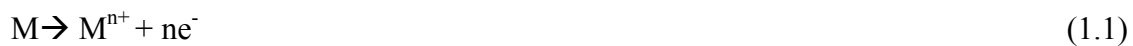
The electron liberated during anodic dissolution flow through the metal to the cathode where they are consumed. Depending upon the pH and oxygen availability, various reduction reactions may take place at the cathode. In acidic and neutral solution, following reactions are often observed.

$$2H_2O + O_2 + 4e^- \rightarrow 4OH^- \text{ (neutral or basic solution)} \tag{1.2}$$

$$2H^+ + 2e^- \rightarrow H_2 \qquad \text{(acid solution)} \tag{1.3a}$$

$O_2+4H^++4e^- \rightarrow 2H_2O$ (1.3b)
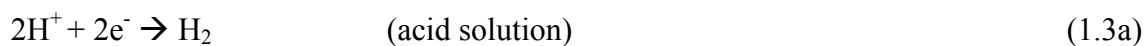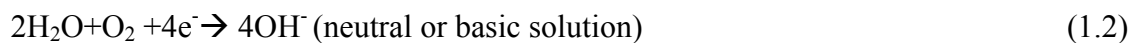
Water will be reduced in the absence of other reduction reactions.[8]

$2H_2O + 2e^- \rightarrow H_2 + 2OH^-$ (1.4)

1.3. Corrosion of steel and aluminum alloys

Two of the most widely used structural materials are steel and aluminum alloys. They are used as the load bearing materials for many structural applications. However the issue of corrosion must be addressed in order to ensure their optimal performance. Usually they are selected not for their corrosion resistance but for their strength, ease of fabrication, cost, etc., and hence the issue of corrosion has to be addressed post fabrication. Both steel and aluminum alloys are prone to corrosion under atmospheric or most working conditions.

1.3.1. Steel

Rusting of steel is perhaps the best example of metallic corrosion. Steel is widely used as structural backbone in buildings and skyscrapers. It is used in bridges, tanks, pipelines, vehicles, major appliances, heavy equipments such as bulldozers, railway line and car etc. It is subject to corrosion in aqueous solutions. In the presence of water/moisture, salts and oxygen, it corrodes to form oxides and mixed species. In the presence of oxidizing species a passivating hydrated iron oxide layer can form on the surface. Such an oxide layer might be loose or imperfect depending upon the alloy content and type. Low and non-alloyed steels form loose iron oxide products on the surface and are unable to protect the underlying metals from further corrosion.[9]

The reactivity of iron in aqueous solution can be further understood by the Pourbaix diagram.[10] At pH below ~9 and a potential above ~-0.6, iron tends to exists as Fe^{+2}

implying that it will corrode under these conditions. At higher pH and potential, iron is mostly passive. Below approximately -0.5V iron is immune to corrosion.

1.3.2. Aluminum alloys

Pure aluminum (Al) is a light and soft metal with very good corrosion resistance property due to the formation of a strong, resistive adherent oxide layer. Upon contact with dioxygen it forms a very thin (1-100nm) but strongly adherent and impermeable aluminum oxide layer which can protect the underlying Al substrate from environmental attack such as oxygen, water and other reactive chemicals. However, pure Al is highly ductile and lacks tensile strength. This has hindered it from being used in structural applications.[11]

To enhance its mechanical properties Al is alloyed with elements such as Cu, Zn, Mg, Mn and Si.[12] Two such alloys are AA-2024 T3 and AA-7075 T6, which are widely used in aerospace industry due to their enhanced mechanical property and high strength to weight ratio. Figure 1.2a and 1.2b depicts the microstructure of AA-2024 T3 and AA-7075 T6. Their high strength is derived from the phase separated intermetallic compounds that are present within the bulk alloy matrix and grain boundaries. However these intermetallic-compounds provide galvanic corrosion sites and render the alloys susceptible to localized corrosion.[13-15] Therefore, protecting these alloys from corrosion becomes essential to prevent service failure of Al alloys and obtain useful lifetimes of material performance.

1.4. Corrosion preventive strategies

To increase the lifetime of structures in use and obtain maximum performance, corrosion preventive strategies have to be implemented. Apart from appropriate material selection, proper design and material modification, two other strategies of material

protection exist that are widely in use. They are the use of sacrificial/ cathodic protection of structures and protective coatings to act as barriers to corrosive environments.
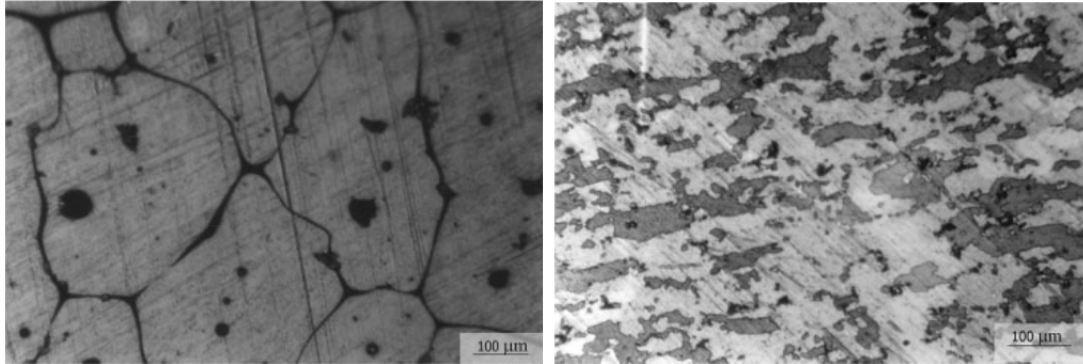
Figure 1.2: Microstructure of the Al alloys, rolling direction, a) 2024-T3, and b) 7075-T6. [Khoshnaw et al., *Materials and Corrosion* 2007, *58* (5), 345-347].

1.4.1. Cathodic/Sacrificial protection

Cathodic or sacrificial protection is based on the concept that the structure to be protected is converted into the cathode of an electrochemical cell. Since metallic dissolution or anodic reaction is corrosion, being the cathode where only reduction reactions take place, means no metallic dissolution and true protection. Cathodic protection of ship hulls, concrete rebar and pipelines are some examples of the use of this technology.

Cathodic/sacrificial protection can be achieved in two ways. Firstly, by impressing an externally generated cathodic current on the substrate forcing electrons towards the structure to be protected so that only the reduction reaction is favored at the structure and secondly, by the use of a sacrificial anode that is more active than the structure to be protected. Zinc and magnesium are some examples of active anodes used for sacrificial protection.[16-18] The sacrificial anode used during this process must be galvanically more active than the structure to be protected. Figure 1.3 lists galvanic series of various metal

and alloys in sea water. An understanding of galvanic series is essential in order to ensure proper protection of structures by sacrificial means.

Cathodic (noble)
Platinum
Gold
Graphite
Titanium
Silver
Zirconium
AISI Type 316, 317 Stainless steels (passive)
AISI Type 304 Stainless steels (passive)
AISI Type 430 Stainless steels (passive)
Nickel (passive)
Copper-Nickel (passive)
Bronzes
Copper
Brass
Nickel (active)
Naval brass
Tin
Lead
AISI Type 316, 317 stainless steels
AISI Type 304 stainless steels (active)
Cast iron
Steel or iron
Aluminum alloy 2024
Cadmium
Aluminum alloy 1100
Zinc
Magnesium and magnesium alloys
Anodic

Noble Metal

Reactive Metal

Figure 1.3: Galvanic series of various metal and alloys in sea water. [Jones D.A., 2nd edition, *Principles and Prevention of Corrosion* 1996, Macmillan Publishing Company, USA, 14].

6

1.4.2. Coatings

Coatings are seen almost everywhere. Chances are that they are the first things that we see around us. A primary use of coating is corrosion protection. However, they may also provide aesthetic and specialty functions.[19-22] Among the coatings used to protect various structures, organic coatings are widely used today and have gained huge significance. Organic coating film consists of a polymeric binder in addition to additives and pigments in its final form. The binder may be natural (e.g. rubber) or synthetic (e.g. polyurethane, epoxy) and to a large extent govern the coating properties. The binder binds together other constituents of the coatings, adhere to the substrate and form a continuous film. Various binder systems that are currently in use in coating industries are epoxies, polyurethanes, drying oils, alkyds, silicones, acrylics, phenolics, polyesters, and amines.[23] The end use of organic coatings include bridges, buildings and skyscrapers, aircrafts, transportation, wood flooring, pipelines, plastic and metal coil stock. Depending upon the choice of substrate and environment, certain coating systems is chosen.

The use of coating for corrosion prevention is primarily based on the concept that it isolate the substrate from interaction with the environment. There can be three ways by which a coating system can protect structures from corrosion.[24] They are 1) barrier protection 2) cathodic/sacrificial protection and 3) inhibitive protection. In the barrier protection mode intact coating provides protection to the substrate by blocking the transport of oxygen, water and electrolyte ions such as Cl^-, SO_4^{2-}, Na^+, K^+, NH_4^+ and Ca^{2+} to the substrate surface. In the absence of these chemicals at the metal-coating interface any electrochemical corrosion reaction or physical delamination of the coating is prevented and the substrate is protected. Not only this, the transport of ionic and electronic charge is also

7

blocked and this property has been considered to be important for barrier protection and a distinguishing feature of good coating.[24]

A barrier coating succeeds by blocking the anodic reaction, cathodic reaction or conductive pathways between the anode and the cathode. A good wet adhesion between the coating and the substrate ensure no substrate exposure for corrosion reaction to take place. For systems where pigments are used it must be ensured that the pigment volume concentration (PVC) does not exceed the critical pigment volume concentration (CPVC) to obtain barrier properties. Above the CPVC the onset of voids can allow easy access of ions and electrolytes to the substrate. Moreover, coating designed to act as barriers, must be thick or be applied in multiple layers.[24, 25]

In the inhibitive protection mode, corrosion inhibitors are loaded into the coating matrix so that when the coating is damaged and the substrate is exposed the inhibitors can act by passivating the metal surface and blocking the corrosion reaction. Inhibitors can be defined as a chemical compound which when present in a small amount in corrosive environment of a metal can effectively decrease its corrosion rate. Inhibitors may be organic or inorganic in composition. Inorganic inhibitors often act by undergoing reduction at the damaged or active corrosion sites and forming insoluble precipitates. These precipitates deposit and provides barrier to the permeation of species such as electrolytes, water and oxygen. Examples include phosphates, molybdates, tungstate and the highly efficient chromates.[26-29] Chromates, owing to their slight solubility in water, strong oxidizing behavior and passive nature of their corrosion products are very effective and are widely used in aerospace pretreatment and primer. They are however, carcinogenic and are in the verge of legally being phased out. Efforts at replacement of chromates with benign

8

environmentally friendly substitutes are on its way.[14, 30] Among the organic pigments used include aliphatic and aromatic amines such as ethylenediamine, ammonia, cyclohexylamine, benzylamine, aniline, methylaniline, dimethylaniline, phenylhydrazine, phenylenediamine, ortho and para toluidine. Aromatic organic inhibitors inhibit corrosion by forming an adsorbed layer on the metal surface.[31] It is widely believed that a prerequisite for organic inhibitors to be effective is their attachment to the metal surface. They also act by increasing the local pH and thereby providing passivation of the substrate. It has been reported that when the corrosive environment is comprised of dissolved oxygen, salts and weak acids inorganic inhibitors have been successfully used to minimize corrosion. When strong acids, acid brines, high temperatures and microbial actions constitute corrosive environment, the polar organic compounds and colloidal organic materials have been found to be better corrosion inhibitors.[32]

The third form of protection is similar to galvanic protection as discussed in section 1.4.1 except that the active metallic particles are loaded in the coating matrix in pigment form and are an integral part of the coating system. They are added to the matrix in certain amount such that the pigment particles are in contact among themselves and also with the substrate for which protection is desired. Under such condition the OCP of the system is a mixed potential that is between the rest potential of the substrate and the sacrificial pigment particles. The substrate is cathodically polarized and is protected from corrosion.[33] Common examples of sacrificial pigment containing primer is the traditional Zn based primer system used to protect steel substrate and the more recent Mg rich primer system designed for the protection of aluminum alloys.[14, 34-37]

1.5. Evaluating coating performance

Prior to the application of the coating it is important to verify the ability of the coating to provide the intended properties for which it is designed for. Depending upon the intended application the requirements may vary. Long term corrosion protection remains one of the most important requirement for which a coating is designed for. Exposing the coating in the real life exposure condition is the best way of evaluating its performance. Such tests however may take months or even years and is quite impractical. Acceleration of the failure is necessary to provide reasonable development times.

Current accelerated conventional coating evaluation methods such as salt spray (ASTMB117), Prohesion (ASTM G85) and Prohesion/QUV tests are aggressive methods that were designed to simulate the atmospheric condition such as humidity, temperature, UV radiation, and salt concentration in the laboratory and induce coating failure in a shorter time. Ideally, the parameters that lead to coating degradation are attempted to be amplified without changing in the failure mechanism. Salt spray test consists of exposing the coating to a continuous fog of 5 wt% NaCl at 35°C whereas Prohesion® tests involve repeated cyclic exposure of the coated panel in wet and dry environment for 1 hour each. The wet cycle consists of exposing the coated panel in a fog of dilute Harrison's solution [0.05% wt. NaCl and 0.35 wt. % $(NH_4)_2SO_4$] at 25°C whereas the dry cycle consists of exposing the samples in air at 35°C. Prohesion/QUV test is a cyclic test alternating weekly between Prohesion and QUV. QUV stage consists of exposing the coating to 4 hours of UV light at 60°C and 4 hours of condensation at 50°C repeatedly for a week until the next Prohesion step.

Figure 1.4: Picture of ASTM B117 salt spray chamber. [Source CPM, NDSU]

These evaluation methods are, however, qualitative in nature and monitoring of coating performance is done by visual inspection of the coating. Therefore, the evaluation is subjective and prone to inaccurate judgments. Coating is considered failed only when visual defects are observed. The process of corrosion however may start earlier than the observed ability of defects. Such test methods also do not exactly simulate conditions to which the coatings will be exposed to during service and hence any conclusions based on such tests might be erroneous. For example, a sample may perform well on one test and fail on other. Also for coating systems that are robust enough the time to failure during such test conditions may be very long as was observed by Bierwagen et al.,[38] for aircraft coating system under Prohesion exposure condition. The coatings displayed excellent barrier property even after 2 years of Prohesion exposure. Test methods such as B117 and Prohesion have been under criticism too. Today almost every automotive company has their own standard corrosion test.[24, 39-41]

1.6. Coating characterization by electrochemical techniques

Since the corrosion process is electrochemical in nature, electrochemical characterization techniques are more appropriate and are widely used in understanding the

corrosion behavior of structures and protective performance of organic coatings. These techniques also circumvent the disadvantage of subjective and qualitative evaluation of coatings performed with the exposure testing methods. Two widely used electrochemical methods are electrochemical noise method (ENM) and electrochemical impedance spectroscopy (EIS).

1.6.1. Electrochemical Noise Methods (ENM)

Electrochemical noise methods (ENM) involve the analysis of spontaneous fluctuations of potential and current from a naturally corroding electrode. In ENM, the electrochemical noise measurement is carried out between two nominally identical panels that acts as the two working electrodes filled with aqueous electrolyte and connected by a salt bridge. A reference electrode is placed in one of the cells. Current noise is measured as fluctuation in noise between two 'identical' working electrodes connected by a zero resistance ammeter so that they are at the same working potential. Potential noise is measured as fluctuation in potential between a working electrode and a reference electrode. ENM has found growing applications in investigation related to corrosion and in evaluating performance of organic coating.[42-47]

ENM is highly sensitive and is completely non-intrusive since only spontaneous fluctuations in current and potential is measured. This method provides rapid ranking and furnishes quantitative information on the protective properties of organic coating. ENM also facilitates *in-situ* monitoring of corrosion processes. A good correlation and reproducibility between ENM results and results from other electrochemical testing techniques such as linear polarization and electrochemical impedance spectroscopy (EIS) has been observed.[48-50]
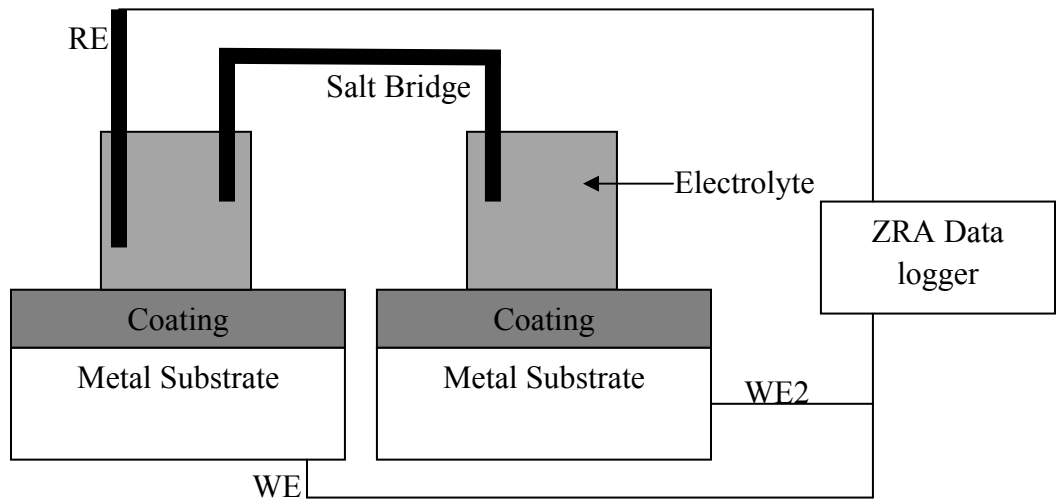
Figure 1.5: A typical three electrode two metal substrate ENM configuration.

Modification of the ENM method has been done in order to facilitate field application. Mabbutt et al.,[51] devised a single substrate configuration also called the reverse three electrode ENM configuration that was a modification of the traditional three electrode configuration. In this configuration a single substrate contained two electrolytic cells and the salt bridge was obviated. This method however required a connection to the substrate. A further modification known as "No Connection to the Substrate" (NOCS) was done obviating the need for connection to the substrate. In this method a single substrate contained three electrolytic cells, one of which was a reference electrode, the other two being the two working electrodes. Figure 1.6 depicts the NOCS configuration method of ENM measurement. It was also observed that the results obtained from such measurement were consistent with measurements made from traditional ENM and the reverse ENM method.[51]

13
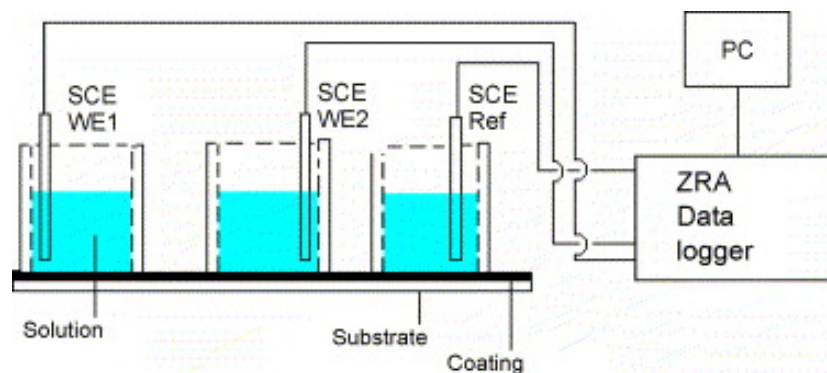
Figure 1.6: NOCS configuration for ENM measurements. [S. Mabbutt, D.J. Mills, C.P. Woodcock, *Progress in Organic Coatings*, 59 (2007) 192-196].

Recently the successful use of embedded sensors in coatings to perform electrochemical measurements was performed using these more simple electrochemical noise measurement methods which have possible use in field application. The complex set up of the conventional design is obviated and measurements are more convenient. In one such study by Quan Su et al.,[52] ENM measurement was performed using two sensors embedded on the coating that worked as the two working electrode whereas the substrate acted as the reference electrode. It was demonstrated that noise resistance, R_n, measured using sensors were similar to the impedance data obtained using EIS. Bierwagen et al.,[53] had earlier observed that the results obtained from conventional ENM measurement for same sample was very close to the ENM measurement performed using embedded sensors. Allahar et al.,[48] also has demonstrated the utility of sensors in the ENM measurements in coated substrates.

The sources of electrochemical noise have been classified into three major types: Thermal noise, shot noise and flicker noise.[54]

14

1.6.1.1. Thermal noise: Thermal noise is the result of thermally activated motion of charge carriers such as electrons, ions or charge movement at the interface. The motion results in random separation of charges across resistors and generates a voltage noise given by

$$\psi_E = 4kTR \qquad\qquad (1.5)$$

where ψ_E is the thermal potential noise, k is the Boltzmann constant, T is the absolute temperature and R is the resistance.[55] Thermal noise is white since ψ_E is frequency independent and is associated with the low frequency plateau in the power spectral density (PSD) plot. For passive metals and coated samples the impedance of the metal-solution interface may be high and thermal noise can be significant.[54, 56]

1.6.1.2. Shot noise: Shot noise is based on the assumption that the charge is quantized and is composed of packet of charge passing a given point. For independently moving charge carriers the current noise is given by

$$\Psi_I = 2qI = 2f_n q^2 \qquad\qquad (1.6)$$

Where Ψ_I is the power spectral density (PSD) of the current noise, q is the charge on charge carrier, I is the mean current and f_n is the mean frequency of charge emission. Some assumptions when Shot Noise theory is used for the analysis of electrochemical noise signals are; [54, 56-58]

- Current is generated by pulses of same shape and charge.
- Pulses are independent statistically.
- Cathodic reaction is considered noiseless.
- The two working electrodes corrode at the same rate.
- Solution resistance is zero.

Under these assumptions, by using low frequency PSD value of voltage noise and current noise, q and f_n can be obtained.

$$q = \frac{\sqrt{\Psi_E}\,\sqrt{\Psi_I}}{B} \qquad (1.7)$$

and

$$f_n = \frac{B^2}{\Psi_E A} \qquad (1.8)$$

Where ψ_E is the PSD of potential noise, B is the Stern-Geary coefficient and A is the electrode exposed area.

1.6.1.3. Flicker noise: Flicker noise is also known as 1/f noise and is the noise whose amplitude is inversely proportional to frequency. It is widely observed in a range of physical systems. For Flicker noise, the PSD α f^n , where n < 0 and f is the frequency. No theoretical treatment exists that suggest that electrochemical systems should exhibit flicker noise.[54, 56]

1.6.1.4. Data analysis from ENM:

1.6.1.4.1. Time domain analysis and frequency domain analysis

Data from ENM measurement are initially obtained in the time domain as potential noise and current noise. Statistical analysis of these data can furnish important information on the state of the coating and the metal substrate beneath. Two significant parameters of the time domain analysis are the Noise resistance R_n and Localization Index LI.[59, 60] R_n is defined as

$$R_n = \frac{\sigma_V}{\sigma_I} \qquad (1.9)$$

Where σ_V and σ_I are the standard deviations of potential noise and current noise respectively. R_n is associated with the barrier protection property of the coating and is

comparable to the polarization resistance R_p and low frequency impedance.[59, 61-64]

Localization index, LI is another important parameter obtained in the time domain during

ENM measurement. LI can be defined as

$$LI = \frac{\sigma_I}{I_{rms}}$$ (1.10)

Where I_{rms} is the root mean square of the current noise. LI can furnish information about

the corrosion mechanism of the metal substrate. A LI value less than 10^{-3} indicates uniform

corrosion whereas an LI value larger than 0.1 indicates localized corrosion. A value

between the two indicates mixed corrosion.[53]

In addition to the statistical analysis of ENM data transformation of the original

noise data from the time domain to the frequency domain can be done using mathematical

algorithm calculations. The normal approach used to characterize a random signal is to

estimate its power spectral density (PSD) which is the distribution of the power of the

signal in the frequency domain. Two methods are employed to obtain the PSD of noise

signals. One is the Fast Fourier Transform (FFT) and the other is the Maximum entropy

Method (MEM). MEM has several advantages over FFT: It is faster than FFT since it does

not need ensemble averaging, it gives continuous and smooth spectra compared to FFT and

it also allows computation of the spectrum at frequencies that are lower than the inverse of

the acquisition time, which is the lowest frequency calculated by the FFT. [65, 66]

The PSD of the current noise (Ψ_I) and potential (Ψ_V) noise obtained by the

transformation can be used to obtain the spectral noise resistance $R_{sn}(f)$.[67]

$$R_{sn}(f) = \sqrt{\frac{\Psi_V}{\Psi_I}}$$ (1.11)

$R_{sn}(f)$ can also be defined as $R_{sn}(f) = |V_{FFT}(f)/I_{FFT}(f)|$, where $V_{FFT}(f)$ and $I_{FFT}(f)$ are the FFTs of potential and current fluctuations respectively.[68, 69] For spectral noise plot independent of frequency, $R_n = R_{sn\ f \to 0} = R_p = |Z|_{f \to 0}$.[46, 66]

The shot noise parameters such as charge of events, q, and frequency of events, f_n, obtained using the power spectral density of potential noise and current noise can also furnish important information regarding the nature of corrosion of the metal substrate. A large value of f_n is indicative of a uniform corrosion whereas smaller value indicates localized corrosion. The charge of event, q, is indicative of the intensity of the corrosion process. Values of q however should be interpreted with caution when using them for studying corrosion mechanism.[54]

1.6.2. Electrochemical Impedance Spectroscopy (EIS)

EIS has been well established as a very powerful technique that is used for investigation in areas such as understanding the mechanisms of electrochemical reactions, transport, and dielectric and barrier properties of materials and for the investigation of passive surfaces. It has also been used by many groups to study the properties of organic coating system.[25, 38, 70-74] In the EIS technique, a small AC potential perturbation, typically a sine wave of amplitude $\sim \pm 10mV$, is applied on a system with respect to its open circuit potential over a wide range of frequency (typically from 10^5 -10^{-2} Hz or 10^{-3} Hz) and the response of the current is measured at each frequency.

The excitation signal expressed as a function of time is of the form

$$V(t) = V_o \sin(\omega t) \qquad\qquad\qquad (1.12)$$

where V(t) is the applied AC potential perturbation , V_o is the amplitude of the excitation

signal, t is the time and $\boldsymbol{\omega}$ is the angular frequency representing the number of cycles in one seconds. $\boldsymbol{\omega}$ is related to the temporal frequency f by

$$\boldsymbol{\omega}=2\pi f \qquad (1.13)$$

In a linear system, the response of the potential perturbation is a current signal I(t) that is shifted in phase by ϕ and has the amplitude of I_o and is given by

$$I(t) = I_o sin(\boldsymbol{\omega}t- \phi) \qquad (1.14)$$

For a purely resistive system ϕ is zero and the impedance is given by resistance of the system. However for systems displaying non resistive behavior the impedance is given by

$$Z=\frac{V(t)}{I(t)} = V_o sin(\boldsymbol{\omega}t)/I_o sin(\boldsymbol{\omega}t- \phi) \qquad (1.15)$$

$$= |Z| (cos \phi + jsin \phi) \qquad (1.16)$$

Where $|Z|$ is the modulus of impedance and is given by V_o/I_o. The impedance Z can be also be expressed by complex number as

$$Z = Z' + jZ'' \qquad (1.17)$$

where Z' is the real part and Z'' is the imaginary part of the complex impedance and $j^2=-1$. Resolving the real and the imaginary parts the following equations are obtained:

Real $Z= Z' = |Z| cos\phi \qquad (1.18)$

Imaginary $Z=Z'' = |Z|sin\phi \qquad (1.19)$

The phase angle is given by

$$\Phi = tan^{-1}(Z''/Z') \qquad (1.20)$$

and the modulus of the impedance is given by

$$|Z| = [(Z')^2+ (Z'')^2]^{1/2} \qquad (1.21)$$

The EIS technique also has several advantages. It is considered to be a non-destructive technique since the system is perturbed very minimally during measurement.

Rapid acquisition of data is possible except at low frequencies. Moreover, the results are quantitatively similar to ENM.[75]

For EIS studies on metal/coated system, a three electrode configuration is normally used. The metal substrate acts as the working electrode. Platinum mesh, graphite rods, or any other noble metal can act as the counter electrode. A saturated calomel electrode generally is used as the reference electrode. However, other reference electrodes such as silver/silver chloride or mercury/mercury sulfate can also be used.[76] Figure 1.7 depicts the most commonly used or "conventional" EIS set up.
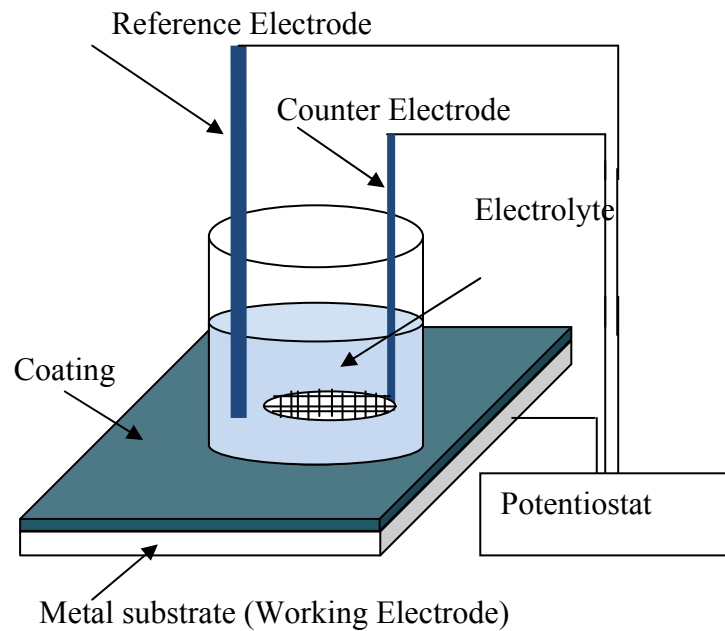
Figure 1.7: Schematic of conventional EIS set up.

For conditions where reference electrode cannot be used, other configurations such as two electrode EIS measurements have been employed with the counter electrode acting both as counter and a pseudo reference electrode.[77] A 2 electrode setup is sufficient for performing EIS measurement of barrier coatings, since precise knowledge of the potential of the substrate is not required.[78]

The EIS data are analyzed via two major plots, the Nyquist plot and the Bode plot. The Nyquist plot is a plot of real component of impedance in the abscissa and imaginary value of impedance as the ordinate. An advantage of the Nyquist plot is that it provides a clear signature of diffusion effects (e.g. a 45° line for infinite diffusion). The Bode plot is a plot of log of modulus of impedance and phase angle as the ordinate and log of frequency as the abscissa. Advantage of the Bode plot is its ability to display large variation in the Z values. The low frequency Z value is related to the barrier performance of the coating and can be used to estimate polarization resistance.[79]

In order to understand the various physical processes occurring in the coating system under investigation fitting of the EIS data to an equivalent circuit can be done. A direct connection between the idealized circuit model and the behavior of the real system often exists. However only simple circuits provides unambiguous description of experimental data. [80] Each circuit element obtained by fitting the EIS data correlates to the corrosion properties of the system and the extracted values of the circuit elements provides quantitative information of the processes involved.[80, 81] Figure 1.8b and 1.9b represent an equivalent circuit model of an intact coating and a degraded coating corresponding to their bode plot in Figure 1.8a and 1.9a respectively. The coating whose metal-coating interface is intact is represented by a parallel circuit consisting of a capacitance known as the coating capacitance C_c and a resistance known as coating resistance R_c (sometimes known as pore resistance R_{po}). For coating that has degraded whose interface has been compromised an additional resistance and capacitance element is added to the circuit known as the charge transfer resistance R_{ct} and the double layer

capacitance C_{dl}. These circuit parameters are used to specify the coating disbondment and

interfacial corrosion attack.[71, 82, 83]
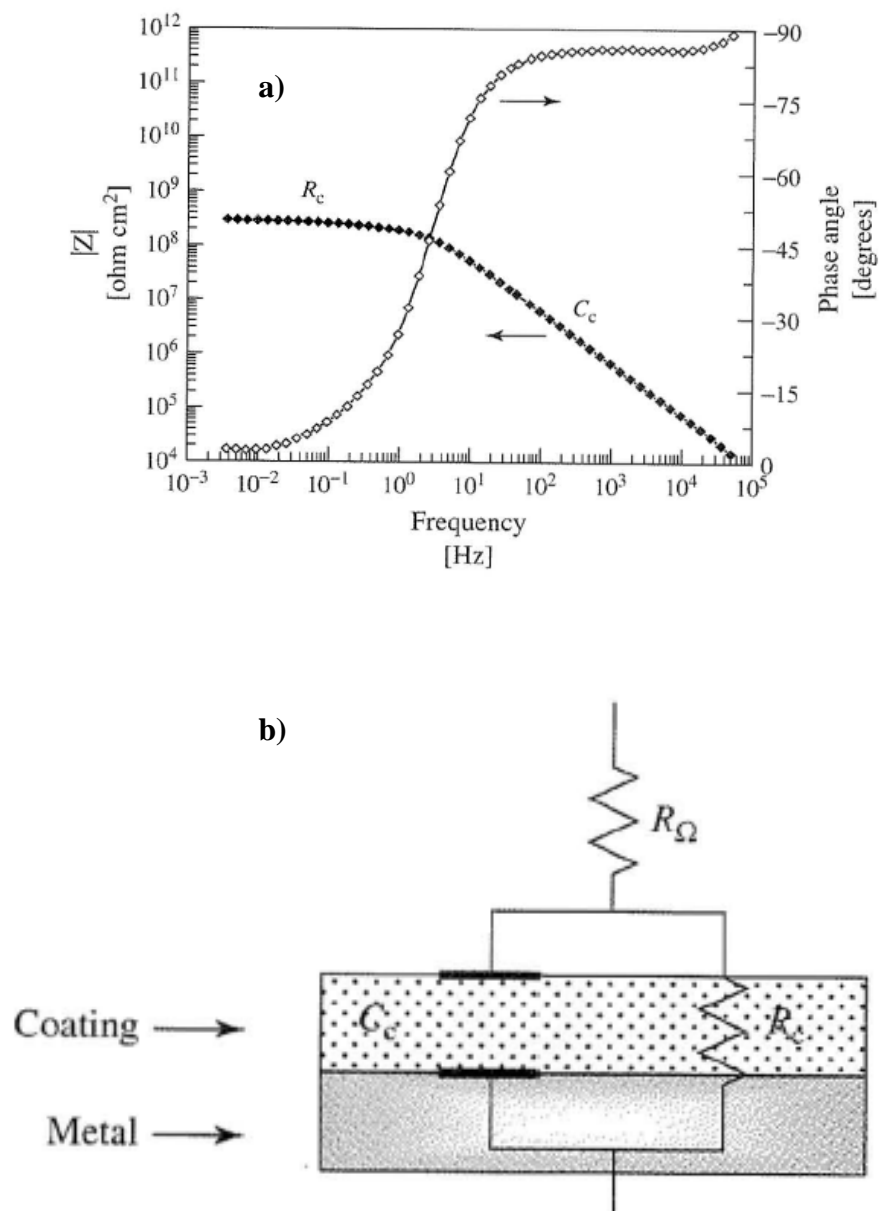
Figure 1.8: a) EIS Bode plot of an undamaged coating and b) its equivalent circuit. [Taken from Grundmeier et al., *Encyclopedia of Electrochemistry*, Vol. 4, Chapter 5.4, page 521].
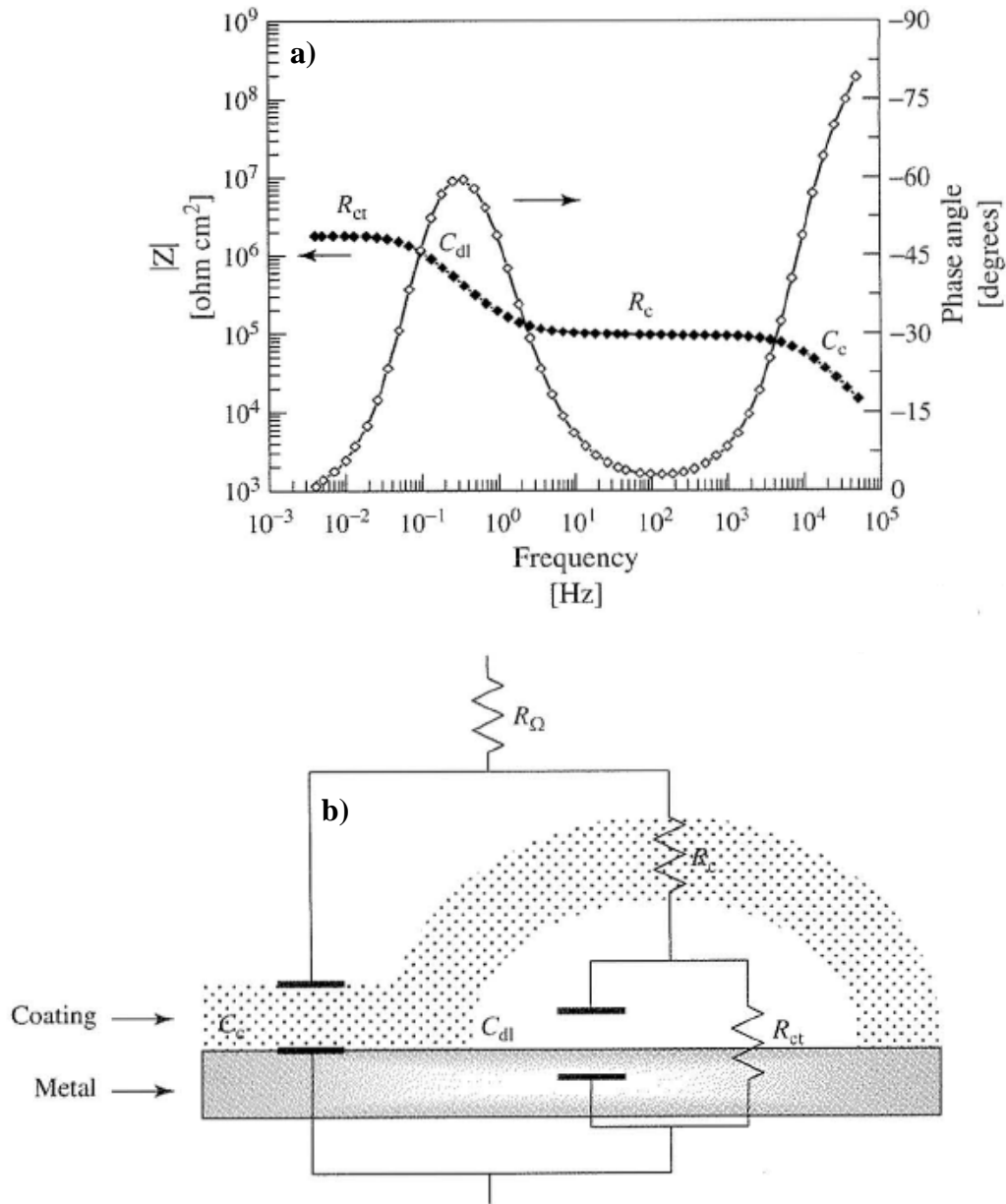
Figure 1.9: a) EIS Bode plot of a damaged coating whose corrosion has occurred under the blisters and b) its equivalent circuit. [Taken from Grundmeier et al., *Encyclopedia of Electrochemistry*, Vol. 4, Chapter 5.4, page 522].

In addition to the impedance measurement, the EIS technique can also be used to understand the capacitance behavior of the coating, which may allow the estimation of volume fraction of water uptake by the coating and rate of water uptake or diffusion

coefficient. EIS has been successfully used to measure the water uptake and diffusion behavior in coating systems.

The transport of water in an organic coating that obeys Fick's second law can be written in mathematical expression of the form

$$\frac{\delta c(z,t)}{\delta t} = D \frac{\delta^2 c(z,t)}{\delta z^2} \qquad (1.22)$$

Where c is the concentration of water at a position z normal to the coating surface, t is the exposed time and D is the diffusion coefficient. An approximate short time one dimensional solution to this equation is given by

$$\frac{M_t}{M_s} = \sqrt{\frac{4Dt}{L^2 \pi}} \qquad (1.23)$$

Where M_t and M_s are the mass of the absorbed water at time t and at saturation respectively. L is the coating thickness. D is assumed to be independent of c.[84, 85] The diffusion coefficient of water can be obtained by relating Brasher and Kingsbury equation[86] that has the volume fraction of absorbed water with the mass fraction of absorbed water as obtained from Fick's second law. The volume fraction of coating occupied by water, ϕ_t, as obtained from Brasher and Kingsbury equation is given by[86, 87]

$$\phi_t = \frac{Log\{\frac{C(t)}{C(o)}\}}{Log\varepsilon_{H_2 O}} \qquad (1.24)$$

Where C(t) and C(o) are the capacitance of the coating at time t and at zero time respectively and ε is the dielectric constant of water.

Capacitance can be obtained by single frequency EIS (SFEIS) measurement. The imaginary impedance value (Z_{imag}) from the SFEIS measurement measured at a frequency f (usually $f > 10^3$Hz) is related to the capacitance of the coating C and can be written as

$$Z_{imag} = \frac{-1}{2\pi f C(t)} \qquad (1.25)$$

24

Since capacitance of a coating is a function of its dielectric properties, changes in these will changes the capacitance of the coating.[88] Polymer has dielectric constant of around 3-5 whereas the dielectric constant of water is around 80 at room temperature.[89, 90] Therefore as water is absorbed by the coating the dielectric of the coating increases resulting in increase in capacitance that is manifested as an increase in the imaginary impedance during the single frequency EIS measurement. Equation 1.24 can also be written in the form;

$$\frac{\phi_t}{\phi_s} = \frac{Log\{\frac{C(t)}{C(o)}\}}{Log\{\frac{C(s)}{C(o)}\}} \qquad (1.26)$$

where $\frac{\phi_t}{\phi_s}$ is a measure of the degree of saturation and is the ratio of volume fraction of coating that is occupied by water at time t and at saturation respectively and C(s) represents the capacitance of the coating at saturation. Equation 1.23 and 1.26 can be equated and we get an equation of the form

$$\frac{Log\{\frac{C(t)}{C(o)}\}}{Log\{\frac{C(s)}{C(o)}\}} = \sqrt{\frac{4Dt}{L^2\pi}} \qquad (1.27)$$

From this equation the value of D can be obtained by plotting the left hand side (LHS) as ordinate and √t as the abscissa, the slope of the curve being $\sqrt{\frac{4D}{L^2\pi}}$.

1.7. References

[1] http://corrosion.ksc.nasa.gov/corr_fundamentals.htm (12-01-2011), in.

[2] D.A. Jones, Principles and Prevention of Corrosion, 2nd ed., 1996.

[3] G.H. Koch, M.P.H. Brongers, N.G. Thompson, Y.P. Virmani, J.H. Payer, Corrosion Cost and Preventive Strategies in the United States (Report No. FHWA-RD-01-156), in, 2001.

[4] D. Miller, Corrosion Control on Aging Aircraft: What is being done?, Materials Performance, 29 (1990) 10-11.

[5] J. Komorowski, N. Bellinger, R. Gould, A. Marincak, R. Reynolds, Quantification of corrosion in aircraft structures with double pass retroreflection, Canadian Aeronautics and Space Journal, 42 (1996) 76-82.

[6] P.R. Roberge, Handbook of corrosion engineering, McGraw-Hill Professional, 2000.

[7] J.R. Davis, Corrosion: understanding the basics, ASM International, 2000.

[8] D.A. Jones, Principles and prevention of corrosion, Macmillan Publishing Company, (1992) 7.

[9] R.A. Dickie, F.L. Floyd, 'Polymeric Materials for Corrosion Control: An Overview, in, ACS Publications, pp. 1–16.

[10] M. Pourbaix, Atlas of electrochemical equilibria in aqueous solutions, 2nd English edition, Copyright NACE International 1974 and CEBELCOR.

[11] A.W. Apblett, Aluminum: Inorganic Chemistry, in: Encyclopedia of Inorganic Chemistry, John Wiley & Sons, Ltd, 2006.

[12] J.R. Davis, J. Davis, Aluminum and aluminum alloys, Asm Intl, 1993.

[13] P. Campestrini, H. Terryn, A. Hovestad, J.H.W. de Wit, Formation of a cerium-based conversion coating on AA2024: relationship with the microstructure, Surface and Coatings Technology, 176 (2004) 365-381.

[14] M. Nanna, G. Bierwagen, Mg-rich coatings: A new paradigm for Cr-free corrosion protection of Al aerospace alloys, Journal of Coatings Technology and Research, 1 (2004) 69-80.

[15] S. Lamaka, M. Zheludkevich, K. Yasakau, M. Montemor, M. Ferreira, High effective organic corrosion inhibitors for 2024 aluminium alloy, Electrochimica acta, 52 (2007) 7231-7247.

[16] C. Christodoulou, G. Glass, J. Webb, S. Austin, C. Goodier, Assessing the long term benefits of Impressed Current Cathodic Protection, Corrosion Science, 52 (2010) 2671-2679.

[17] C. Rousseau, F. Baraud, L. Leleyter, O. Gil, Cathodic protection by zinc sacrificial anodes: Impact on marine sediment metallic contamination, Journal of Hazardous Materials, 167 (2009) 953-958.

[18] G.T. Parthiban, T. Parthiban, R. Ravi, V. Saraswathy, N. Palaniswamy, V. Sivan, Cathodic protection of steel in concrete using magnesium alloy anode, Corrosion Science, 50 (2008) 3329-3335.

[19] A. Greenberg, R. Kusy, A survey of specialty coatings for orthodontic wires, J Dent Research, 58 (1979) A21.

[20] A. Roa, D. Kanttkar, A. PARAB, Some specialty coatings from radiation curable poly (acrylic) combination, Progress in Organic Coatings, 25 (1995) 221-223.

[21] E. Scrinzi, S. Rossi, The aesthetic and functional properties of enamel coatings on steel, Materials & Design, 31 (2010) 4138-4146.

[22] S. Rossi, F. Deflorian, E. Scrinzi, Comparison of different abrasion mechanisms on aesthetic properties of organic coatings, Wear, 267 (2009) 1574-1580.

[23] Z. Wicks, F. Jones, S. Pappas, D. Wicks, Organic coatings: science and technology, Wiley-Interscience, 2007.

[24] G.P. Bierwagen, Reflections on corrosion control by organic coatings, Progress in Organic Coatings, 28 (1996) 43-48.

[25] M. Bethencourt, F.J. Botana, M.J. Cano, R.M. Osuna, M. Marcos, Lifetime prediction of waterborne acrylic paints with the AC-DC-AC method, Progress in Organic Coatings, 49 (2004) 275-281.

[26] R. Twite, G. Bierwagen, Review of alternatives to chromate for corrosion protection of aluminum aerospace alloys, Progress in Organic Coatings, 33 (1998) 91-100.

[27] G. Mu, X. Li, Q. Qu, J. Zhou, Molybdate and tungstate as corrosion inhibitors for cold rolling steel in hydrochloric acid solution, Corrosion Science, 48 (2006) 445-459.

[28] F.M. Donahue, K. Nobe, Theory of organic corrosion inhibitors, Journal of the electrochemical Society, 112 (1965) 886.

[29] A. Braig, Organic Corrosion Inhibitors for Coatings, in: Proceedings of the Symposium on Advances in Corrosion Protection by Organic Coatings, The Electrochemical Society, 1998, pp. 18.

[30] L. Reynolds, R. Twite, M. Khobaib, M. Donley, G. Bierwagen, Preliminary evaluation of the anticorrosive properties of aircraft coatings by electrochemical methods, Progress in Organic Coatings, 32 (1997) 31-34.

[31] C.A. Mann, B.E. Lauer, C.T. Hultin, Organic Inhibitors of Corrosion Aromatic Amines, Industrial & Engineering Chemistry, 28 (1936) 1048-1051.

[32] J.N. Breston, Corrosion Control with Organic Inhibitors, Industrial & Engineering Chemistry, 44 (1952) 1755-1761.

[33] D. Battocchi, A.M. Simões, D.E. Tallman, G.P. Bierwagen, Electrochemical behaviour of a Mg-rich primer in the protection of Al alloys, Corrosion Science, 48 (2006) 1292-1306.

[34] D. Battocchi, A.M. Simões, D.E. Tallman, G.P. Bierwagen, Comparison of testing solutions on the protection of Al-alloys using a Mg-rich primer, Corrosion Science, 48 (2006) 2226-2240.

[35] R.A. Armas, C.A. Gervasi, A.D. Sarli, S.G. Real, J.R. Vilche, Zinc-Rich Paints on Steels in Artificial Seawater by Electrochemical Impedance Spectroscopy, CORROSION, 48 (1992) 379-383.

[36] C.A. Gervasi, A.R. Di Sarli, E. Cavalcanti, O. Ferraz, E.C. Bucharsky, S.G. Real, J.R. Vilche, The corrosion protection of steel in sea water using zinc-rich alkyd paints. An assessment of the pigment-content effect by EIS, Corrosion Science, 36 (1994) 1963-1972.

[37] O.Ø. Knudsen, U. Steinsmo, M. Bjordal, Zinc-rich primers--Test performance and electrochemical properties, Progress in Organic Coatings, 54 (2005) 224-229.

[38] G. Bierwagen, D. Tallman, J. Li, L. He, C. Jeffcoate, EIS studies of coated metals in accelerated exposure, Progress in Organic Coatings, 46 (2003) 149-158.

[39] C.G. Oliveira, M.G.S. Ferreira, Ranking high-quality paint systems using EIS. Part I: intact coatings, Corrosion Science, 45 (2003) 123-138.

[40] G. Davis, L. Krebs, C. Dacres, Coating evaluation and validation of accelerated test conditions using an in-situ corrosion sensor, Journal of Coatings Technology, 74 (2002) 69-74.

[41] N. LeBozec, N. Blandin, D. Thierry, Accelerated corrosion tests in the automotive industry: a comparison of the performance towards cosmetic corrosion, Materials and Corrosion, 59 (2008) 889–894.

[42] G. Bierwagen, C. Jeffcoate, J. Li, S. Balbyshev, D. Tallman, D. Mills, The use of electrochemical noise methods (ENM) to study thick, high impedance coatings, Progress in Organic Coatings, 29 (1996) 21-29.

[43] B.S. Skerry, D.A. Eden, Characterisation of coatings performance using electrochemical noise analysis, Progress in Organic Coatings, 19 (1991) 379-396.

[44] G.P. Bierwagen, Calculation of noise resistance from simultaneous electrochemical voltage and current noise data, Journal of The Electrochemical Society, 141 (1994) L155.

[45] D.A. Eden, M. Hoffman, B.S. Skerry, Application of Electrochemical Noise Measurements to Coated Systems, in: Polymeric Materials for Corrosion Control, American Chemical Society, 1986, pp. 36-47.

[46] F. Mansfeld, L.T. Han, C.C. Lee, G. Zhang, Evaluation of corrosion protection by polymer coatings using electrochemical impedance spectroscopy and noise analysis, Electrochimica Acta, 43 (1998) 2933-2945.

[47] D. Mills, S. Mabbutt, G. Bierwagen, Investigation into mechanism of protection of pigmented alkyd coatings using electrochemical and other methods, Progress in Organic Coatings, 46 (2003) 176-181.

[48] K.N. Allahar, V. Upadhyay, G.P. Bierwagen, V.J. Gelling, Monitoring of a military vehicle coating under Prohesion exposure by embedded sensors, Progress in Organic Coatings, 65 (2009) 142-151.

[49] G. Gusmano, S. Pacetti, A. DAmico, A. Petitti, G. Montesperelli, Electrochemical noise resistance as a tool for corrosion rate prediction, CORROSION, 53 (1997).

[50] C. Jeyaprabha, S. Muralidharan, G. Venkatachari, M. Raghavan, Applications of Electrochemical Noise Measurements In Corrosion Studies: A Review, Corrosion Reviews, 19 (2001) 301-314.

[51] S. Mabbutt, D.J. Mills, C.P. Woodcock, Developments of the electrochemical noise method (ENM) for more practical assessment of anti-corrosion coatings, Progress in Organic Coatings, 59 (2007) 192-196.

[52] Q. Su, K. Allahar, G. Bierwagen, Embedded electrode electrochemical noise monitoring of the corrosion beneath organic coatings induced by ac-dc-ac conditions, Electrochimica Acta, 53 (2008) 2825-2830.

[53] G. Bierwagen, X. Wang, D. Tallman, In situ study of coatings using embedded electrodes for ENM measurements, Progress in Organic Coatings, 46 (2003) 163-175.

[54] R.A. Cottis, Interpretation of Electrochemical Noise Data, Corrosion, 57 (2001) 265.

[55] R.A. Cottis, Interpretation of Electrochemical Noise Data, CORROSION, 57 (2001) 265-285.

[56] U. Bertocci, F. Huet, Noise Analysis Applied to Electrochemical Systems, Corrosion, 51 (1995) 131.

[57] J.M. Sanchez-Amaya, R.A. Cottis, F.J. Botana, Shot noise and statistical parameters for the estimation of corrosion mechanisms, Corrosion Science, 47 (2005) 3280-3299.

[58] H.A.A. Al-Mazeedi, R.A. Cottis, A practical evaluation of electrochemical noise parameters as indicators of corrosion type, Electrochimica Acta, 49 (2004) 2787-2793.

[59] A. Aballe, A. Bautista, U. Bertocci, F. Huet, Measurement of the noise resistance for corrosion applications, CORROSION, 57 (2001).

[60] D. Eden, Electrochemical Noise-The First Two Octaves, in, CORROSION, 1999.

[61] J. Li, C. Jeffcoate, G. Bierwagen, D. Mills, D. Tallman, Thermal Transition Effects and Electrochemical Properties in Organic Coatings: Part 1 Initial Studies on Corrosion Protective Organic Coatings, CORROSION, 54 (1998).

[62] B.S. Skerry, D.A. Eden, Electrochemical testing to assess corrosion protective coatings, Progress in organic Coatings, 15 (1987) 269.

[63] G.P. Bierwagen, S. Balbyshev, D.J. Mills, D.E. Tallman, Proceedings of the Symposium on advances in Corrosion Protection by Organic Coatings II, 95-13 (1995) 82.

[64] D.A. Eden, US Patent, No 0149594 A1 (2002).

[65] U. Bertocci, J. Frydman, C. Gabrielli, F. Huet, M. Keddam, Analysis of electrochemical noise by power spectral density applied to corrosion studies, Journal of The Electrochemical Society, 145 (1998) 2780.

[66] T. Schauer, H. Greisiger, L. Dulog, Details on MEM analysis of electrochemical noise data and correlation with impedance measurements for organic coatings on metals, Electrochimica Acta, 43 (1998) 2423-2433.

[67] H. Greisiger, T. Schauer, On the interpretation of the electrochemical noise data for coatings, Progress in Organic Coatings, 39 (2000) 31-36.

[68] F. Mansfeld, L. Han, C. Lee, C. Chen, G. Zhang, H. Xiao, Analysis of electrochemical impedance and noise data for polymer coated metals, Corrosion Science, 39 (1997) 255-279.

[69] F. Mansfeld, L. Han, C. Lee, Analysis of electrochemical noise data for polymer coated steel in the time and frequency domains, Journal of The Electrochemical Society, 143 (1996) L286.

[70] F. Mansfeld, Electrochemical impedance spectroscopy (EIS) as a new tool for investigating methods of corrosion protection, Electrochimica Acta, 35 (1990) 1533-1544.

[71] F. Mansfeld, Use of electrochemical impedance spectroscopy for the study of corrosion protection by polymer coatings, Journal of Applied Electrochemistry, 25 (1995) 187-202.

[72] J. Li, C.S. Jeffcoate, G.P. Bierwagen, D.J. Mills, D.E. Tallman, Thermal Transition Effects and Electrochemical Properties in Organic Coatings: Part 1 --- Initial Studies on Corrosion Protective Organic Coatings, CORROSION, 54 (1998) 763-771.

[73] H. Leidheiser, Electrical and electrochemical measurements as predictors of corrosion at the metal--organic coating interface, Progress in Organic Coatings, 7 (1979) 79-104.

[74] J.N. Murray, Electrochemical test methods for evaluating organic coatings on metals: an update. Part I. Introduction and generalities regarding electrochemical testing of organic coatings, Progress in Organic Coatings, 30 (1997) 225-233.

[75] J.R. Scully, D.C. Silverman, M.W. Kendig, Electrochemical impedance: analysis and interpretation, ASTM International, 1993.

[76] E. Van Westing, G. Ferrari, F. Geenen, J. De Wit, In situ determination of the loss of adhesion of barrier epoxy coatings using electrochemical impedance spectroscopy, Progress in Organic Coatings, 23 (1993) 89-103.

[77] A.K. Manohar, O. Bretschger, K.H. Nealson, F. Mansfeld, The use of electrochemical impedance spectroscopy (EIS) in the evaluation of the electrochemical properties of a microbial fuel cell, Bioelectrochemistry, 72 (2008) 149-154.

[78] J. Vogelsang, W. Strunz, New interpretation of electrochemical data obtained from organic barrier coatings, Electrochimica Acta, 46 (2001) 3817-3826.

[79] J.N. Murray, Electrochemical test methods for evaluating organic coatings on metals: an update. Part III: Multiple test parameter measurements, Progress in Organic Coatings, 31 (1997) 375-391.

[80] E. Barsoukov, J.R. Macdonald, Impedance spectroscopy: theory, experiment, and applications, Wiley-Interscience, 2005.

[81] F. Mansfeld, Models for the impedance behavior of protective coatings and cases of localized corrosion, Electrochimica Acta, 38 (1993) 1891-1897.

[82] M.T. Rodríguez, J.J. Gracenea, S.J. García, J.J. Saura, J.J. Suay, Testing the influence of the plasticizers addition on the anticorrosive properties of an epoxy primer by means of electrochemical techniques, Progress in Organic Coatings, 50 (2004) 123-131.

[83] P.P. D. Loveday, B. Rodgers, Evaluation of Organic Coatings with Electrochemical Impedance Spectroscopy. Part 2: Application of EIS to Coatings, JCT Coatings Tech, (2004) 88-93.

[84] F. Bellucci, L. Nicodemo, Water transport in organic coatings, CORROSION, 49 (1993).

[85] J. Crank, The mathematics of diffusion, Oxford University Press, New York, 1989.

[86] D. Brasher, A. Kingsbury, Electrical measurements in the study of immersed paint coatings on metal. I. Comparison between capacitance and gravimetric methods of estimating water uptake, Journal of Applied Chemistry, 4 (1954) 62-72.

[87] F. Deflorian, L. Fedrizzi, S. Rossi, P.L. Bonora, Organic coating capacitance measurement by EIS: ideal and actual trends, Electrochimica Acta, 44 (1999) 4243-4249.

[88] S. Lindqvist, Theory of dielectric properties of heterogeneous substances applied to water in a paint film, CORROSION, 41 (1985) 69-75.

[89] D. Bogdal, A. Prociak, Microwave-enhanced polymer chemistry and technology, John Wiley and Sons, 2007.

[90] J.A. Brydson, Plastics materials, Butterworth-Heinemann, 1999.

CHAPTER 2. GOAL OF THIS DISSERTATION, LITERATURE REVIEW OF ACCELERATED COATING CHARACTERIZATION AND SENSORS FOR SUBSTRATE AND COATING MONITORING

2.1. Goal of the Dissertation

The use of advanced electrochemical techniques such as electrochemical impedance spectroscopy (EIS), electrochemical noise method (ENM) and coulometry to extract information about the coating system is the focus of this Dissertation research. Three areas of research were explored. Firstly, this dissertation examined whether AC-DC-AC technique can discriminate two different coating systems and whether the total charge passing through the coating during the DC step of the AC-DC-AC test determines when a coating fails. Secondly, the use of embedded sensors in coatings in detecting variations in environmental changes via electrochemical techniques has been explored. Research in the use of embedded sensors to locate defects in coatings is also scarce. An attempt has also been made to study if embedded sensors in coatings can track defects in coatings by electrochemical means. Influence of topcoat on embedded sensors has also been studied.

Thirdly, in a novel attempt, this dissertation also examined systematically the influence of polymer structure and composition variations on the electrochemical properties of unpigmented coating films as measured by EIS. Novel thermosetting glycidyl carbamate (GC) functional polymers were designed with structure (branching) as well as composition (monomer and concentration) variations. The designed polymers were mixed with amine and coated on steel substrate and cured. EIS measurements were performed on the coating films and the influence of polymer structural and compositional variation on the EIS response was investigated. The effect of such changes on the absorption and desorption

behavior of water was also investigated. A new method to rank the stability of organic coating has also been proposed.

2.2. Accelerated methods of coating evaluation

The prolonged use of outdoor metallic structures is made possible by the application of organic coatings that act as a barrier between the substrate and the environment. They prevent the interaction of corrosive ions and electrolytes from the environment with the substrate whose protection is desired. Organic coatings are also used to store corrosion inhibitors and other pigments for a number of functional requirements but its barrier protection remains the primary means for which coatings are employed. Metallic coatings and cathodic or anodic protections are also used in conjunction with the robust barrier protection provided by organic coatings in preventing water and ionic species transporting from the environment to the metal surface.[1, 2]

Coatings are designed to last as long as possible during service use. Prior to application they are evaluated for their ability to function for the intended purpose. The best approach to evaluate them is to expose them to natural conditions where they are intended to be used. This approach is however impractical since it may require months or even years under natural outdoor exposure condition for a coating to fail. Conventional methods for the performance evaluation of organic coatings are designed to test the barrier protection under controlled simulated and accelerated conditions and include methods such as salt-fog (ASTM B117), Prohesion (ASTM G85 annex A5), and the Prohesion®/QUV® (ASTM D 5894) methods. These methods attempt to simulate worst-case weathering conditions in the laboratory such that coating failure is promoted in shorter time as compared to actual service lifetime.[3] The inherent assumption associated with these

accelerated test methods is that the failure mechanisms promoted by the testing conditions are consistent with that of natural weathering conditions. A brief discussion of these test methods are given below.

2.2.1. ASTM B117 salt spray test

In this test method samples, metals or coated metals, are continuously exposed to a controlled corrosive atmosphere consisting of a fog of 5% NaCl at 35°C to study the corrosion resistance information of the specimen. Ranking are based on visual inspection of coatings. Coated panels are routinely taken out of the exposure to evaluate corrosion protection performance. This method is widely used. However this method has also been under criticism due to its lack of resemblance with the natural exposure.[1, 4]

2.2.2. ASTM G-85 Prohesion test (Annex A5)

This test method also known as the Prohesion test consists of a cyclic wet and dry step. The wet step consists of exposing the samples in a fog of dilute Harrison's solution consisting of 0.35 wt. % $(NH_4)_2SO_4$ and 0.05 wt. % NaCl at 25°C for 1 hour whereas the dry step consists of drying the sample in air for 1 hour at 35°C.

2.2.3. ASTM D5894 Prohesion/QUV test

In this test method the Prohesion test method is coupled with a QUV accelerated test method in order to study the influence of the sunlight or UV radiation on the coating in addition to the Prohesion wet-dry conditions. QUV test method consists of exposing the coated panel to alternating cycles of 4 hours of UV light at 60°C followed by 4 hours of water condensation at 50°C. In the Prohesion/QUV test the coated sample is alternately placed in a Prohesion chamber for 1 week followed by QUV chamber for another week and

so on. Periodical visual inspection is performed to evaluate the corrosion protection performance of the coating.

The test methods mentioned above are purely qualitative and rely on visual inspection for ranking the corrosion protective performance of the coating. Moreover coatings that are robust might require months or even years to fail under these conditions as was observed for a standard Aircraft polyurethane topcoat/chromate epoxy primer system on AA 2024-T3 which showed little change in barrier property during 2 years of exposure to Prohesion®/QUV® conditions.[5] More recent approaches to expedited coating testing are the thermal cycling method and the AC-DC-AC test methods.

2.2.4. Thermal cycling method

Another approach of ranking and differentiating coating systems is the thermal cycling method where the coating is subjected to a temperature change in a cyclic manner in an immersed condition. The coating is subjected to water as well as temperature cycling. Post cycling treatment electrochemical techniques, such as EIS and ENM, are used to study the state of the coating. Electrochemical techniques such as electrochemical noise methods and electrochemical impedance spectroscopy have been described in detail in section 1.6 and 1.7 respectively. The increase in temperature is intended to reduce the barrier property of the coating film by facilitating increased rate of electrolyte diffusion into the film and expediting coating failure due to physical and chemical ageing resulting from thermal fatigue effect and di-electric variation due to more open polymer structure.[6, 7] With every cycle the damage that accumulates in the film increases, thus, enhancing film deterioration. Figure 2.1 is a schematic of the thermal cycle test method performed by Bierwagen et al.,[7] to study the effect of thermal cycling in different pretreatments and

coating systems on their corrosion resistance properties. It was observed that for some samples the |Z| value at low frequency failed to merge at room temperature during subsequent runs indicating that an irreversible permanent damage of the sample was induced by the thermal cycling. The thermal cycling method took just one week to rank coating that would normally take 8-12 weeks in Prohesion exposure indicating that thermal cycling method is an accelerated method and has potential to examine the performance of coated system in quick time.

RT (23°C)	--Heating-->	35°C/EIS	--Heating-->	55°C/EIS	--Heating-->
75°C/EIS	--Heating-->	85°C/EIS	--Cooling-->	75°C/EIS	--Cooling-->
55°C/EIS	--Cooling-->	35°C/EIS	--Cooling-->	RT (23°C)	
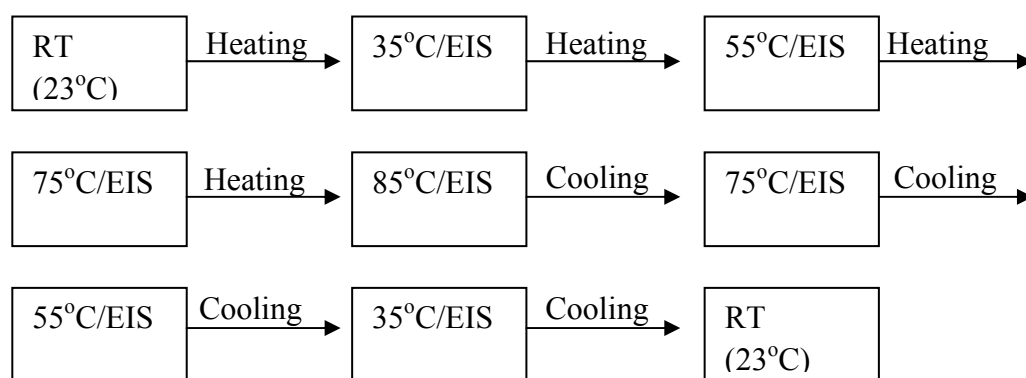
Figure 2.1: Schematic of thermal cycle test method. [Taken from Bierwagen et al., *Progress in Organic Coatings* 2000, *39* (1), 67-78].

Li, et al.,[8] have written an extensive analysis of thermal (and aqueous) effects on electrochemical properties of organic coatings that reviewed the literature through 1997 and extensively surveyed the effects of water and temperature especially on epoxy-based corrosion protective coatings. They observed that the use of coating at temperature above the glass transition temperature (T_g) results in much reduced barrier performance of the coating film. Fedrizzi et al., also have verified the use of a thermal ageing method in quickly ranking the behavior of the coated system and obtaining precise information concerning their barrier and adhesion behavior.[6] Moreover it has also been observed that the irreversible changes induced by thermal conditions have similar degradation mechanisms as compared to natural atmospheric conditions.[7, 9, 10] Sensors embedded in

coatings have also been used to study the performance of coating subjected to thermal treatment. Further studies on the water and thermal effects on coatings have also been reported.[11-16]
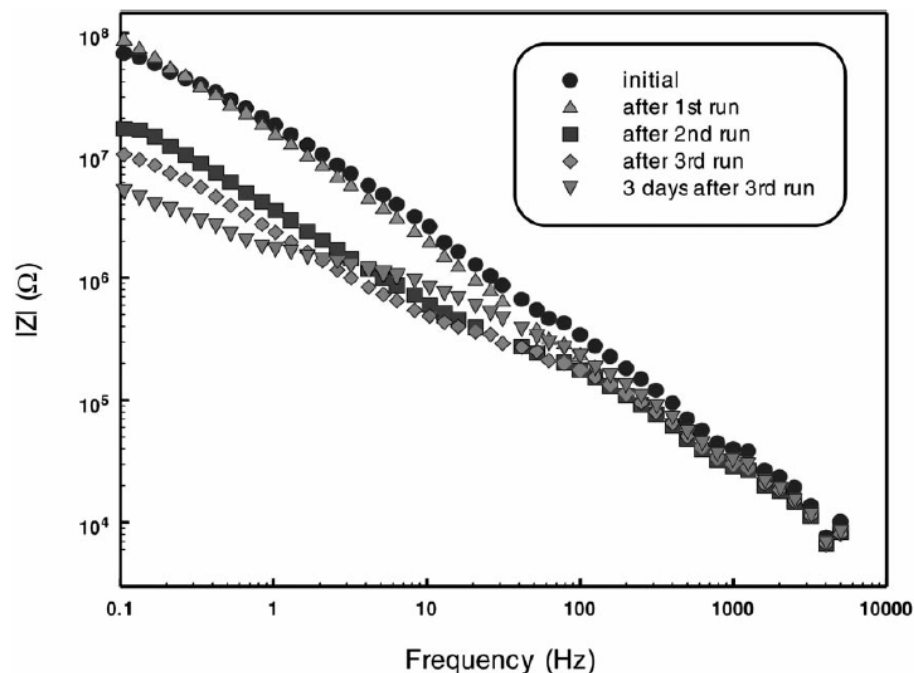
Figure 2.2: Impedance modulus |Z| at room temperature as a function of frequency: irreversible behavior after thermal cycle runs where one cycle consisted of three runs. [Taken from Bierwagen et al., *Progress in Organic Coatings* 2000, *39* (1), 67-78].

2.2.5. AC-DC-AC accelerated test methods

The AC-DC-AC method is another unconventional accelerated method that promotes the degradation of coatings through the application of a direct current (DC).[17] This method is the fusion of an AC multi frequency EIS technique with the DC technique that is used to expedite coating failure as shown in Figure 2.3. The fist AC of the AC-DC-AC method measures the existing state of an immersed coated system. This is followed by a DC step that is intended to expedite electron flow at the working electrode/substrate and induce coating failure via enhanced reduction reaction at the metal coating interface by producing hydroxyl ions and hydrogen gas and resulting in coating degradation and

delamination. In addition the negatively charged substrate attracts the positively charged ions from the electrolyte and results in coating deterioration and pore formation.[18, 19] Post DC, the system is allowed to relax to its new open circuit potential and subsequently an AC multi frequency EIS measurement is performed again to study the new state of the coating system. AC-DC-AC measurement can be performed in cycles until the coating fails and is an accelerated test method that has been used to induce coating failure, to rank the coating barrier and protective properties and to predict their lifetime.[18-21]
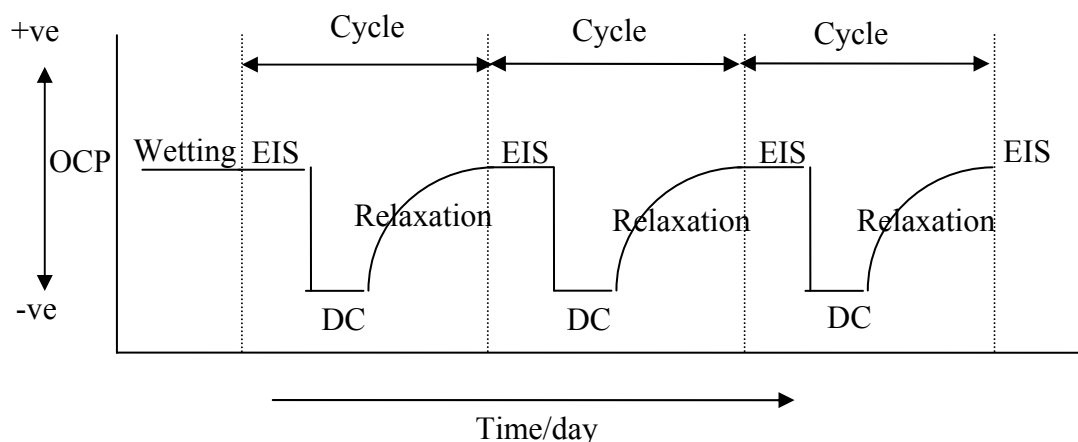
Figure 2.3: Schematic of AC-DC-AC method.

A complete cycle of an AC-DC-AC procedure may vary depending upon the parameters used. Two important parameters that can be varied to expedite the coating failure are the length of the DC polarization and the magnitude of DC polarization. Su et al.,[22] however observed that the extent of cathodic potential was more significant in expediting coating failure. But depending upon the coating system, the length and magnitude of polarization may be varied. For instance Bethencourt et al., [20] used -2V for 20 minutes to degrade waterborne acrylic paints in his study on the qualitative lifetime prediction using the AC-DC-AC method. Garcia et al.,[23] have used AC-DC-AC method

to rank commercial anticorrosive epoxy coating system. At the DC step they used -4V for 20 minutes to induce coating failure followed by 3 hours of relaxation. Rodríguez et al.,[18] applied -2V for 10 min to induce coating failure with 3 hours relaxation on an epoxy resin based on bisphenol. Bierwagen and Allahar et al.,[24, 25] have varied the DC potential from -1V to -8V and the time of polarization from 0.5 hours to 8 hours while working with army and air force primers.

AC-AC-AC technique has also been used jointly with single frequency EIS measurement techniques in order to study the influence of DC on the water uptake and diffusion behavior of the coating system. Coating properties such as water diffusion coefficient and capacitance provides a useful measure of coating degradation and transport process.[24] Allahar et al.,[24] have jointly used AC-DC-AC with the single frequency EIS measurement technique to understand the effect of DC on the capacitance and diffusion coefficient behavior of an Army primer MIL-P-53022B Type II on steel substrate. They observed for all but one AC-DC-AC cycles that the water uptake behavior followed Fick's second law and the uptake behavior was not much affected by the DC cycles. However a relatively increased diffusion coefficient was observed when the coating was compared with a control sample indicating the influence of DC on the rate of water diffusion through the coating.

Other useful information obtained from the AC-DC-AC method is from the relaxation behavior after the DC step. After the application of DC the coating system is allowed to relax to its new open circuit potential. Depending upon the nature of the coating the relaxation potential profile changes and displays a unique signature characteristic of the state of the coating. Qualitative interpretation of the relaxation profile have been reported

by Rodriguez et al.,[18] Two important processes are expected to be caused by the DC polarization step.
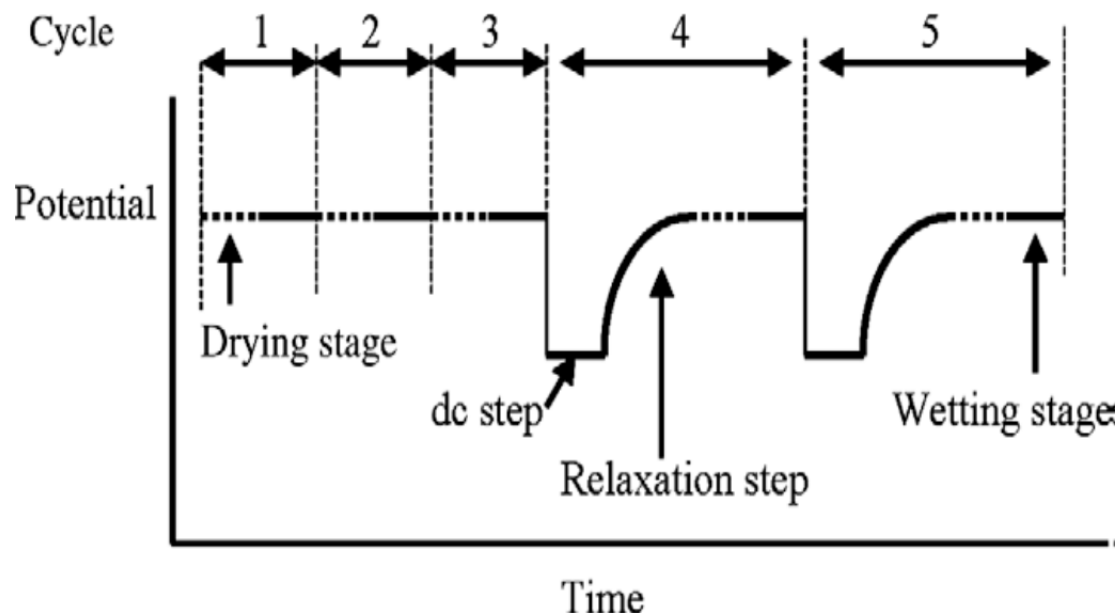
Figure 2.4: Modified AC-DC-AC method used to obtain water uptake behavior of coating. [Allahar et al., *Corrosion Science* 2010, 52, 1106].

1) The transport of ions such as H^+ and Na^+ through the coating due to the applied negative potential to the metal substrate. Such forced ion transport can cause coating deterioration and pore formation.

2) Cathodic reaction on the substrate surface.

$$2H_2O \ (l) + 2e^- \rightarrow H_2 \ (g) + 2OH^- \qquad (2.1)$$

This reaction will be favored if the electrolyte can penetrate the coating film and will depend upon the film properties such as adhesion, ion permeability, local defects, and the applied potential. Cathodic reaction at the interface will result in coating delamination and blister formation as a result of hydrogen gas formation and the alkaline nature of the interface.[26-30]

44

The relaxation potential profile after DC application, depending upon the affect of DC on the coating, displays behavior that can identify an intact coating from a deteriorated one. As the DC is withdrawn, the potential relaxation can occur via two different mechanisms.

1)   Had a cathodic reaction occured at the interface during DC step, the potential would have had a first rapid relaxation corresponding to the stop of the cathodic reaction   and a second relaxation corresponding to the exit of ions and electrolytes from the coating. The time required for the system to reach its new open circuit potential would be high since the ions will have to pass through the coating thickness.

2)   If no cathodic reaction occured at the interface, then a relaxation process corresponding to the exit of ions and electrolytes from the coating would be observed. Deeper penetration of ions and electrolytes would require longer time to relax. However this time would be shorter than the time taken by the ions and electrolyte had they reached the interface. Figure 1.3 is a relaxation potential profile post DC of an epoxy coating subjected to AC-DC-AC test. It can be observed that two relaxation processes exists, a fast one corresponding to the stop of the cathodic reaction and a second one that corresponds to the exit of ions and electrolytes from the coating.

Quantitative interpretation of the relaxation process has also been attempted. Vogelsang et al.,[31] interpreted the potential relaxation behavior of coating with three physicochemical processes, the dielectric relaxation, diffusion and charge transfer. Allahar et al.,[32] subjected an army primer to various AC-DC-AC cycles and modeled the relaxation potential profile post DC using three different equations consisting of one time

constant, two time constants and three time constants respectively and observed that the

model fitted well with the equation with three time constants, the equation being

$$E = A_1 \exp(t_1/t) + A_2 \exp(t_2/t) + A_3 \exp(t_3/t) + y \tag{2.2}$$
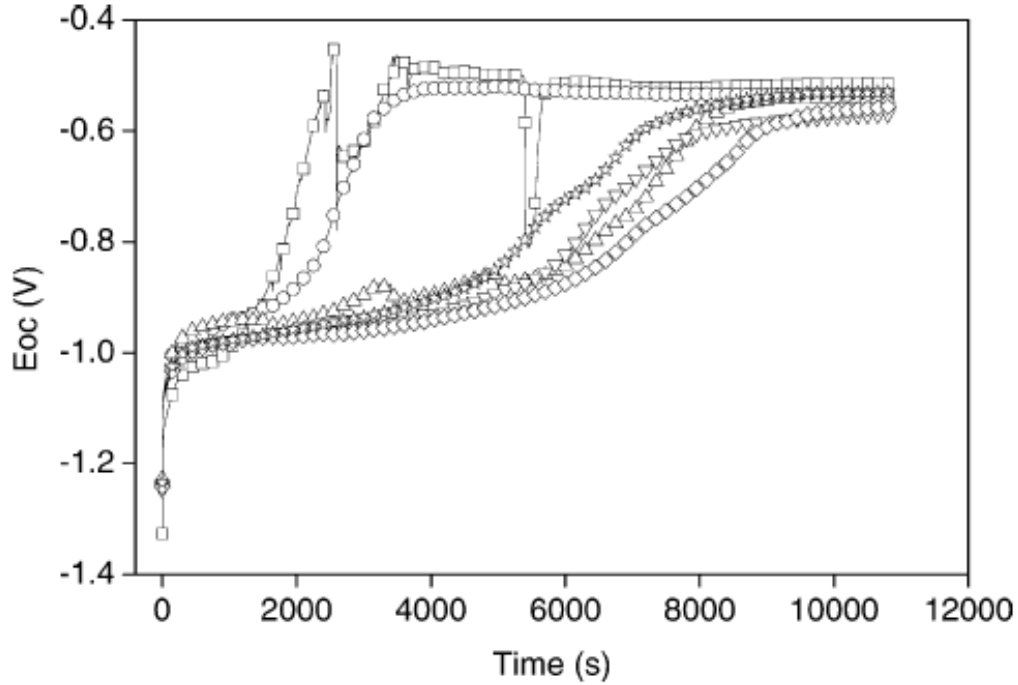
Figure 2.5: Relaxation profile post DC for one cycle (□), two cycles (o), three cycles (Δ), four cycles (∇), five cycles (◊) and six cycles (☆) during AC-DC-AC test.[Rodríguez et al., *Progress in Organic Coatings* 2004, 50 (2), 129].

where t_1, t_2, and t_3 are the characteristic times, A_1, A_2, and A_3 are the pre-exponential

factors and y is a constant. Three time constant were also suggested by Vogelsang et al.[31]

It was observed that t1> t2> t3 and were assumed to be associated with charge transfer at

the metal coating interface, coating dielectric relaxation, and transport of ions through the

coating, respectively. The process identified with charge transfer displayed the fastest

decay independent of the number of cycles whereas the influence of repeated cycles was

observed for coating dielectric and transport properties.[24]
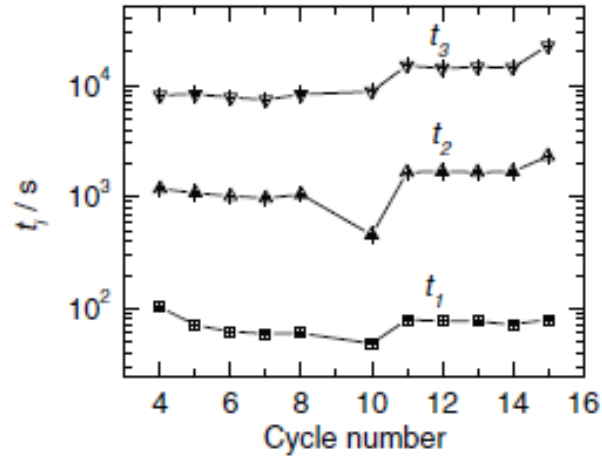
Figure 2.6: Characteristic time parameter values as a function of cycle number. [Allahar et al., *Corrosion Science* 2010, 52 (4), 1106-1114].

2.3. Sensors for structural health monitoring

To ensure enhanced corrosion protection of structures it is essential to identify when the structure starts to deteriorate so that timely repair can be performed. Structures such as pipelines running through remote location are as susceptible to fail compared to structures in accessible areas. Locating defect /corrosion at the application site is tedious and might be time consuming since it requires travel to the site for inspection. Sometimes the detection of defect might be too late for any further protective action to be implemented and might necessitate installing new structure instead of repair. Moreover the lifetime prediction of structures based on their evaluation at the laboratory simulated conditions might not be accurate and the structure may fail early. The use of sensors to monitor corrosion might therefore be a prudent approach to facilitate timely detection of defect and to avoid any catastrophic damage. Sensors also provide a unique and convenient feature and facilitate remote *in-situ* measurements. Sensor technologies have been used to monitor structures such as such as bridges, pipelines, and storage tanks.[33, 34] [35] Sensing techniques are used to monitor bare metal structure as well as coated systems.

2.3.1. Sensors for metal corrosion detection

2.3.1.1. Optical fiber corrosion sensor

An optical fiber corrosion sensor (OFCS) is based on the concept of changes in the optical properties of light due to the formation of corrosion product, detection of chemicals and pH changes associated with corrosion as well as changes in strain of the corroding sample.[36, 37] OFCS system consists of a light source, a sensing element, optical fiber for transmitting light and a detector. Some of the emerging applications of OFCS include detection of pH and moisture in aircraft lap joints, monitoring health of the bridges and rebar corrosion .[37, 38]

Optical fiber has many advantages in corrosion sensing studies due to their flexibility, light weight, and small size. The fiber allows signals to be transmitted over long distances without significant loss, allowing remote monitoring of corrosion. Optical fiber also resists adverse environments and is a great advantage as it is constantly exposed to such environment during usage. Moreover, optical fiber is also immune to electromagnetic interference, therefore radio waves and power transmission lines do not have any effect on the signals inside the fiber. OFCS, therefore are ideally suited for use on large structures such as transmission towers, offshore drilling platforms, bridges, etc. OFCS have been widely used both in research and application to corrosion sensing.[36, 38-44]

A typical corrosion sensing technique using optical fiber is the corrosion fuse technique. In this technique the fiber is bent into a loop and is held by a thin metallic wire. The wire also known as "corrosion fuse" is a corrodible material. As light passes through the fiber a decrease in the intensity of light is observed due to light refraction as a result of the bend. The corrosion fuse is exposed to the environment where it corrodes and breaks.

48

This results in a relaxation of the fiber from the bend position to straight position as a result of which the intensity of light is increased. The amount of corrosion required for the fuse to break will be equivalent to specific amount of corrosion in the structure that is monitored. The corrosion rate of the sensor is correlated to the corrosion rate of the material under investigation.[39]
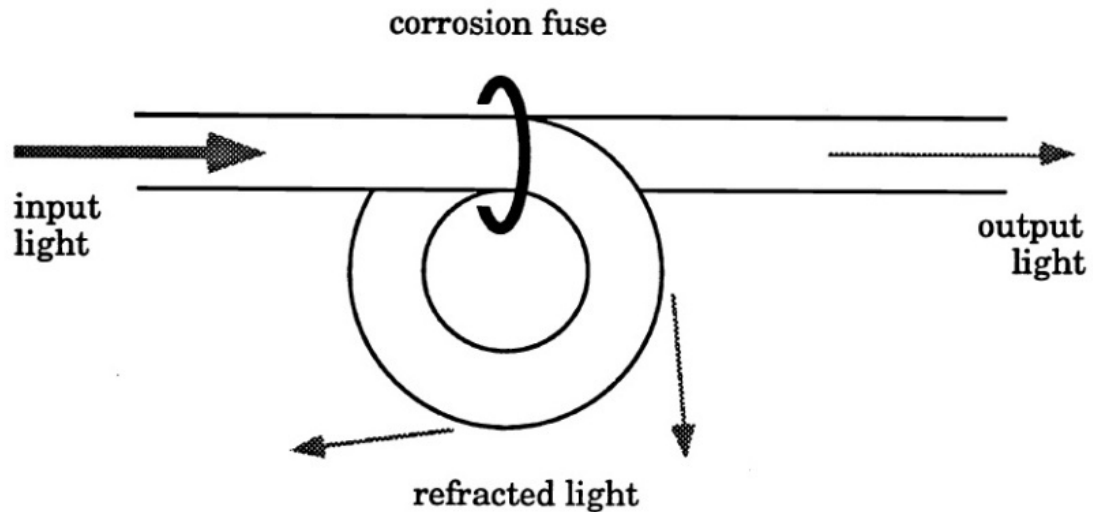
Figure 2.7: A Fiber optic corrosion sensor. When corrosion attacks the sensor and the fuse breaks, the fiber straightens, increasing the light at the output. [Bennett et al., *SPIE* 1995, p 48].

OFCS has been used to monitor the corrosion behavior of various metals and alloys such as steel[39], aluminum[45, 46], aluminum alloys[47], copper[48] and nickel.[49] OFCS can detect corrosion under different aggressive environmental conditions. The kinetics and the corrosion mechanism could also be deduced using optical signal. OFCS can also detect humidity in structures and discriminate different metallic corrosion rate.[40, 48, 50]

2.3.1.2. Wireless corrosion sensors

Wireless sensor corrosion monitoring techniques obviate the need for long wires tethered to the sensor and thus reduces the system complexity and labor cost. The sensing

mode can be passive or active. Passive wireless sensors measure structural responses due to static and dynamic loading. Examples include the radio frequency identification sensors that can capture signal from a remote reader and communicate its measurement back. Active sensors can interact or excite a structure at will. An active sensor such as piezoelectric pad is ideally suited for localized structural health monitoring (SHM).[51, 52] Wireless sensors have been widely used for health monitoring of structures such as reinforced concrete and bridges.[53, 54] The Golden Gate bridge at the entrance to the San Francisco bay has been one of the favorite test site for researchers studying sensors for SHM and houses the largest wireless sensor network ever installed for the purpose of SHM.[55] Tests have also been performed on other structures such as buildings, aircrafts, offshore oil platform and naval ships.[56-59]

Wireless sensors consist of three to four functional units. They are the sensing interface, computational core, wireless transceiver and, in some cases, an actuation interface. They are mostly powered by batteries. Recent innovation in this area has been the self powered wireless corrosion sensors. Qiao et al.,[60] reported a method to power wireless corrosion sensor used to monitor reinforced concrete structures by using the current generated during the corrosion process. A supercapacitor was used to store charge generated during the corrosion process for using it to power sensor system. Similar auto powering sensor for corrosion monitoring has also been reported.[61, 62] Wireless sensors based on induction-capacitor (LC) circuit to monitor corrosion via the resonant frequency signal have also been explored. The breakage, due to corrosion, of the steel wire attached to the capacitor in the LC circuit results in circuit configuration change resulting in changes in the resonant frequency of the sensor and facilitating corrosion monitoring.[63]

2.3.1.3. Galvanic corrosion sensors

A galvanic sensor consists of a galvanic set up where two dissimilar metals are in electrical and ionic contact. The more active metal acts as the anode and is corroded while the electrons released during corrosion are consumed at the other electrode (cathode). The current measured between them is the galvanic current. Galvanic sensor for corrosion monitoring is mainly based on the correlation of the output of a galvanic set up acting as sensor to that of the structure under investigation. The monitoring process is non-destructive and the onset of corrosion, corrosion rate as well as the ingress by corrosive element such as chloride ions in the structure can be predicted.[64, 65] Depending upon the environment of the structure under study certain galvanic couple sensor might be favored compared to others. For instance, for high resistance environment galvanic couples that can drive large current is favored.[65] Factors affecting current output may be cathode/anode ratio, the distance of separation between the anode and the cathode and the throwing power of the anode. Temperature has also been observed to affect the current density.[66, 67]

Multi electrode galvanic sensors have also been developed for corrosion monitoring. Macro cell multi electrode sensors consisting of a number of anodes in the form of ladder or rings has been used to monitor the ingress of chloride ions into the reinforcement and to monitor the time to corrosion.[68] Coupled multi-electrode array sensors have also been widely tested for in-situ corrosion monitoring of carbon steel, stainless steels, and nickel base alloys. Such sensors have been reported to give real time measurement of the corrosivity of the environment besides monitoring metal corrosion mechanism especially localized corrosion. Corrosion can also be measured in bulk electrolytes using galvanic sensors.[69]

51

2.3.1.4. Acoustic corrosion sensors

When a metal corrodes low level elastic waves or acoustic signals are emitted during the corrosion process. Acoustic emission (AE) sensors such as resonant piezoelectric transducer can be used to detect acoustic signals which is then filtered and amplified. The wave forms and the acoustic parameter of each signal as well as the electrochemical parameters are extracted. Parameter such as event number, amplitude, rise time, count number and duration are used for the corrosion analysis.[70, 71] Corrosion behavior of various metals and alloys such as carbon steel, stainless steel, aluminum alloys and titanium alloys have been studied using AE sensors.[71-73]
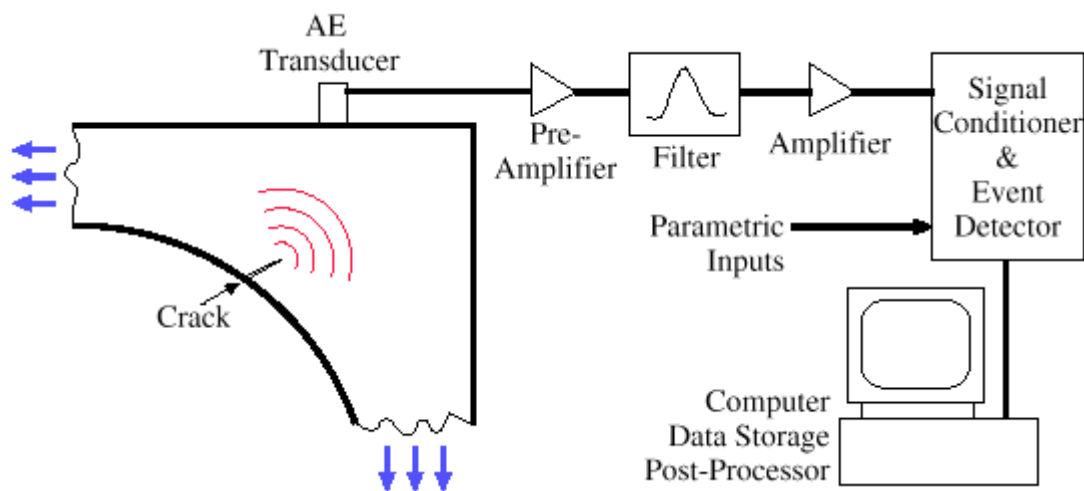
Figure 2.8: Typical Acoustic Emission system setup. [Huang et al., JOM 1998, 50,1-14].

Acoustic corrosion sensors have been widely used in research as well as in industry. It has been used in the industries for detection of leakage or faults in pressure vessels, tanks, piping system and for reinforcement corrosion.[74, 75] It has also been used to detect many types of corrosion such as uniform corrosion, crevice corrosion, pitting corrosion, erosion corrosion, intragranular corrosion, hydrogen embrittlement, stress corrosion cracking, fatigue crack and exfoliation corrosion.[71, 76-81] It is also highly

sensitive to the detection of initiation and propagation of cracks.[81, 82] It can also be used

to study low and high temperature corrosion phenomena and in the determination of active-

passive transition of metal surface.[72]
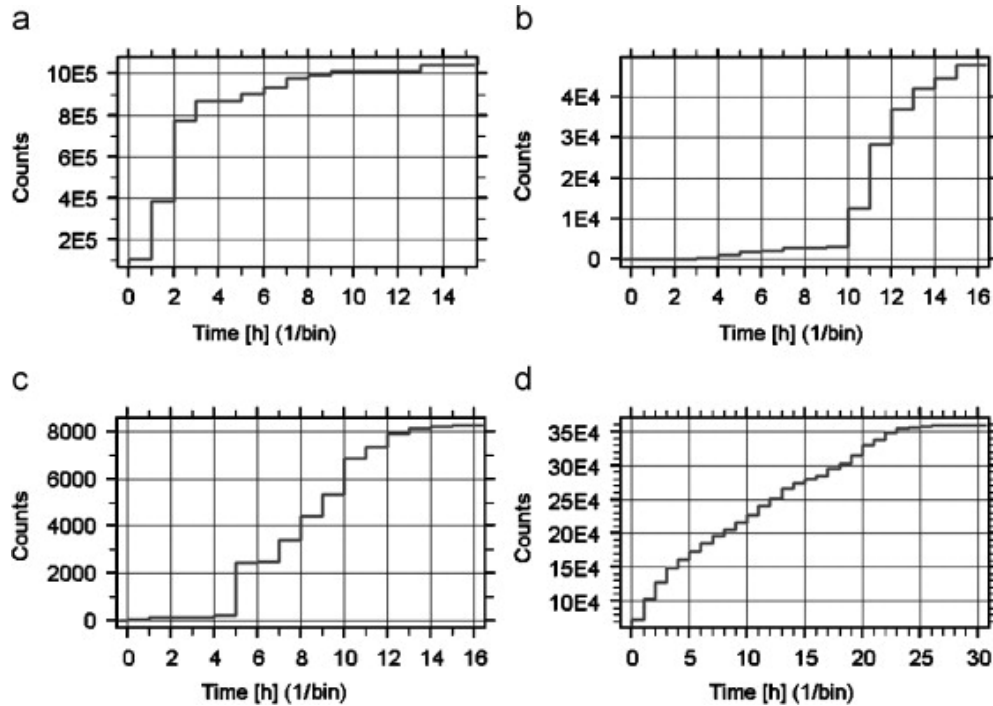
Figure 2.9: Count rates for (a) uniform, (b) pitting, (c) crevice corrosion and (d) SCC as measured from acoustic emission sensor. [Jomdecha et al., *NDT & E International* 2007, 40 (8), 584-593].

Figure 2.9 displays graph where AE discriminates various corrosion types.[76]

Various processes have been cited to be associated with acoustic emission (AE). Darowicki

et al.,[83] attributed AE to the hydrogen evolution while investigating pitting corrosion of

stainless steel. Cakir et al.,[84] attributed AE to the rupture of corrosion products deposited

on the pits and/or evolution of hydrogen gas. Magaino et al.,[85] have attributed stress

change on metal surface to be the cause of AE signal. Acoustic emission sensors are

however limited to qualitative information only.[74]

2.3.1.5. Corrosion sensing using weight loss method

In weight loss method, test specimens are exposed to similar environment of operating condition for certain amount of time and the weight loss of the specimen is calculated by the weight loss method. Corrosion rate is determined using ASTM G4-95. Measurement does not cover electrochemical technique. This method is perhaps the oldest and one of the most reliable one. The results might however be influenced by the initial sample preparation and the cleaning process of the weathered sample.

2.3.1.6. Electrical and polarization resistance corrosion sensors

Sensors using linear polarization resistance measurement techniques based on the Stern-Geary equation are widely used for measuring corrosion rate and structural lifetime. Measurement of polarization resistance using this method is well established for the corrosion rate measurement of structures such as reinforcement steels in concrete.[86-88] The corrosion rate is determined using the Stern Geary equation $I_{corr} = B/R_p$, where I_{corr} is the instantaneous corrosion current density, R_p is the polarization resistance in Ωcm^2 and B is Stern-Geary constant in volts given by $b_a.b_c/[(2.3(b_a+b_c)]$, b_a and b_c being the anodic and cathodic Tafel slopes, respectively. The corrosion rate can be expressed in various units such as mm/year and represents the volume loss of the metal with time and can be calculated using the corrosion current density and applying Faraday's law provided that the density of the metal is known. For example for a corrosion current density of 1 $\mu A/cm^2$ for steel substrate the corrosion rate or V_{corr} (mm/yr) is equal to 0.0116 I_{corr} ($\mu A/cm^2$). Some assumptions are made in using this technique for corrosion measurement. Corrosion is believed to be uniform and activation controlled for both the cathodic and anodic reactions.

A single anodic and a single cathodic reaction is assumed with negligible solution resistance.[89, 90]

The Linear Polarization Resistance sensor has been widely used for monitoring of steels in reinforced concrete structures.[86, 91, 92] A small polarization perturbation, usually an overpotential of 10-30 mV, is applied to the steel reinforcing bar and the resulting current response is measured to obtain polarization resistance, $R_p = \Delta V / \Delta I$. However, a few modifications are done in this technique so as to confine the polarized current within a certain area of the steel rebar so that accurate corrosion rate can be measured. A Potentiostatic guard ring electrodes are used to maintain a confinement current and to prevent the applied perturbation current from spreading a known area. It has been observed that the temperature and the atmospheric conditions also influence the corrosion rate. It has also been stated that the Stern Geary equation can be used in limited corrosion cases only and the constant B that is typically between 25-52mV in most cases is not acceptable for measurements, especially on passivated systems that has a diffusion controlled cathodic process.[93]

Polarization resistance sensors have also been designed by modifying the 'time of wetness sensor". This sensor consists of a stack of tiny metal plates separated by insulators. As the surface of the plates becomes wet, a small voltage is applied to the plates resulting in current flowing between them, the current being proportional to the corrosion rate of the metal plates acting as anodes. The instantaneous corrosion rate can be obtained from this current using the linear polarization resistance method.[94, 95] However a true corrosion rate measurement requires the use of a conversion factor.

Another type of electrical corrosion sensor measures in a relatively simple manner and obviates the need to remove coupons from service. It is based on the concept that the resistance of the sensor coupon is a function of the sensor thickness and is given by $R=\rho L/A$, where ρ is the resistivity of the sensor coupon, L is the length and A is its cross section. As the area decreases due to corrosion, the resistance increases, giving an indication of corrosion. Based on this concept, corrosion sensors have been designed to detect the changes in the metal resistance and have been converted to the corrosion rate of the metal.[96, 97] Such sensors are available commercially and are widely used in industries (such as oil and gas industries) for corrosion measurement.[98, 99]

2.3.2. Sensors in coatings

Amongst the strategies used for the protection of structures from corrosion the use of organic coating ranks first. Protective organic coatings are widely used in most of the structures such as buildings, vehicles, aircrafts, tanks, pipelines. However the permeable nature of organic polymers leads to slow but certain penetration of corrosive species such as ions, oxygen and electrolytes through the coating towards the metal substrate which eventually leads to corrosion of the substrate. A Coating can also degrade under natural weathering conditions such as UV, rain, chloride ions or under stresses of dry and wet cycles during day and night. Therefore gradually with time the protective ability of coating decreases and eventually the coating fails. In order to ensure maximum protection of structures timely detection of coatings protective property is necessary. There are many indicators that can confirm a coating failure such as rust spots, detection of corrosive species, excess local alkaline or acidic condition, and detection of certain species like chloride ions on the surface of metal or reduction in the resistance of the coating. Therefore

if there are sensors that can monitor coating activity with respect to time than the repair and maintenance of the coating can be performed much earlier enhancing the lifetime of the structure under protection and sometimes preventing catastrophic failure. *In-situ* monitoring of coating via the use of such sensors or the use of such sensors to detect failure activity can therefore be a strategy that can be applied for enhanced protection. Sensors that detect pH change due to corrosion, corrosive species and resistance of the coating have been developed.

2.3.2.1. Chemical sensors for coatings

During the corrosion process the anode often has acidic pH whereas cathode has an alkaline pH.[100] Therefore, chemicals that respond to pH change can be used to sense anodic and cathodic region. Coating incorporated with microcapsules that rupture and releases color or fluorescent dye on certain pH can indicate corrosion of the metal. Research on pH sensitive microcapsule has been performed at NASA Corrosion Technology Laboratory. Coatings incorporated with corrosion indicator (pH indicator) were successfully examined and the coating displayed color change at the corrosion site.[101, 102] Further works on pH-triggered release microcapsules that can detect and protect a damaged coating is currently underway at the Coatings and Polymeric Materials department at North Dakota State University by Professor Victoria Gelling and her groups in collaboration with NASA. Earlier works on detecting corrosion using pH sensitive color and fluorescent dyes also have been reported by White and Zhang among others.[103-105] White demonstrated the use of pH sensitive fluorescent dye for the detection of corrosion in integrated circuits. Zhang used pH sensing (color changing or fluorescing) indicator in clear acrylic paint matrix system to detect corrosion or the pH change associated with the

cathodic reaction during the corrosion process. The Color change could be observed due to the transparent nature of the coating system by unaided eye. Fluorescing and color changing dyes also have been used to identify corrosion products.[103-105]
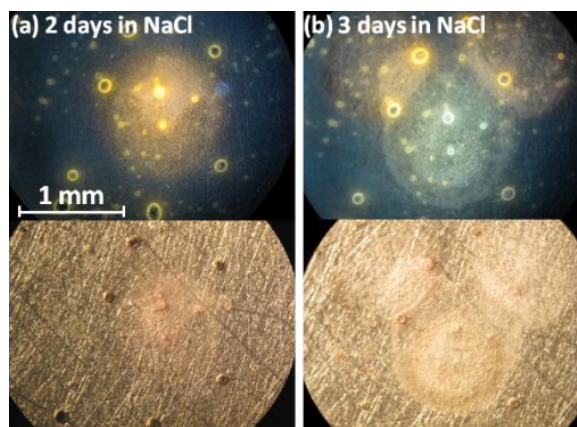
Figure 2.10: Images of Al 1052 coated with a spirolactam containing, clear epoxy coating after (a) 2 days and (b) 3 days of exposure to 3.5% NaCl solution. [Augustyniak et al., *Progress in Organic Coatings* 2011, *71* (4), 406-412].

A very recent finding in corrosion sensing in coatings has been the concept of "turn on" fluorescent spectroscopy. This technique uses a spirolactam to fluoresce at low pH. The spirolactum was embedded in an epoxy matrix primer in an aluminum substrate. On pitting sites fluorescence were observed (Figure 2.10). It was reported that the spirolactum was converted into a fluorescing agent on protonation at acidic pH.[106] Sensing of pH has also been performed using microelectrode sensors and has been used to sense pH changes in thin films.[100] In addition sensors that can detect certain ions detrimental to structural health, such as chloride ions in reinforced concrete have also been reported. [107]

2.3.2.2. Electrochemical sensors for coatings

Electrochemical techniques are widely used to study the protective behavior of coating system. They provide quantitative information and can give early warning signs. However the complex nature of the electrochemical set up as well as the need for

electrolytes, bulky reference and counter electrodes during measurement have made them unfit for in-situ field measurement unless modification in the design is made. Efforts have been made to modify the technique to facilitate *in-situ* field measurements. As early as in 1987, modification in the design of the EIS set up was made by Kihira et al.,[108] His design consisted of sealing the electrolyte holding chamber with a mass of sponge to prevent electrolyte spill. The counter electrode was installed in the closed chamber. An EIS measurement could be performed in the field and the coatings protective ability could be monitored. A further modification was made to this design by using a super absorbent polymer to absorb the electrolyte and using a screen to cover the opening portion of the chamber.[109] Later the use of solid electrolyte had also been reported.[110] Davis et al., [4, 111] used conductive ink deposited on the coating and used it as a sensor to perform EIS measurement. He also reported the use of permanent sensor applied to the coating surface and a hand held sensor that is pressed against the surface of the coating to perform EIS measurement. Simpson reported surface sensor made of thin gold layer and performed EIS to evaluate the effect of acidic deposition on coated substrate.[112] It has however been observed that surface sensors are prone to degradation due to their interaction with the environment and hence measurement made using such sensors might lack accuracy as well as long lifetime.[113] Moreover, surface sensor techniques are complicated and require sophisticated deposition method such as physical vapor deposition/electron beam deposition, vacuum condition, considerable processing work such as the use of photo resist, UV exposure, baking, etching etc.

An approach used to circumvent the problem arising out of surface sensor is the use of embedded sensors in coatings. These sensors are similar to the surface sensor except that

they are covered with a protective topcoat to protect them from external influence. The topcoat also provides additional advantages such as improved isolation between sensors, better adhesion to the underlying films, improved measurement and higher sensitivity to small changes in coating impedance. Bierwagen et al.,[114] first conceived and implemented the idea of embedded sensors in coatings and combining them with EIS and ENM measurement to monitor the health of the coating in-situ. Since then embedded sensors have been used in many coating research. Kittel et al.,[115] used gold comb like embedded sensors deposited on the primer via physical vapor deposition and top coated by a second coat layer embedding it. He used a four electrode technique with the gold comb sensor acting as a reference probe for EIS measurement. The impedance of the primer was obtained by measuring potential between the sensor and the substrate and current between the substrate and an external counter electrode consisting of Pt grid in solution. Impedance of top coat was obtained by measuring the potential between the sensor and the Pt electrode and current between the substrate and the Pt electrode. Similar work using nickel sensor was also performed.[116] This approach, however, still required solution where the counter electrode was immersed and therefore was inconvenient for field application.

In their first such study, Bierwagen et al.,[117] demonstrated the in-situ use of embedded sensors to monitor the performance of the coating degradation and substrate corrosion using ENM technique and demonstrated that the variation of electrochemical parameters such as R_n, LI and R_{sn} were consistent with the change in environmental (Prohesion) condition. Such embedded sensor measurement could provide a strategy for in-situ monitoring of the coatings with potential for field applications. It was earlier observed that the results obtained from conventional ENM measurement for same sample was very

60

close to the ENM measurement performed using embedded sensors.[117] Since then the department of Coatings and Polymer Materials at North Dakota State University has been at the forefront of research on embedded sensors for coating applications. Su et al.,[22] applied DC on sensor embedded coatings and studied the behavior of coating using non standard ENM configuration with substrate as the reference electrode. It was observed that the coating degraded using DC could be measured by embedded sensors using ENM and the R_n value obtained was comparable with $|Z|$. Embedded sensors have also been used to monitor the behavior of coating *in-situ* under constant immersion condition and to evaluate the performance of coating under accelerated thermal cycling method using EIS and ENM.[11, 118] Sensors have also been used to study coating behavior under certain environmental conditions such as QUV/Prohesion and Prohesion.[117-119] More recently Allahar et al.,[120] have demonstrated the feasibility of substrate monitoring without the substrate being acting as electrode. He has concluded that the data obtained by EIS measurement made between two sensors in a non-substrate configuration agrees with the data obtained by EIS measurement made between embedded electrode and the substrate.
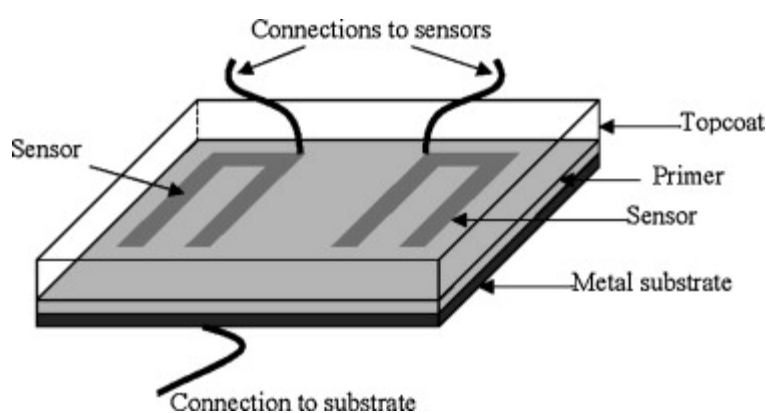
Figure 2.11: Embedded sensors between primer and topcoat. [Allahar et al. *Progress in Organic Coatings* 2010, 67, 180-187].

Other researchers also have contributed to this area with valuable findings. Embedded sensors in coatings have been used to study water uptake behavior in the two layers of a primer/topcoat system.[115, 116] Miszczyk et al.,[121] used conductive ink as embedded sensor to evaluate the performance of interlayer adhesion of a coating system using EIS. Two sensor electrodes embedded in the basecoat were used as working and counter/reference electrode respectively. It was also observed that the interlayer adhesion is affected by both temperature and humidity. In a simulation study supported with experimental results Nogueira et al.,[122] demonstrated that the coating impedance measured between two embedded sensors is a function of frequency, metal-coating interface and the relative impedance of the coating and the current mostly take the least resistive path. Allahar et al.,[120] have suggested 5 possible routes for current passage when EIS measurements between two embedded sensors are made.

2.4. References

[1] G.P. Bierwagen, Reflections on corrosion control by organic coatings, Progress in Organic Coatings, 28 (1996) 43-48.

[2] Z.W. Wicks Jr, F.N. Jones, S.P. Peppas, Organic coatings: Science and technology, 2 ed., Wiley-Interscience, 1999.

[3] G.P. Bierwagen, D.E. Tallman, Choice and measurement of crucial aircraft coatings system properties, Progress in Organic Coatings, 41 (2001) 201-216.

[4] G. Davis, L. Krebs, C. Dacres, Coating evaluation and validation of accelerated test conditions using an in-situ corrosion sensor, Journal of Coatings Technology, 74 (2002) 69-74.

[5] G. Bierwagen, D. Tallman, J. Li, L. He, C. Jeffcoate, EIS studies of coated metals in accelerated exposure, Progress in Organic Coatings, 46 (2003) 149-158.

[6] L. Fedrizzi, A. Bergo, F. Deflorian, L. Valentinelli, Assessment of protective properties of organic coatings by thermal cycling, Progress in Organic Coatings, 48 (2003) 271-280.

[7] G.P. Bierwagen, L. He, J. Li, L. Ellingson, D.E. Tallman, Studies of a new accelerated evaluation method for coating corrosion resistance -- thermal cycling testing, Progress in Organic Coatings, 39 (2000) 67-78.

[8] J. Li, C. Jeffcoate, G. Bierwagen, D. Mills, D. Tallman, Thermal Transition Effects and Electrochemical Properties in Organic Coatings: Part 1 Initial Studies on Corrosion Protective Organic Coatings, CORROSION, 54 (1998).

[9] A. Miszczyk, K. Darowicki, Accelerated ageing of organic coating systems by thermal treatment, Corrosion Science, 43 (2001) 1337-1343.

[10] A. Miszczyk, K. Darowicki, Effect of environmental temperature variations on protective properties of organic coatings, Progress in Organic Coatings, 46 (2003) 49-54.

[11] Q. Su, K.N. Allahar, G.P. Bierwagen, Application of embedded sensors in the thermal cycling of organic coatings, Corrosion Science, 50 (2008) 2381-2389.

[12] G. Bierwagen, L. He, D. Tallman, Time-temperature effects in polymer coatings for corrosion protection as analyzed by EIS, Macromolecular Symposia, 187 (2002) 909-918.

[13] C. Jeffcoate, T. Wocken, G. Bierwagen, Electrochemical assessment of spray-applied thermoplastic coating barrier properties, Journal of Materials Engineering and Performance, 6 (1997) 417-420.

[14] C. Jeffcoate, J. Li, G. Bierwagen, Problems Encountered in Electrochemical Corrosion Testing of Flame Sprayed Powder Coatings, Electrochemical Soc. Symposium Proceedings 95-16, S.R.Taylor, H. Isaacs, & E. Brooman, eds. (1995) p.1960.

[15] B.R. Hinderliter, K.N. Allahar, G.P. Bierwagen, D.E. Tallman, S.G. Croll, Thermal Cycling of Epoxy Coatings Using Room Temperature Ionic Liquids, Journal of The Electrochemical Society, 155 (2008) C93-C100.

[16] S. Touzain, Q.L. Thu, G. Bonnet, Evaluation of thick organic coatings degradation in seawater using cathodic protection and thermally accelerated tests, Progress in Organic Coatings, 52 (2005) 311-319.

[17] E.L. J. Hollaender, S. Hillebrand, Proceedings of the Fifth International Tinplate Conference,London, (1992) 300.

[18] M.T. Rodríguez, J.J. Gracenea, S.J. García, J.J. Saura, J.J. Suay, Testing the influence of the plasticizers addition on the anticorrosive properties of an epoxy primer by means of electrochemical techniques, Progress in Organic Coatings, 50 (2004) 123-131.

[19] S.J. García, J. Suay, Anticorrosive properties of an epoxy-Meldrum acid cured system catalyzed by erbium III trifluromethanesulfonate, Progress in Organic Coatings, 57 (2006) 319-331.

[20] M. Bethencourt, F.J. Botana, M.J. Cano, R.M. Osuna, M. Marcos, Lifetime prediction of waterborne acrylic paints with the AC-DC-AC method, Progress in Organic Coatings, 49 (2004) 275-281.

[21] M. Poelman, M.G. Olivier, N. Gayarre, J.P. Petitjean, Electrochemical study of different ageing tests for the evaluation of a cataphoretic epoxy primer on aluminium, Progress in Organic Coatings, 54 (2005) 55-62.

[22] Q. Su, K. Allahar, G. Bierwagen, Embedded electrode electrochemical noise monitoring of the corrosion beneath organic coatings induced by ac-dc-ac conditions, Electrochimica Acta, 53 (2008) 2825-2830.

[23] S.J. García, J. Suay, A comparative study between the results of different electrochemical techniques (EIS and AC/DC/AC): Application to the optimisation of the cataphoretic and curing parameters of a primer for the automotive industry, Progress in Organic Coatings, 59 (2007) 251-258.

[24] K.N. Allahar, G.P. Bierwagen, V.J. Gelling, Understanding ac-dc-ac accelerated test results, Corrosion Science, 52 (2010) 1106-1114.

[25] G.P. Bierwagen, K.N. Allahar, Q. Su, V.J. Gelling, Electrochemically characterizing the ac-dc-ac accelerated test method using embedded electrodes, Corrosion Science, 51 (2009) 95-101.

[26] J. Castle, J. Watts, Cathodic Disbondment of Well Characterized Steel/Coating Interfaces, Corrosion Control by Organic Coatings. Ed H. Leidheiser Jr, (1981) 78-86.

[27] J. Ritter, Ellipsometric studies on the cathodic delamination of organic coatings on iron and steel, J. Coat. Technol., 54 (1982) 51-57.

[28] J. Mayne, D. Mills, The effect of the substrate on the electrical resistance of polymer films, J. Oil Color Chem. Assoc, 58 (1975) 155.

[29] J.I. Skar, U. Steinsmo, Cathodic disbonding of paint films-transport of charge, Corrosion Science, 35 (1993) 1385-1389.

[30] D. Greenfield, J.D. Scantlebury, Blistering and Delamination Processes on Coated Steel, Journal of Corrosion Science and Engineering, 2 (2000).

[31] J. Vogelsang, W. Strunz, New interpretation of electrochemical data obtained from organic barrier coatings, Electrochimica Acta, 46 (2001) 3817-3826.

[32] K.N. Allahar, V. Upadhyay, G.P. Bierwagen, Characterizing the Relaxation of the Open-Circuit Potential during an AC-DC-AC Accelerated Test, Corrosion, 66 (2010) 095001.

[33] V.V. Shah, J.R. Birchak, W. Han, B.H. Storm, R.M. Amin, B. Kalpakci, F. Fleyfel, Guided acoustic wave sensor for pipeline build-up monitoring and characterization, in, US, 2003.

[34] A. Ramirez, W. Daily, A. Binley, D. LaBrecque, D. Roelant, Detection of leaks in underground storage tanks using electrical resistance methods, J. Environ. Eng. Geophys, 1 (1996) 189–203.

[35] R. Maaskant, T. Alavie, Fiber-optic Bragg grating sensors for bridge monitoring, Cement and Concrete Composites, 19 (1997) 21-33.

[36] Y. Wang, H. Huang, Optical fiber corrosion sensor based on laser light reflection, Smart Materials and Structures, 20 (2011) 085003.

[37] R. Roberge Pierre, Handbook of corrosion engineering, McGraw-Hill, 2000.

[38] J.R. Casas, Fiber optic sensors for bridge monitoring, Journal of bridge engineering, 8 (2003) 362.

[39] K.D. Bennett, L. McLaughlin, Monitoring of corrosion in steel structures using optical fiber sensors, SPIE, 2446 (1995) 48.

[40] S. Wade, C. Wallbrink, G. McAdam, S. Galea, B. Hinton, R. Jones, A fibre optic corrosion fuse sensor using stressed metal-coated optical fibres, Sensors and Actuators B: Chemical, 131 (2008) 602-608.

[41] G. McAdam, P. Newman, I. McKenzie, C. Davis, B. Hinton, Fiber optic sensors for detection of corrosion within aircraft, Structural Health Monitoring, 4 (2005) 47.

[42] P.L. Fuhr, D.R. Huston, Corrosion detection in reinforced concrete roadways and bridges via embedded fiber optic sensors, Smart Materials and Structures, 7 (1998) 217.

[43] X.M. Li, W. Chen, Z.Q. Huang, S. Huang, K.D. Bennett, Fiber optic corrosion sensor fabricated by electrochemical method, in, SPIE, 1998, pp. 126-133.

[44] S. Dong, Y. Liao, Q. Tian, Z. Qiu, Y. Luo, S. Song, Study on different preparing methods of the metallized fiber core for optical fiber corrosion sensor, in: Advanced Sensor Systems and Applications II, SPIE, Beijing, China, 2005, pp. 627.

[45] S. Dong, Y. Liao, Q. Tian, Sensing of corrosion on aluminum surfaces by use of metallic optical fiber, Applied optics, 44 (2005) 6334-6337.

[46] S. Dong, Y. Liao, Q. Tian, Sensing of corrosion on aluminum surfaces by use of metallic optical fiber, Appl. Opt., 44 (2005) 6334-6337.

[47] S. Dong, Y. Liao, Q. Tian, Intensity-based optical fiber sensor for monitoring corrosion of aluminum alloys, Applied optics, 44 (2005) 5773-5777.

[48] M. Benounis, N. Jaffrezic-Renault, G. Stremsdoerfer, R. Kherrat, Elaboration and standardization of an optical fibre corrosion sensor based on an electroless deposit of copper, Sensors and Actuators B: Chemical, 90 (2003) 90-97.

[49] A.M. Cardenas-Valencia, R.H. Byrne, M. Calves, L. Langebrake, D.P. Fries, E.T. Steimle, Development of stripped-cladding optical fiber sensors for continuous monitoring: II: Referencing method for spectral sensing of environmental corrosion, Sensors and Actuators B: Chemical, 122 (2007) 410-418.

[50] M. Benounis, N. Jaffrezic-Renault, Elaboration of an optical fibre corrosion sensor for aircraft applications, Sensors and Actuators B: Chemical, 100 (2004) 1-8.

[51] G. Park, H. Sohn, C.R. Farrar, D.J. Inman, Overview of piezoelectric impedance-based health monitoring and path forward, Shock and Vibration Digest, 35 (2003) 451-464.

[52] J.P. Lynch, A. Sundararajan, K.H. Law, H. Sohn, C.R. Farrar, Design of a wireless active sensing unit for structural health monitoring, in, SPIE, 2004, pp. 157-168.

[53] M.M. Andringa, D.P. Neikirk, N.P. Dickerson, S.L. Wood, Unpowered wireless corrosion sensor for steel reinforced concrete, in, IEEE, 2005, pp. 4 pp.

[54] J.T. Simonen, M.M. Andringa, K.M. Grizzle, S.L. Wood, D.P. Neikirk, Wireless sensors for monitoring corrosion in reinforced concrete members, in: Proc. SPIE, SPIE, San Diego, CA, USA, 2004, pp. 587.

[55] S. Kim, S. Pakzad, D. Culler, J. Demmel, G. Fenves, S. Glaser, M. Turon, Health monitoring of civil infrastructures using wireless sensor networks, in: IPSN '07, ACM, 2007, pp. 254-263.

[56] L. Salvino, R. Swartz, A.T. Zimmerman, J.P. Lunch, J. Rosario, T. Brady, K.H. Law, Hybrid Wireless Hull Monitoring System for Naval Combat Vessels, in, NAVAL SURFACE WARFARE CENTER CARDEROCK DIV BETHESDA MD, 2010.

[57] R.A. Swartz, Hybrid wireless hull monitoring system for naval combat vessels, in, DTIC Document, 2010.

[58] Z.B. Popovi Wireless powering for low-power distributed sensors, Serbian Journal of Electrical Engineering, 3 (2006) 149-162.

[59] Y. Yu, J. Ou, Wireless sensing experiments for structural vibration monitoring of offshore platform, Frontiers of Electrical and Electronic Engineering in China, 3 (2008) 333-337.

[60] G. Qiao, G. Sun, Y. Hong, Y. Qiu, J. Ou, Remote corrosion monitoring of the RC structures using the electrochemical wireless energy-harvesting sensors and networks, NDT & E International, 44 (2011) 583-588.

[61] G. Sun, G. Qiao, B. Xu, Corrosion Monitoring Sensor Networks with Energy Harvesting, Sensors Journal, IEEE, 1-1.

[62] M.J. Hamel, S.W. Arms, C.P. Townsend, D.L. Churchill, Energy harvesting for wireless sensor operation and data transmission, in, US, 2006.

[63] J. Wu, W. Wu, Study on wireless sensing for monitoring the corrosion of reinforcement in concrete structures, Measurement, 43 (2010) 375-380.

[64] J.-H. Yoo, Z.-T. Park, J.-G. Kim, L. Chung, Development of a galvanic sensor system for detecting the corrosion damage of the steel embedded in concrete structures: Part 1. Laboratory tests to correlate galvanic current with actual damage, Cement and Concrete Research, 33 (2003) 2057-2062.

[65] Z.-T. Park, Y.-S. Choi, J.-G. Kim, L. Chung, Development of a galvanic sensor system for detecting the corrosion damage of the steel embedded in concrete structure: Part 2. Laboratory electrochemical testing of sensors in concrete, Cement and Concrete Research, 35 (2005) 1814-1819.

[66] C. Arya, P.R.W. Vassie, Influence of cathode-to-anode area ratio and separation distance on galvanic corrosion currents of steel in concrete containing chlorides, Cement and Concrete Research, 25 (1995) 989-998.

[67] E.V. Pereira, R.B. Figueira, M.M.L. Salta, I.T.E. da Fonseca, A Galvanic Sensor for Monitoring the Corrosion Condition of the Concrete Reinforcing Steel: Relationship Between the Galvanic and the Corrosion Currents, Sensors, 9 (2009) 8391-8398.

[68] M. Raupach, P. Schießl, Macrocell sensor systems for monitoring of the corrosion risk of the reinforcement in concrete structures, NDT & E International, 34 (2001) 435-442.

[69] L. Yang, N. Sridhar, C.S. Brossia, D.S. Dunn, Evaluation of the coupled multielectrode array sensor as a real-time corrosion monitor, Corrosion Science, 47 (2005) 1794-1809.

[70] H. Wadley, C. Scruby, J. Speake, Acoustic emission for physical examination of metals, International Metals Reviews, 25 (1980) 41-64.

[71] F. Bellenger, H. Mazille, H. Idrissi, Use of acoustic emission technique for the early detection of aluminum alloys exfoliation corrosion, NDT & E International, 35 (2002) 385-392.

[72] F. Ferrer, T. Faure, J. Goudiakas, E. Andrès, Acoustic emission study of active-passive transitions during carbon steel erosion-corrosion in concentrated sulfuric acid, in: Corrosion Science, 2002, pp. 1529-1540.

[73] J. Sieniawski, M. Gieron, W. Ziaja, Application of resistance and acoustic emission measurements in fatigue tests of two phase [alpha] + [beta] titanium alloys, Journal of Materials Processing Technology, 53 (1995) 363-372.

[74] M. Huang, L. Jiang, P.K. Liaw, C.R. Brooks, R. Seeley, D.L. Klarstrom, Using acoustic emission in fatigue and fracture materials research, JOM, 50 (1998) 1-14.

[75] H. Idrissi, A. Limam, Study and characterization by acoustic emission and electrochemical measurements of concrete deterioration caused by reinforcement steel corrosion, NDT & E International, 36 (2003) 563-569.

[76] C. Jomdecha, A. Prateepasen, P. Kaewtrakulpong, Study on source location using an acoustic emission system for various corrosion types, NDT & E International, 40 (2007) 584-593.

[77] J. Onoro, C. Ranninger, Exfoliation corrosion behaviour of welded high strength aluminium alloys, British corrosion journal, 28 (1993) 137-141.

[78] B. Knowlton, A. Siddiqui, S. Jihan, Stress corrosion monitoring of 7000 series aluminium alloy welded specimens using acoustic emission, British corrosion journal, 32 (1997) 249-253.

[79] F. Ferrer, T. Faure, J. Goudiakas, E. Andrès, Acoustic emission study of active-passive transitions during carbon steel erosion-corrosion in concentrated sulfuric acid, Corrosion Science, 44 (2002) 1529-1540.

[80] J. Kovac, C. Alaux, T.J. Marrow, E. Govekar, A. Legat, Correlations of electrochemical noise, acoustic emission and complementary monitoring techniques during intergranular stress-corrosion cracking of austenitic stainless steel, Corrosion Science, 52 (2010) 2015-2025.

[81] A. Berkovits, D. Fang, Study of fatigue crack characteristics by acoustic emission, Engineering fracture mechanics, 51 (1995) 401-409.

[82] D. Kohn, P. Ducheyne, J. Awerbuch, Sources of acoustic emission during fatigue of Ti-6Al-4V: effect of microstructure, Journal of materials science, 27 (1992) 1633-1641.

[83] K. Darowicki, A. Mirakowski, S. Krakowiak, Investigation of pitting corrosion of stainless steel by means of acoustic emission and potentiodynamic methods, Corrosion Science, 45 (2003) 1747-1756.

[84] A. Cakir, S. Tuncell, A. Aydin, Ae response of 316L SS during SSR test under potentiostatic control, Corrosion Science, 41 (1999) 1175-1183.

[85] S.-i. Magaino, A. Kawaguchi, A. Hirata, T. Osaka, Spectrum Analysis of Corrosion Potential Fluctuations for Localized Corrosion of Type 304 Stainless Steel, Journal of The Electrochemical Society, 134 (1987) 2993-2997.

[86] J. Broomfield, Techniques to Assess the Corrosion Activity of Steel-Reinforced Concrete Structures, ASTM STP, 1276 (1996) 91–106.

[87] H.W. Song, V. Saraswathy, Corrosion Monitoring of Reinforced Concrete Structures-A, Int. J. Electrochem. Sci, 2 (2007) 1-28.

[88] D. Law, S. Millard, J. Bungey, Linear polarisation resistance measurements using a potentiostatically controlled guard ring, NDT & E International, 33 (2000) 15-21.

[89] M. Stearn, A. Geary, Electrochemical Polarization No. 1: Theoretical Analysis of the Shape of Polarization Curve, Journal of Electrochemical Society, 104 (1957) 56-63.

[90] C. Andrade, C. Alonso, Test methods for on-site corrosion rate measurement of steel reinforcement in concrete by means of the polarization resistance method, Materials and Structures, 37 (2004) 623-643.

[91] D.W. Law, S.G. Millard, J.H. Bungey, Linear polarisation resistance measurements using a potentiostatically controlled guard ring, NDT & E International, 33 (2000) 15-21.

[92] S.G. Millard, D. Law, J.H. Bungey, J. Cairns, Environmental influences on linear polarisation corrosion rate measurement in reinforced concrete, NDT & E International, 34 (2001) 409-417.

[93] G. Song, Theoretical analysis of the measurement of polarisation resistance in reinforced concrete, Cement and Concrete Composites, 22 (2000) 407-415.

[94] F.J. Ansuini, R.E. Howe, Corrosion sensor for measuring the corrosion loss and the instantaneous corrosion rate, in, US, 1988.

[95] F. Mansfeld, S. Jeanjaquet, M. Kendig, D. Roe, A New atmospheric corrosion rate monitor--development and evaluation, Atmospheric Environment (1967), 20 (1986) 1179-1192.

[96] Y.G. Kim, S.M. Lee, Y.T. Kho, H.S. Song, D.S. Won, Electric resistance sensor for measuring corrosion rate, in, US, 2002.

[97] S. Li, S. Jung, K.-w. Park, S.-M. Lee, Y.-G. Kim, Kinetic study on corrosion of steel in soil environments using electrical resistance sensor technique, Materials Chemistry and Physics, 103 (2007) 9-13.

[98] J.P. Cai, S.B. Lyon, A mechanistic study of initial atmospheric corrosion kinetics using electrical resistance sensors, Corrosion Science, 47 (2005) 2956-2973.

[99] L. Cooper, Sensing Probes and Instruments for Electrochemical and Electrical Resistance Corrosion Monitoring, Corrosion Monitoring in Industrial Plants Using Nondestructive Testing and Electrochemical Methods, (1984) 237-250.

[100] F.J. Maile, T. Schauer, C.D. Eisenbach, Evaluation of corrosion and protection of coated metals with local ion concentration technique (LICT), Progress in Organic Coatings, 38 (2000) 111-116.

[101] W. Li, L.M. Calle, Controlled Release Microcapsules For Smart Coatings, in: CORROSION 2007, NACE International, Nashville, Tennessee, 2007.

[102] L.M. Calle, W. Li, Coatings and methods for corrosion detection and/or reduction, in, US 2010.

[103] L.K. White, R.B. Comizzoli, C.A. Deckert, G.L. Schnable, The Detection of Corrosion Phenomena with pH-Sensitive Fluorescent Dyes on Aluminum- and Gold-Metallized IC Devices, Journal of The Electrochemical Society, 128 (1981) 953-956.

[104] J. Zhang, G.S. Frankel, Corrosion-Sensing Behavior of an Acrylic-Based Coating System, Corrosion, 55 (1999) 957.

[105] N.E. Cipollini, Visual Detection of Hydrated Aluminum Oxide by Staining with Fluorescing and Nonfluorescing Dyes, Journal of The Electrochemical Society, 129 (1982) 1517.

[106] A. Augustyniak, W. Ming, Early detection of aluminum corrosion via "turn-on" fluorescence in smart coatings, Progress in Organic Coatings, 71 (2011) 406-412.

[107] M.F. Montemor, J.H. Alves, A.M. Simões, J.C.S. Fernandes, Z. Lourenço, A.J.S. Costa, A.J. Appleton, M.G.S. Ferreira, Multiprobe chloride sensor for in situ monitoring of reinforced concrete structures, Cement and Concrete Composites, 28 (2006) 233-236.

[108] H. Kihira, S. Ito, T. Murata, S. Sakamoto, K. Yamamoto, Method and apparatus for diagnosing degradation of coating film on metal material, in, US, 1989.

[109] K. Homma, H. Kihira, S. Ito, K. Matsuoka, N. Hirosawa, Sensor for electrochemical measurement and method for diagnosing corrosion protective properties of metal surface coating by using the sensor, in, US, 1990.

[110] A. Gonzalez-Martin, J. Kim, D. Hodko, C. Salinas, Electrochemical impedance evaluation and inspection sensor, in, US, 2004.

[111] G.D. Davis, C.M. Dacres, Electrochemical sensors for evaluating corrosion and adhesion on painted metal structures, in, US, 1999.

[112] T. Simpson, H. Hampel, G. Davis, C. Arah, T. Fritz, P. Moran, B. Shaw, K. Zankel, Evaluation of the effects of acidic deposition on coated steel substrates, Progress in Organic Coatings, 20 (1992) 199-216.

[113] X. Wang, Study on novel electrode configurations for in-situ corrosion monitoring on coated systems, Chapter 3 in: CPM, North Dakota State University, Fargo, 2002.

[114] G.P Bierwagen, D. Mills, D.Tallman, Proceedings of the 12th International Corrosion Congress, paper 576, NACE, Houston, (1993) 4208.

[115] J. Kittel, N. Celati, M. Keddam, H. Takenouti, New methods for the study of organic coatings by EIS:: New insights into attached and free films, Progress in Organic Coatings, 41 (2001) 93-98.

[116] J. Kittel, N. Celati, M. Keddam, H. Takenouti, Influence of the coating-substrate interactions on the corrosion protection: characterisation by impedance spectroscopy of the inner and outer parts of a coating, Progress in Organic Coatings, 46 (2003) 135-147.

[117] G. Bierwagen, X. Wang, D. Tallman, In situ study of coatings using embedded electrodes for ENM measurements, Progress in Organic Coatings, 46 (2003) 163-175.

[118] D. Wang, D. Battocchi, K.N. Allahar, S. Balbyshev, G.P. Bierwagen, In situ monitoring of a Mg-rich primer beneath a topcoat exposed to Prohesion conditions, Corrosion Science, 52 (2010) 441-448.

[119] Q.S. K. N. Allahar, G. P. Bierwagen1, D. H. Lee, Monitoring of the AC-DC-AC Degradation of Organic Coatings Using Embedded Electrodes, Corrosion, 64 (2008) 773.

[120] K. Allahar, Q. Su, G. Bierwagen, Non-substrate EIS monitoring of organic coatings with embedded electrodes, Progress in Organic Coatings, 67 (2010) 180-187.

[121] A. Miszczyk, T. Schauer, Electrochemical approach to evaluate the interlayer adhesion of organic coatings, Progress in Organic Coatings, 52 (2005) 298-305.

[122] A. Nogueira, X.R. Nóvoa, C. Pérez, On the possibility of using embedded electrodes for the measurement of dielectric properties in organic coatings, Progress in Organic Coatings, 59 (2007) 186-191.

CHAPTER 3. ELECTROCHEMICALLY CHARACTERIZING THE DEGRADATION OF ARMY PRIMERS BY THE AC-DC-AC ACCELERATED TEST METHOD AND EXTRACTING NEW INFORMATIONS

3.1. Introduction

The extended use of outdoor metallic structures are enabled by the application of organic coatings that act as a barrier between substrate and the environment.[1] Organic coatings can also be used to store corrosion inhibitors but its barrier protection remains the primary means for which coatings are employed. Metallic coatings and impressed cathodic or anodic protection are often less favored than the robust barrier protection provided by organic coatings in preventing water and ionic species transporting from the environment to the metal surface. Conventional methods for the performance evaluation of organic coatings are designed to test the barrier protection and include the salt-fog (ASTM B117) and the Prohesion®/QUV® (ASTM D 5894) methods. These methods attempt to simulate worst-case weathering conditions such that coating failure occurs in shorter times than actual service lifetime. Even under the severe Prohesion®/QUV® condition, the barrier property of organic coatings can remain intact, as is the case for a standard aircraft polyurethane topcoat/chromate epoxy primer system on AA 2024-T3, which showed little change in barrier property during 2 years of exposure to Prohesion®/QUV® conditions.[2]

The inherent assumption associated with conventional accelerated test methods is that the failure mechanisms promoted by the testing conditions are the same as those caused by natural weathering. Unconventional accelerated test methods have been used to yield coating performance ranking in considerable less time than conventional test methods. The thermal cycling method involves exposure of coated panels to cyclic

temperature changes under constant immersion and has been supported by observations that the irreversible changes induced by thermal conditions had similar degradation mechanisms as compared to natural atmospheric conditions.[3-6]

The AC-DC-AC method is another unconventional accelerated test method that promotes the degradation of coatings through the application of cycles of direct current (DC) exposure.[7-13] The AC-DC-AC method refers to three step testing process that begins with a multi frequency EIS (MF-EIS) impedance measurement of the coating followed by a DC polarization of the substrate which is again followed by a MF-EIS measurement. The first MF-EIS step measures the existing state of a coating system. In the DC step, a negative DC polarization is applied to the substrate. During this step the positive ions such as Na^+ and H^+ at the electrolyte are forced through the coating to reach the metal coating interface. If these ions and electrolytes get to the interface, they will cause coating deterioration since the forceful ion transport through the coating would result in the formation of pores and reduction in barrier property. Moreover the products of the reduction reactions such as H_2 and OH^- can cause film delamination and adhesion loss thus causing film deterioration.[14-17]

This step is followed by shutting off the applied DC potential and allowing the system to relax to its open circuit potential. Once the applied DC is removed, the ions and electrolytes no longer move towards the substrate and return to their original position via charge transfer processes at the metal coating interface, dielectric relaxation of the coating and the transport of the ionic species out of the coating. Modeling of the relaxation profile has been attempted to quantitate the contributions by these processes.[18] The signature of the potential relaxation profile can also be interpreted qualitatively to help describe coating

behavior. A single short relaxation time can indicate an intact coating whereas a single longer relaxation time indicate that the ions have penetrated the coating and hence require a longer time to relax and reach their state at open circuit potential. The ions have to pass through the network of polymers, and hence require longer times. The relaxation times will be greater the deeper the ions and electrolytes have penetrated the film and would be longest if the electrolytes and ions have managed to reach the metal-coating interface. If cathodic reactions were to take place at the metal-coating interface then two relaxations would be observed, first one corresponding to the reversing of the reactions at the metal-coating interface and second due to exit of ions and electrolytes from the film[14].

At the new open circuit potential that develops after the relaxation processes, measurement by MF-EIS is performed to assess the state of the coating after DC. This second MF-EIS provides information about the effect on the coating of the DC polarization. AC-DC-AC can be performed in cycles until failure is induced in the coating. Hollaender, Bierwagen, Allahar, Garcia, Suay, Bethencourt, Poelman, Rodriguez etc. have made significant contributions towards understanding the AC-DC-AC method, and have used it to extract information about the coating system [9-11, 13, 14, 19-22]. Further extraction of information from this method has been explored in this chapter and an attempt is made to extend the past work. In this chapter AC-DC-AC method is used to first discriminate between two different Army primers and then to investigate the possible correlation between coating failure and total charge transferred across at the metal coating interface, induced to the coating during DC polarization step of AC-DC-AC. First AC-DC-AC method is applied to two standard Army primers on steel substrates under immersion in

79

3.5 wt. % NaCl. After the AC-DC-AC test on the two primers, one of the primers was selected for studying the importance of total charge to coating failure.

3.2. Experimental

Two standard Army primers were used for this work and were exposed to the AC-DC-AC accelerated test method. One was a 2-component primer consisting of an epoxy resin and curing agent manufactured by Sherwin Williams, meeting primer specification of MIL-P-53022B Type II. This primer was designated as S-primer. The other primer was a similar 2-component primer with an epoxy resin and curing agent that also had a primer specification of MIL-P-53022B Type II and was manufactured by Deft. This primer is identified as D-primer. The primers were applied unto steel panels of dimensions 3 x 6 inches (Q-panels of Cleveland, Ohio). The as-received panels were sandblasted and cleaned with n-hexane before use. Each of the primers was prepared according to the manufacturer's specifications and applied by regular air spray. The primers were cured for one week at room temperature. The manufacturers listed the primers as containing a corrosion inhibitor and free of lead and chromate. After inspection for uniformity of the panels prepared two panels were selected for each primer.

Careful visual inspection of the panels was done initially to look for any defects or non-uniformities in the coating. Coatings obtained from S-primer and D-primer was leveled as S-sample and D-sample respectively. The thickness of the area to be investigated was measured using an Elcometer 345 NS supplied by Elcometer Instruments Ltd. of Rochester Hills, MI. The thicknesses of S-sample used in this study were 88 ± 7 μm whereas the thicknesses of the D-sample were 80 ± 7 μm respectively. Two other coated panels used as control during the test were leveled as S-control and D-control respectively.

Perspex cylinders with a surface area of 7.07 cm^2 were mounted on the samples and were clamped with an O-ring insert to facilitate electrochemical measurement.

EIS measurement was performed using the conventional three electrode design as shown in Figure 3.1.[23, 24] Conventional EIS set up consists of the metal substrate as the working electrode (WE) with platinum (Pt) and saturated calomel electrode (SCE) as counter and reference electrodes respectively. A Gamry Instrument R 600 Potentiostat/Galvanostat/ZRA in conjunction with Gamry Framework Version 5.20/EIS 300 software was used for the experiment. The instrument and software were supplied by Gamry Instruments, Inc. of Willow Grove, PA. The impedance response corresponding to the applied frequency of 100 kHz to 0.01Hz was measured with an acquisition rate of 10 points per decade. A 10mV amplitude perturbation potential with respect to the open circuit potential was used during the measurement.
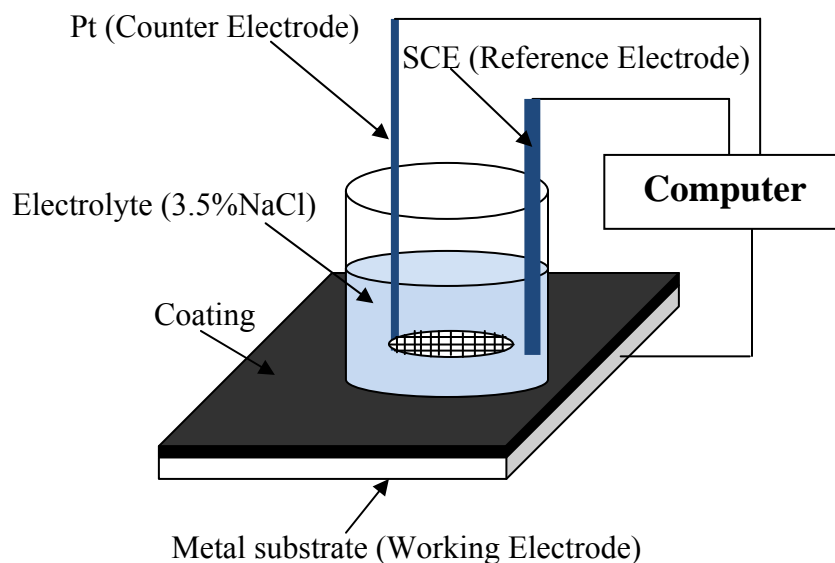
Figure 3.1: Schematic of a conventional three electrode EIS set up.[23, 24]

The AC-DC-AC procedure (stress cycle) as applied in this work is shown schematically in Figure 3.2. It involved three step cycles for a coating panel under

immersion. The first step was an AC step wherein MF-EIS was run on the sample to test the coatings initial properties. In the next step, a negative DC potential was applied to the substrate to force cathodic reactions and formation of hydrogen and hydroxide ion at the metal coating interface. This was followed by withdrawing the applied negative potential and allowing the ions and molecules to relax to its open circuit potential. At the new open circuit potential after relaxation a MF- EIS was performed again to study the new state of the coating after DC polarization.
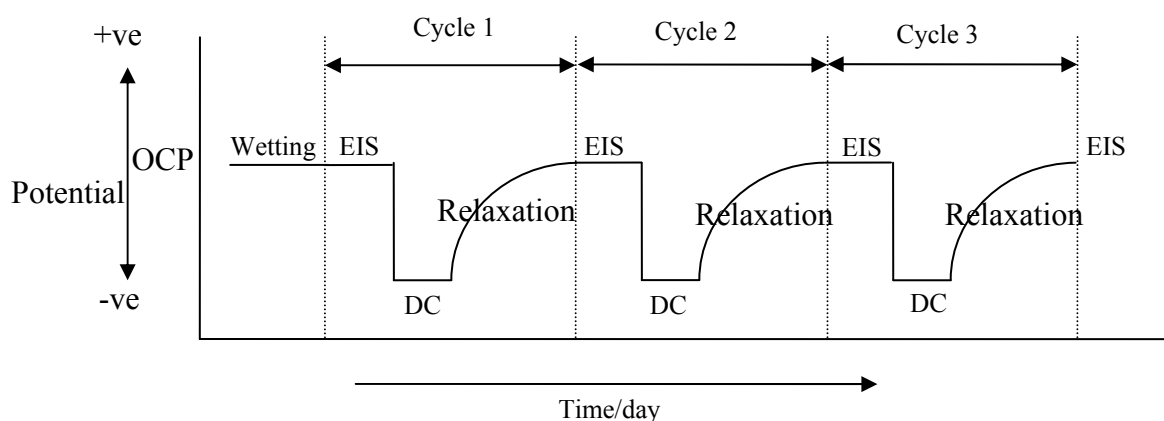
Figure 3.2: Schematic of AC-DC-AC procedure.

During the entire experimental period, all the samples, S-sample, S-control, D-sample and D-control were continuously immersed in 3.5 wt% NaCl solution prepared with DI water. An initial EIS measurement was taken after four days of immersion to monitor the initial state of the coating. This measurement was considered as day 0. Following this measurement, S-sample and D-sample were subjected to AC-DC-AC procedure. In this work the AC-DC-AC was applied in cycles that consisted of a MF-EIS, 4 hours of the DC cathodic polarization, relaxation step of 24 hours followed by a MF-EIS. For the first three cycles, -2 volts were applied on the samples, followed by -4 volts for the next three cycles. Seventh to ninth cycle consisted of -6 volts followed by -8 volts for the rest of the cycles

82

until failure. EIS measurements were performed daily on all control samples, S-control and D-control. Based on the performance of the two samples (S-sample and D-sample), the sample that degraded more rapidly in the applied DC and failed early was used for further investigation to study the correlation between coating failure and the total charge at the metal-coating interface.

3.3. Results and discussions

3.3.1. EIS impedance spectra

The modulus of the impedance (|Z|) and the phase angle as a function of frequency (Bode plots) for both D-sample and S-sample are presented in Figures 3.3 and 3.4 respectively. Bode plots can furnish information about the state of the coating. One time constant indicate intact coating whereas two or more time constants indicate interfacial activity and corrosion at the interface. In addition, low frequency impedance is a measure of coatings barrier properties. A decrease in low frequency impedance indicates degrading barrier properties. Modeling can also be performed on the EIS data to quantitatively extract the contributions by processes involved at the coating and the metal coating interface.[25-27].

Both D-sample and S-sample had undergone AC-DC-AC stress cycles. Cycle 0 corresponds to normal unstressed EIS measurement prior to the application of DC. The bode plots of the D sample corresponding to the third cycles of -2V, -4V and -6V DC stress cycle are depicted in Figure 3a and 3b respectively along with cycle 0. From the figure it is observed that the Bode plot of cycle 0 is superimposed with the plot of cycle 3 suggesting that three cycles of -2V DC potential for 4 hours each could not alter the coating behavior. Moreover the D sample displays two time constants in the phase angle indicating early

interfacial activity. The influence of DC in reducing the coating barrier properties was observed in subsequent cycles with a drop in |Z| (-4V 3rd cycle and -6V 3rd cycle), indicating the influence of the more negative DC potential in degrading the D sample. Cycle 10 corresponds to the first cycle with -8 volts for 4 hours. During cycle 10, the sample failed completely as can be observed in Figure 3.3a and 3.3b. Coatings with an impedance modulus value of $<10^6$ Ωcm^2 has been suggested as a criterion for coating failure by many other researchers.[9, 28-31].
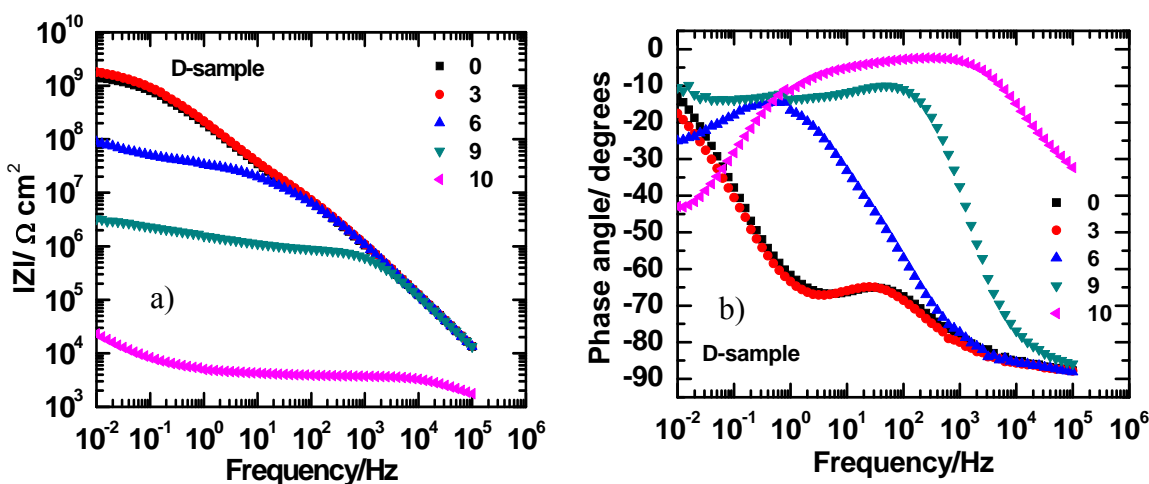
Figure 3.3: a) Bode modulus (left) and b) phase angle (right) representations of the EIS data associated with the testing step for D-sample.
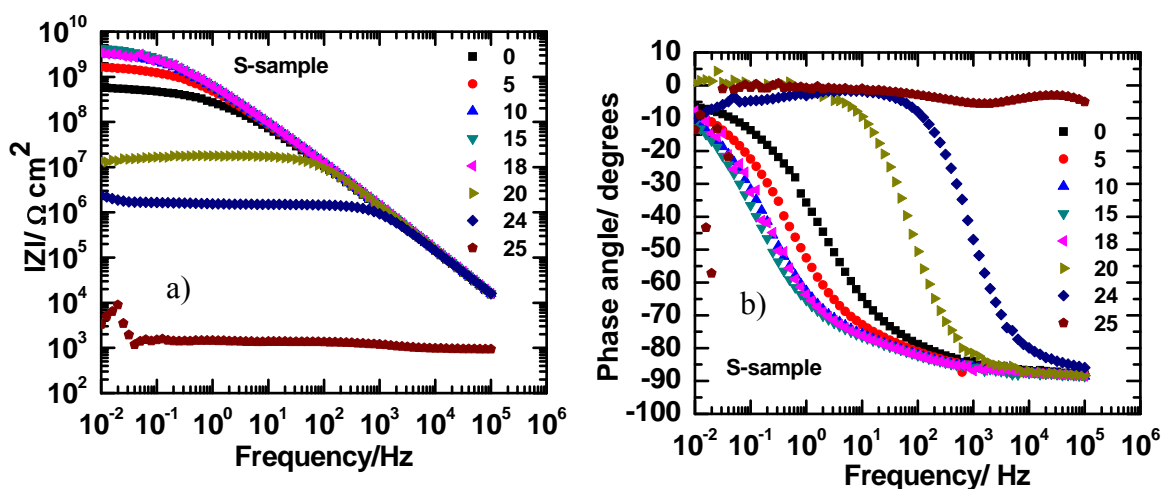
Figure 3.4: a) Bode modulus (left) and b) phase angle (right) representations of the EIS data associated with the testing step for S-sample.

In contrast to the D sample, the S sample displays better barrier performance, as observed by the higher |Z|. Compared to cycle 0 an increase in the low frequency impedance value is observed up to cycle 18. This can be attributed most likely to continued curing of the film. The presence of corrosion inhibitor could also increase the impedance.[9, 32-34] After cycle 18 a gradual reduction in the impedance value and a shift from the capacitive to more resistive behavior is observed indicating higher dielectric loss. On cycle 25 the sample fails. Overall it can be observed that the D sample failed earlier than the S sample in the AC-DC-AC cycling protocol.

3.3.2. Low frequency modulus barrier property

A measure of the barrier properties of an organic coating is the DC resistance of the coating, which is approximately measured by the low frequency modulus of impedance from EIS data.[28, 35] In this work |Z| value at 0.01Hz was used as an approximation to the DC limit and a measure of the barrier properties of the coating system. Figure 3.5a and 3.5b compares D-sample and S-sample with their control samples, D-control and S-control respectively. The control samples did not undergo any DC cycling, but were under continuous immersion throughout the experiment. EIS measurements were performed on the control samples at regular intervals. As observed from Figure 3.5a, the low frequency impedance values remained almost unchanged for D-control, whereas the D-sample showed reduced barrier properties due to the application of DC potential. A reduction in the $|Z|_{0.01Hz}$ value after cycle 5 was observed, suggesting the impact of DC polarization on the barrier performance of the D-sample.

In contrast to the D-sample, the S-sample displayed a different trend as shown in Figure 3.5b. The low frequency modulus for both the S-sample and S-control were almost

similar and kept on increasing after every cycle suggesting an enhancement in the barrier performance after each cycle. Only after cycle 18 a decrease in the $|Z|_{0.01Hz}$ was observed. The increase in the barrier property could be attributed to continued curing of the coating or the inhibitor in the primer. The value for S-control remained high throughout the experiment. When compared with the D-sample, the S-sample withstood larger stress and more stress cycles and displayed a better barrier performance.
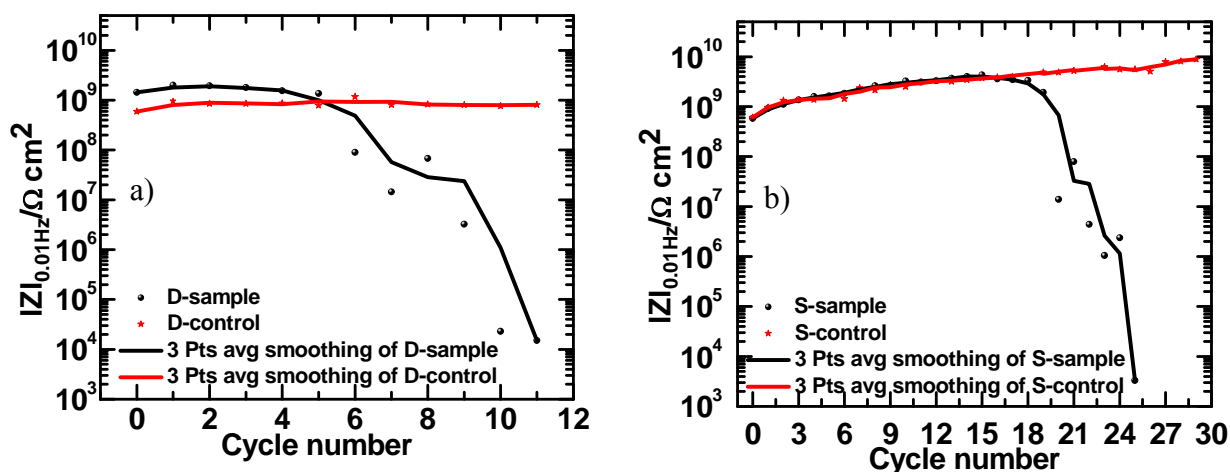
Figure 3.5: Low frequency modulus, $|Z|_{0.01Hz}$, as a function of cycle number for the a) D-sample and D-control and b) S-sample and S-control system. The controls were unstressed samples in continuous immersion.

3.3.3. Current density measurement

A current density measurement during the DC polarization step was performed to help describe the coating performance. The application of the DC potential was aimed to force electrochemical reaction at the metal-coating interface. Hence a change in current density during DC step is to be expected. An increase in current density will suggest enhanced electrochemical activity such as corrosion at the metal-coating interface and a degraded coating. The current density of D-sample as shown in Figure 3.6 is in the range of 10^{-8} to 10^{-9} Acm^{-2} up to cycle 6. However a sharp increase in its value was observed after cycle 6 indicating increased electrochemical activity at the interface. This value increases

constantly until the sample fails. Similar behavior was observed for S-sample. Value of around 10^{-9} Acm^{-2} was observed up to cycle 22. The current density increases monotonically with each polarization cycle until sample failure. These data indicate that current density measurements can also indicate the state of coating after the test cycling.
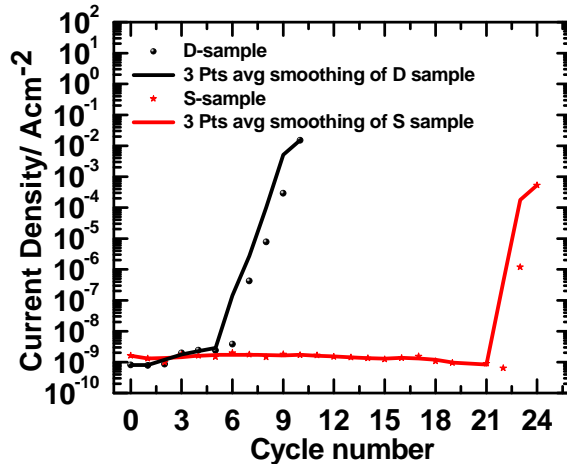
Figure 3.6: Measured current density as a function of cycle number for the D-sample and S-sample that were exposed to the AC-DC-AC procedure.

3.4. Correlation study of coating failure to the total charge induced to the coating during the DC polarization step

In the AC-DC-AC test protocol results, the D-sample failed earlier than the S-sample. Therefore the D-sample was used for further investigation of the total charge correlation to coating failure as this sample should require less time to failure. In this investigation two sets of D-samples were treated separately to AC-DC-AC procedure. Four panels from first set, labeled as set-1, with approximate thicknesses of 55-60μm were subjected to -1V, -2V, -3V and -4V for four hours each respectively (during the DC step of the AC-DC–AC cycle) until failure whereas five panels from the second set, labeled as set-2, were subjected to -1V, -2V, -4V, -5V and -6V for two hours each until failure. The thicknesses of the second set of panels were approximately 70-75 μm.

3.4.1. Results from first set

Figure 3.7a-d depicts the Bode plots for set-1 D-samples subjected to -1V, -2V, -3V and -4V respectively. The DC was applied for 4 hours for all the samples with a relaxation period of 24 hour. The coating failure criteria we used here was again the low frequency impedance, $|Z|_{0.01Hz}$ falling below $10^6 \Omega cm^2$. From the figures it was observed that failure is gradual for samples subjected to low applied DC (-2V, -3V) whereas at -4V failure is fairly rapid. Sample subjected to -1V cycling did not fail during the duration of the experiment as determined by EIS.
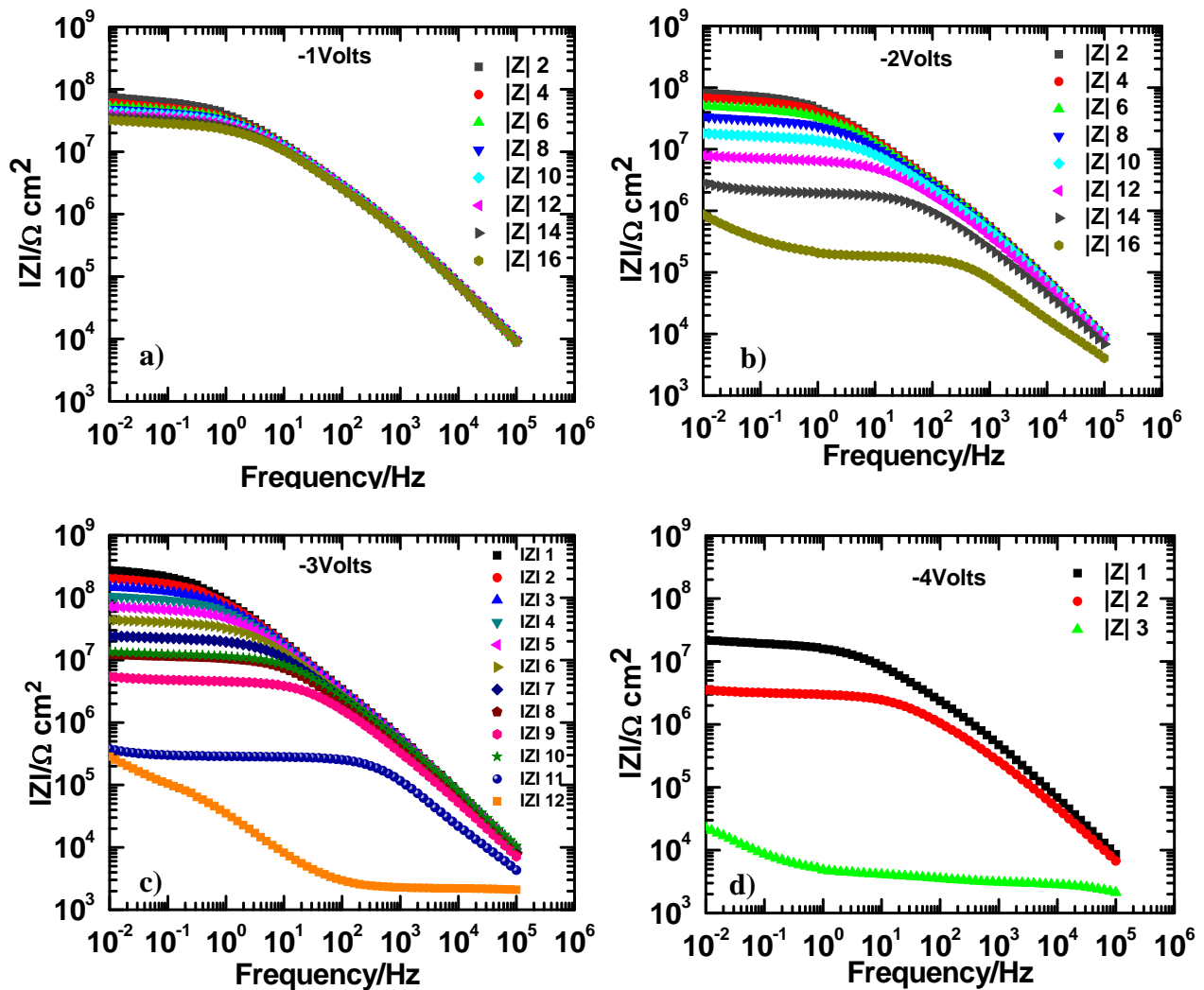
Figure 3.7: EIS Bode plots of set-1 samples subjected to a) -1V b) -2V c) -3V and d) -4V.

Figure 3.8 is the low frequency impedance or the barrier plot depicting the resistance of the coating at 0.01 Hz. The sample treated with -4 volt fails almost instantly after 2 DC cycles whereas the sample treated with -1 volt did not fail at all during the duration of the experiment. The sample treated with -2 volts fails after cycle 15 whereas sample treated with -3 volt fails after cycle 10. The order of the cycle to failure is -1V (did not fail) > -2V (15 cycles) > -3V (10 cycles) > -4V (2 cycles).
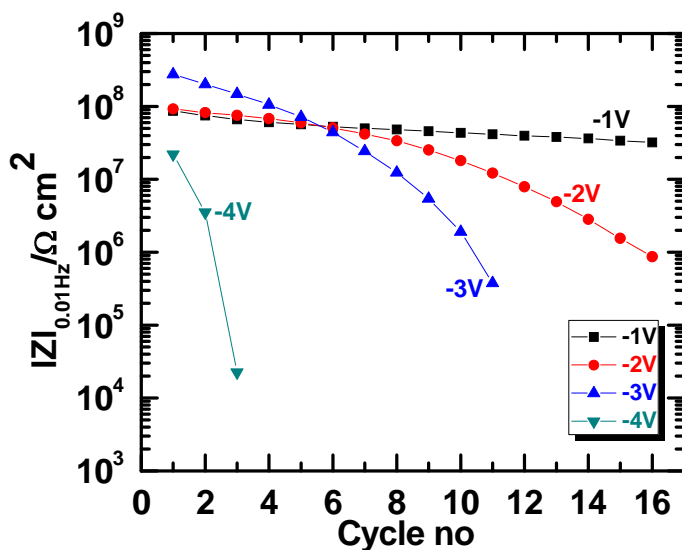
Figure 3.8: Plot of $|Z|_{0.01Hz}$ for all samples of set-1 subjected to -1V, -2V, -3V and -4V during the DC Cathodic polarization step.

Figure 3.9: Total charge passed through the coating film before coating failure as a function of applied DC voltage for set-1 samples subjected to -1V, -2V, -3V and -4V.

Figure 3.9 is a plot of total charge before sample failure as a function of applied DC. The current-time plot obtained at each DC step of the AC-DC-AC cycle was integrated and the charge obtained therein was added until sample failure. Only the current-time plot corresponding to the intact coating was considered and this was verified by the EIS plot succeeding the DC step. $|Z|_{0.01Hz} > 10^6 \Omega cm^2$ was set as the criteria for the coating in the protective range. Therefore, based on EIS prior to the DC step, the total amount of charge corresponding to the coating in the protective region was considered. It was observed that a similar amount of charge was necessary for sample failure independent of the applied DC stress. This can be observed in Figure 3.9. The sample treated with -2V,-3V and -4V all required similar charges before coating failure whereas the sample treated with -1 volt showed slightly lower total charge passed across the film compared to the others, and did not fail up to the time of experiment. This also suggests that by continuing the DC cycle and inducing more charge transfer across the metal coating interface, failure could have been induced in the sample subjected to -1V.

3.4.2. Results from the second set of experiment

Figure 3.10 a-e depicts the Bode plots of the set-2 D-samples subjected to -1V, -2V, -4V, -5V and -6V of the second set of this experiment. The DC was applied for 2 hours for all the samples with a relaxation period of 4 hour. As can be observed from the figures, -1V induced slow and gradual failure whereas -6V induced rapid failure only after the first DC cycle. It took 67 cycles for the coating to fail under -1V, 17 cycles under -2V, 7 cycles under -4V and just 2 DC cycle under -6V. It is also observed that for sample stressed with -1V and -2V the low frequency impedance reaches $\sim 10^6 \Omega cm^2$ before failure. However for samples stressed with the more negative potentials failure was more rapid. Sample stressed

90

with one cycle of -4 volts had $|Z|_{0.01Hz}$ values drop to $\sim 10^7 \Omega cm^2$ and failed in the next DC

cycle. Similarly sample stressed with -6 volts went below the $10^6 \Omega cm^2$ failure value in one

cycle.
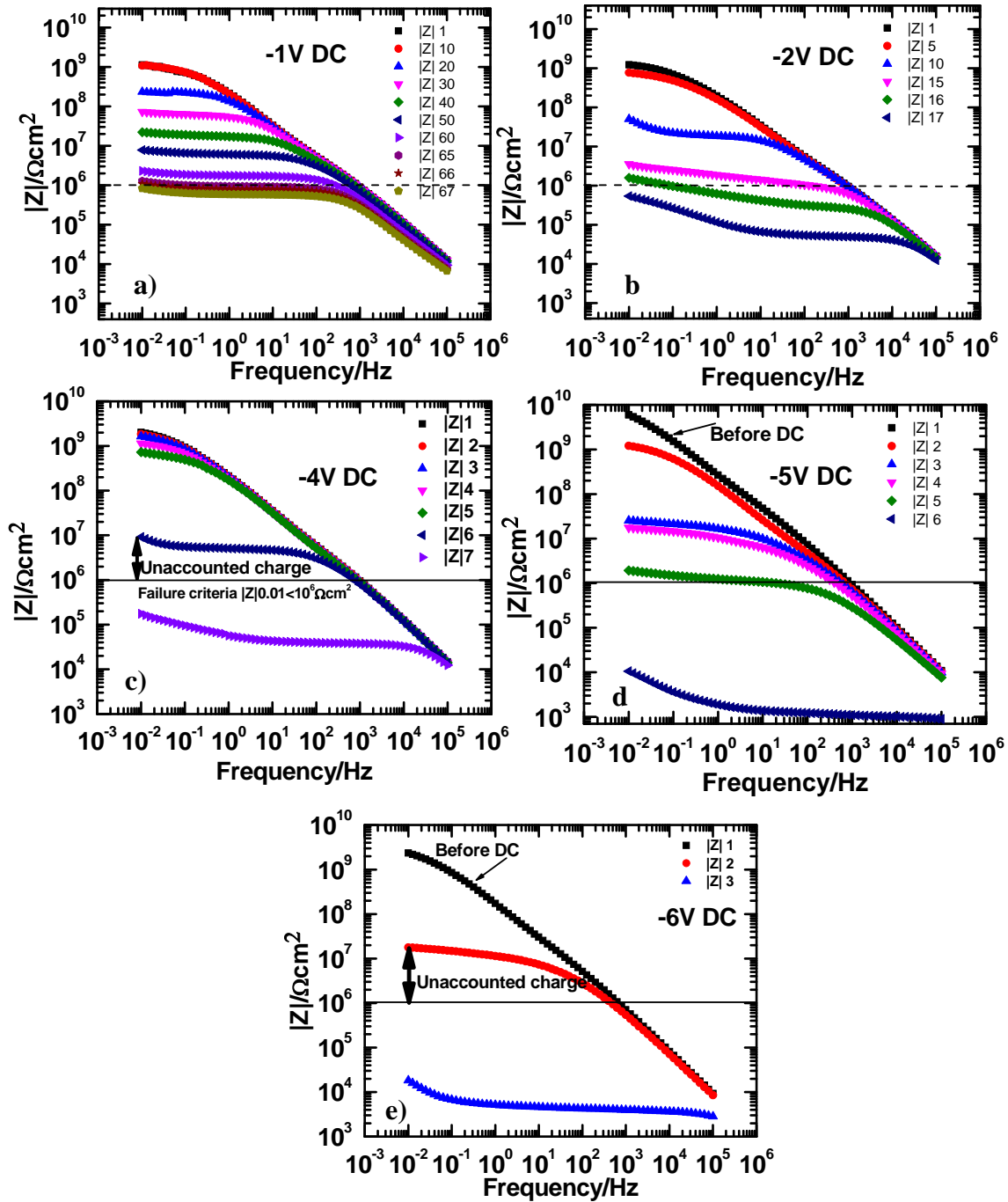
Figure 3.10: EIS Bode plot of set-2 samples subjected to a) -1V b) -2V c) -4V d) -5V and e) -6V during DC polarization.
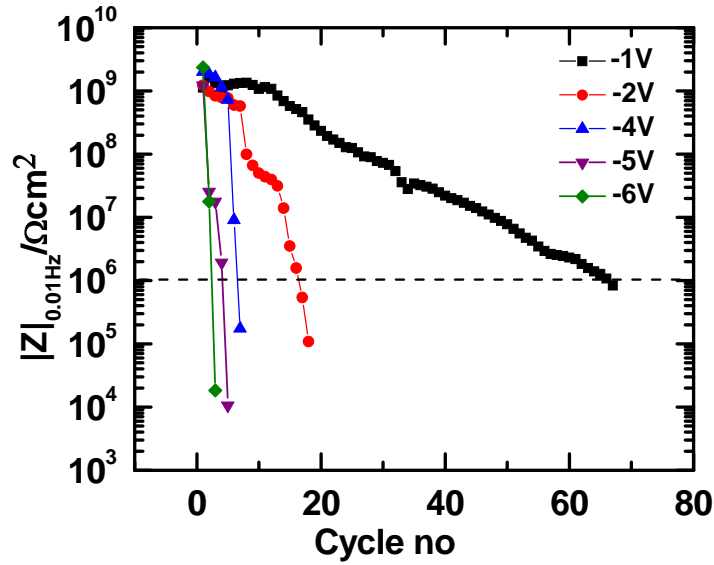
Figure 3.11: Plot of $|Z|_{0.01Hz}$ for all samples of set-2, subjected to -1V, -2V, -4V, -5V and -6V, during the DC cathodic polarization step.
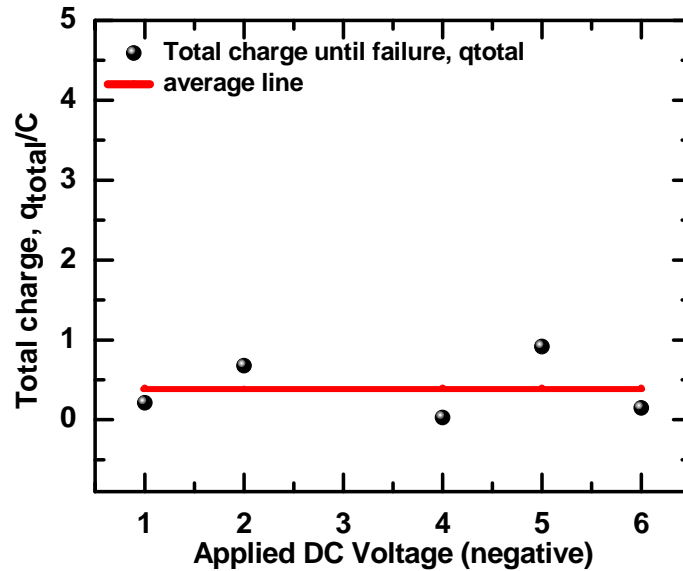
Figure 3.12: Total charge before coating failure as a function of applied DC voltage for set-2 samples subjected to -1V, -2V, -4V,-5V and -6V.

Figure 3.12 depicts the total charge as a function of applied DC voltage for set-2 D-samples. The area of all the studied samples was constant. It was observed that the total charge before coating failure displays values that almost show a linear trend and independent of the applied DC voltage. The fluctuations in the values can perhaps be

92

attributed to the unaccounted charge during the charge summation. For instance for sample stressed to -6V, charge was summed only for the first DC cycles. The subsequent DC fails the coating displaying very low impedance and hence the charge required for coating to reach $10^6 \Omega cm^2$ from $10^7 \Omega cm^2$ could not be measured and was unaccounted. The charge was counted only to the point where the coating impedance reached $\sim 10^7 \Omega cm^2$. Similar is the case with sample stressed with -4 and -5 volts. However a near constancy of total charge is observed in the Figure 3.12 indicating the possible relation of coating failure requiring a fixed total charge transfer, independent of the applied DC.

3.4.3. Further verification using third set of measurements

To further verify the total charge to coating failure correlation a third random approach was undertaken on set-3 D-samples that were 80±5μm thick. In this approach the time during the AC-DC-AC cycle was manipulated such that the coating reaches $10^6 \Omega cm^2$ before it fails so that total charge up to the point where the coating reaches $10^6 \Omega cm^2$ could be measured and a better correlation of total charge to coating failure can be made. The DC parameters used for this experiments were -8V for 30 minute and 15 minutes relaxation, -7V for 1 hour with 30 minute relaxation, -5V for 30 minutes with 15 minutes relaxation, -4V for 30 minutes with 15 minutes relaxation, -3V for 1 hour with 15 minutes relaxation, -2V for 2 hours with 15 minutes relaxation and -1V for 24 hours with 15 minutes relaxation. As can be observed from the low frequency impedance plot of Figure 3.13, all the coatings reached $|Z|_{0.01Hz}$ of $10^6 \Omega cm^2$ before they failed and the total charge up to their preceding DC step was obtained.
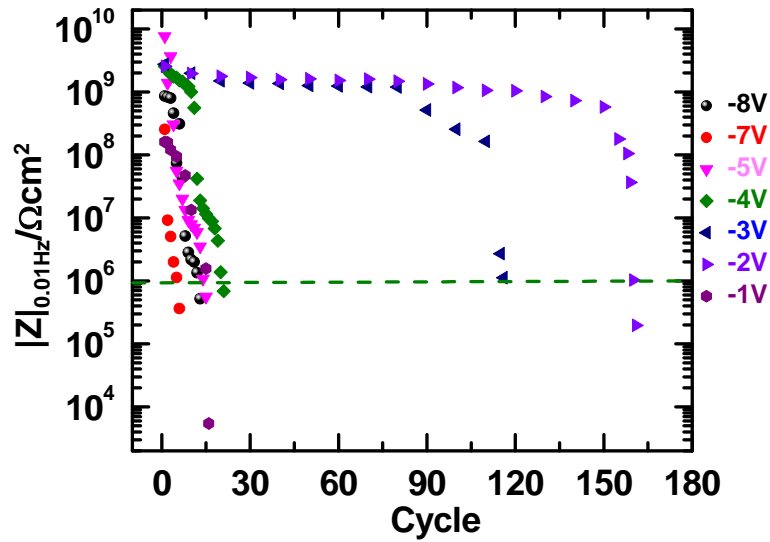
Figure 3.13: Plot of $|Z|_{0.01Hz}$ for all set-3 D-samples subjected to -1V, -2V, -3V, -4V, -5V, -7V and -8V during the DC cathodic polarization step.
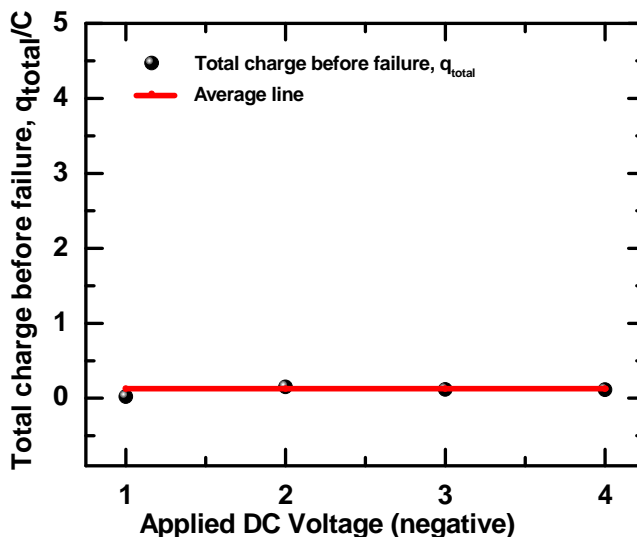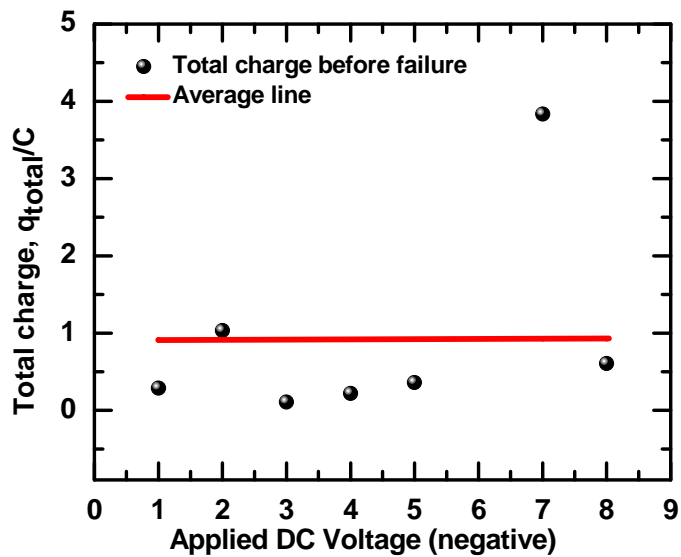

Figure 3.14: Total charge before coating failure as a function of applied DC voltage for set-3 samples subjected to -1V, -2V, -3V, -4V, -5V, -7V and -8V.

Figure 3.14 displays total charge before coating failure for set-3 samples as a function of applied DC polarization. An almost constancy in the plot of total charge to failure is obtained that is independent of the applied DC. This further reinforce our earlier findings with set-1 and set-2 that the failure induced in coating is a function of total

94

induced charge at the metal-coating interface and is independent of the potential that is applied during DC. The effect of higher DC polarization is to induce quicker failure but it seems that the total amount of charge passed across the coating substrate interface determines the coating failure under these conditions of cathodic polarization.

3.5. Conclusions

As an extension to the previous work done on AC-DC-AC method, used to characterize coatings, this chapter focused on extracting new information from this method. In this work, AC-DC-AC method was used to discriminate different primers and to investigate the possible correlation between coating failure and total charge induced to the coating during DC polarization step of AC-DC-AC cycle. It was observed that for failure the coating requires a certain amount of charge, independent of whether the charge was induced via higher DC polarization or low DC polarization. Independent of the applied DC polarization the total amount of charge at failure is constant. This was observed for the three trials performed to examine this hypothesis.

3.6. References

[1] G.H. Koch, M.P.H. Brongers, N.G. Thompson, Y.P. Virmani, J.H. Payer, Corrosion Cost and Preventive Strategies in the United States (Report No. FHWA-RD-01-156), CC Technologies Laboratories, Inc.,/NACE International, Dublin, OH/Houston, TX, (2001).

[2] G. Bierwagen, D. Tallman, J. Li, L. He, C. Jeffcoate, EIS studies of coated metals in accelerated exposure, Progress in Organic Coatings, 46 (2003) 149-158.

[3] G.P. Bierwagen, L. He, J. Li, L. Ellingson, D. Tallman, Studies of a new accelerated evaluation method for coating corrosion resistance--thermal cycling testing, Progress in organic Coatings, 39 (2000) 67-78.

[4] A. Miszczyk, K. Darowicki, Accelerated ageing of organic coating systems by thermal treatment, Corrosion Science, 43 (2001) 1337-1343.

[5] A. Miszczyk, K. Darowicki, Effect of environmental temperature variations on protective properties of organic coatings, Progress in Organic Coatings, 46 (2003) 49-54.

[6] L. Fedrizzi, A. Bergo, F. Deflorian, L. Valentinelli, Assessment of protective properties of organic coatings by thermal cycling, Progress in Organic Coatings, 48 (2003) 271-280.

[7] G.P. Bierwagen, K.N. Allahar, Q. Su, V.J. Gelling, Electrochemically characterizing the ac-dc-ac accelerated test method using embedded electrodes, Corrosion Science, 51 (2009) 95-101.

[8] J. Hollaender, Rapid assessment of food/package interactions by electrochemical impedance spectroscopy (EIS), Food Additives and Contaminants, 14 (1997) 617 - 626.

[9] M. Bethencourt, F.J. Botana, M.J. Cano, R.M. Osuna, M. Marcos, Lifetime prediction of waterborne acrylic paints with the AC-DC-AC method, Progress in Organic Coatings, 49 (2004) 275-281.

[10] M. Poelman, M.G. Olivier, N. Gayarre, J.P. Petitjean, Electrochemical study of different ageing tests for the evaluation of a cataphoretic epoxy primer on aluminium, Progress in Organic Coatings, 54 (2005) 55-62.

[11] S.J. García, J. Suay, Anticorrosive properties of an epoxy-Meldrum acid cured system catalyzed by erbium III trifluromethanesulfonate, Progress in Organic Coatings, 57 (2006) 319-331.

[12] K.N. Allahar, G.P. Bierwagen, V.J. Gelling, Understanding ac-dc-ac accelerated test results, Corrosion Science, 52 1106-1114.

[13] S.J. García, J. Suay, A comparative study between the results of different electrochemical techniques (EIS and AC/DC/AC): Application to the optimisation of the cataphoretic and curing parameters of a primer for the automotive industry, Progress in Organic Coatings, 59 (2007) 251-258.

[14] M.T. Rodríguez, J.J. Gracenea, S.J. García, J.J. Saura, J.J. Suay, Testing the influence of the plasticizers addition on the anticorrosive properties of an epoxy primer by means of electrochemical techniques, Progress in Organic Coatings, 50 (2004) 123-131.

[15] J. Castle, J. Watts, Cathodic Disbondment of Well Characterized Steel/Coating Interfaces, Corrosion Control by Organic Coatings. Ed H. Leidheiser Jr, (1981) 78-86.

[16] J. Ritter, Ellipsometric studies on the cathodic delamination of organic coatings on iron and steel, J. Coat. Technol., 54 (1982) 51-57.

[17] D. Greenfield, J.D. Scantlebury, Blistering and Delamination Processes on Coated Steel, Journal of Corrosion Science and Engineering, 2 (2000).

[18] K.N. Allahar, V. Upadhyay, G.P. Bierwagen, Characterizing the Relaxation of the Open-Circuit Potential during an AC-DC-AC Accelerated Test, CORROSION, 66 095001-095011.

[19] K.N. Allahar, V. Upadhyay, G.P. Bierwagen, Characterizing the Relaxation of the Open-Circuit Potential during an AC-DC-AC Accelerated Test, Corrosion, 66 (2010) 095001.

[20] E.L. J. Hollaender, S. Hillebrand, Proceedings of the Fifth International Tinplate Conference,London, (1992) 300.

[21] K.N. Allahar, G.P. Bierwagen, V.J. Gelling, Understanding ac-dc-ac accelerated test results, Corrosion Science, 52 (2010) 1106-1114.

[22] Q.S. K. N. Allahar, G. P. Bierwagen, and D. H. Lee, Monitoring of the AC-DC-AC Degradation of Organic Coatings Using Embedded Electrodes, Corrosion, 64 (2008) 773.

[23] H. Duan, K. Du, C. Yan, F. Wang, Electrochemical corrosion behavior of composite coatings of sealed MAO film on magnesium alloy AZ91D, Electrochimica Acta, 51 (2006) 2898-2908.

[24] J.N. Murray, Electrochemical test methods for evaluating organic coatings on metals: an update. Part I. Introduction and generalities regarding electrochemical testing of organic coatings, Progress in Organic Coatings, 30 (1997) 225-233.

[25] B.R. Hinderliter, S.G. Croll, D.E. Tallman, Q. Su, G.P. Bierwagen, Interpretation of EIS data from accelerated exposure of coated metals based on modeling of coating physical properties, Electrochimica Acta, 51 (2006) 4505-4515.

[26] F. Mansfeld, Models for the impedance behavior of protective coatings and cases of localized corrosion, Electrochimica Acta, 38 (1993) 1891-1897.

[27] F. Deflorian, L. Fedrizzi, Adhesion characterization of protective organic coatings by electrochemical impedance spectroscopy, Journal of adhesion science and technology, 13 (1999) 629-645.

[28] R.C. Bacon, J.J. Smith, F.M. Rugg, Electrolytic resistance in evaluating protective merit of coatings on metals, Industrial & Engineering Chemistry, 40 (1948) 161-167.

[29] J.M. McIntyre, H.Q. Pham, Electrochemical impedance spectroscopy; a tool for organic coatings optimizations, Progress in Organic Coatings, 27 (1996) 201-207.

[30] G.P. Bierwagen, L. He, J. Li, L. Ellingson, D.E. Tallman, Studies of a new accelerated evaluation method for coating corrosion resistance -- thermal cycling testing, Progress in Organic Coatings, 39 (2000) 67-78.

[31] D. Greenfield, D. Scantlebury, The protective action of organic coatings on steel: a review, Journal of Corrosion Science & Engineering, 3 (2002) 2000-2002.

[32] M.L. Zheludkevich, K.A. Yasakau, A.C. Bastos, O.V. Karavai, M.G.S. Ferreira, On the application of electrochemical impedance spectroscopy to study the self-healing properties of protective coatings, Electrochemistry Communications, 9 (2007) 2622-2628.

[33] I. Thompson, D. Campbell, Interpreting Nyquist responses from defective coatings on steel substrates, Corrosion Science, 36 (1994) 187-198.

[34] R.C. Barik, J.A. Wharton, R.J.K. Wood, K.R. Stokes, R.L. Jones, Corrosion, erosion and erosion-corrosion performance of plasma electrolytic oxidation (PEO) deposited Al2O3 coatings, Surface and Coatings Technology, 199 (2005) 158-167.

[35] Q. Su, K.N. Allahar, G.P. Bierwagen, Application of embedded sensors in the thermal cycling of organic coatings, Corrosion Science, 50 (2008) 2381-2389.

CHAPTER 4. ENVIRONMENTAL HUMIDITY INFLUENCE ON A TOPCOAT/MG-RICH PRIMER SYSTEM WITH EMBEDDED ELECTRODES

4.1. Introduction

Among the engineering metals, magnesium (Mg) is the lightest and is easily corroded/oxidized. It has a standard electrode potential of -2.37V (vs. SHE) and oxidizes readily in aqueous solutions. This high reactivity of magnesium has hindered its application as structural backbone material despite its high strength to weight ratio. However, its readily corroding nature has been wisely innovated by employing it as sacrificial anodes for structures such as underground pipelines, ships and tanks.[1-5]

The concept of using metallic pigments sacrificial anodes in coating is quite old. Zinc (Zn) rich primers have been used to protect steel substrate since 1940s.[6-11] However, the protection of Aluminum (Al) substrate by sacrificial means was not seriously considered until recently.[12] Al alloys are widely used in aerospace structural frames and their current coating system consists of chromates in primers (hexavalent chromium, $SrCrO_4$) and in pretreatments. Zn cannot be used to sacrificially protect Al since Zn is more positive ($E_{Zn^{2+}/Zn}$=-0.76V vs. SHE) compared to Al ($E_{Al^{3+}/Al}$=-1.67V vs. SHE) and would itself be protected instead of providing sacrificial protection to Al. Therefore the use of Zn as sacrificial pigment has been mostly limited to ferrous substrates.

Recently work at NDSU successfully demonstrated that the protection of Al can be achieved by employing Mg particles as sacrificial pigment in primer.[12, 13] This work demonstrated for the first time the use of Mg particles as sacrificial pigments in primers in an effort to replace the highly effective but carcinogenic hexavalent chromate containing primers that is currently in use for the protection of aerospace Al alloys. Unlike chromates

which act as corrosion inhibitor[14, 15], Mg-rich coatings act as a sacrificial primer and can be used in a manner analogous to Zn-rich primers over steel. It was observed that Mg based primers formulated near its CPVC provided sacrificial cathodic protection to Al AA2024-T3 alloys and performed excellently in Prohesion testing. Later studies by Battocchi et al.[16, 17] reinforced the feasibility of Mg rich primers in protecting AA-2024 as well as AA-7075. Battocchi et al. have attributed the protection afforded by Mg based primer to both sacrificial as well as barrier means. The porous $Mg(OH)_2$ formed at higher pH can also inhibit corrosion by barrier mechanism.

Conventional coating evaluation methods include the widely used salt fog ASTM B117 that consists of exposing the coated panel to a continuous fog of 5 wt. % NaCl at $35^{o}C$. Another evaluation method is the ASTM G-85, also known as the Prohesion test, in which the coated samples are exposed to a cyclic wet and dry environment for 1 hour each. The wet cycle exposes the test sample to a fog of dilute Harrison's solution (0.05 wt. % NaCl and 0.35 wt. % $(NH_4)_2SO_4$ at pH 5.0-5.4) at $25^{o}C$ whereas in the dry cycle the panels are dried in air at $35^{o}C$. Prohesion, QUV, prohesion/QUV test are also some other test methods used to study coatings performance. In addition most automotive companies have their own standard corrosion test.[18] For example General Motors uses GMW14872 as one of their standard test protocol for cyclic corrosion test whereas Ford uses Ford APGE. The Society of Automotive Engineer (SAE) recommends SAE J2334 as their standard cyclic corrosion test.

All of these methods are based on the assumption that ions, electrolytes and oxygen are required at the metal coating interface to cause corrosion, and high temperature will increase the transport rates through the coating film to cause accelerated coating

degradation/corrosion. These tests usually exceed normal ambient condition exposure. These exposure test methods mainly rely on visual inspection for ranking the corrosion protective performance of the coating. Very often the simulated environment provided by the laboratory testing conditions are different than the real world exposure conditions and the coating might fail earlier than predicted by conventional tests methods, or may provide different results.[19] Therefore real time coating monitoring in-situ is the best approach to verify the state of the coating-substrate system under protection. However locating defects /corrosion sites at the application site might be tedious and time consuming and require travel to the site for inspection. Further, such sites might be inaccessible without considerable intervention.

The use of sensors in coating is an efficient and improved approach to remotely monitor the performance of a coating system. Sensors can track the coating performance and detect changes in real time, and can also be used to perform electrochemical measurements of the coating system.[20] Embedded sensors can be designed as electrodes of a two electrode electrochemical system that acts as the counter and the pseudo reference electrode and are sandwiched between the layers of a two layered coating system.[20] Actual embeddable reference electrodes are also under study here at NDSU.[21] Advantages of such embedded sensors are that they show insignificant interference with the performance of topcoat/primer system and facilitate in-situ monitoring of electrochemical properties of primer/substrate system beneath topcoat. Coatings are not disturbed during measurement and the robust sensor configuration is not damaged by aggressive environment of exposure since they are protected by the top coat. As a result embedded sensors have tremendous potential for field application.

The uses of embedded sensors have been successfully studied at NDSU under immersion, Prohesion and QUV/Prohesion exposure conditions.[22-27] However information on the ability of sensor to track humidity change, to locate defects in coatings and their response to B117 exposure condition is not yet available. This chapter describes our investigation of the response of the sensors, embedded between Mg rich primer and topcoat, to changing humidity and their ability to distinguish a defect from a defect free region using EIS and ENM.

4.2. Experimental

The coating system used in this work comprised of an epoxy primer and a polyurethane topcoat. The substrate used was a large aluminum AA2024-T3 sheet with dimensions of 60 cm x 30 cm. The substrate was washed with de-ionized water and cleaned with n-hexane before the application of primer. The epoxy primer consisted of Epon 828 crosslinked with Epikure 3164, both procured from Hexion Specialty Chemicals™. An epoxy equivalent to amine hydrogen equivalent ratio of 1:1 was used. Xylene, procured from Sigma-Aldrich®, was the solvent used. The primer contained Mg particles (with a mean diameter of 20 μm) as pigments at 45% pigment volume concentration (PVC) and was supplied by Eckart GmBH, Germany. A brief description of the pigment is given in reference 12. The topcoat used was a 2-component polyurethane PU 03-GY-277 supplied by Deft. The primer was cured for a week at room temperature before the application of topcoat. Between the primer and the topcoat, standard thin Pt sensors were embedded. Both the primer and the topcoat were applied by air spray gun. The dry film thickness of the primer and topcoat were approximately 60μm and 40μm respectively. The back and the edges of the substrate was sealed as is standard procedure using plastic tape.

4.2.1. Sensor set up

After the primer was fully cured, six platinum leaves, approximately 130 nm thick designed as sensors, were adhered on the primer surface. These six sensors were designated as A, B, C, D, E and F respectively. The sensor leaves supported by tissue paper were cut into the designed sensor shape such that the surface area of the sensors was 2.56 cm^2 with the width of each side being 0.4 cm. A schematic of sensor diagram is depicted in Figure 4.1. The adherence of the sensor on the primer was facilitated by an epoxy resin. Epoxy resin D.E.R 331, Ancamide 2353 and methyl ethyl ketone were mixed in the ratio 5:3:5 by weight and a thin layer of the mixture were applied on the primer surfaces where the sensors were to be adhered. Sensors were then placed on top of the epoxy resin and gently pressed. They were adhered to the primer after solvent flash off and cure. The supporting tissue paper was then detached leaving the sensors adhered to the primer. The sensors were then soldered with a copper core electrical conducting wire so that they could be connected externally to the measuring instruments. Sealing of the conducting joint was performed using epoxy resin, D.E.R 331 and ancamide 2353 in the ratio 5:3 by weight. It was left for a day to harden. Topcoat was then applied by air spray such that sensors were embedded in between primer and the topcoat. A wire was also attached to the substrate to give substrate connection to the measuring instruments.
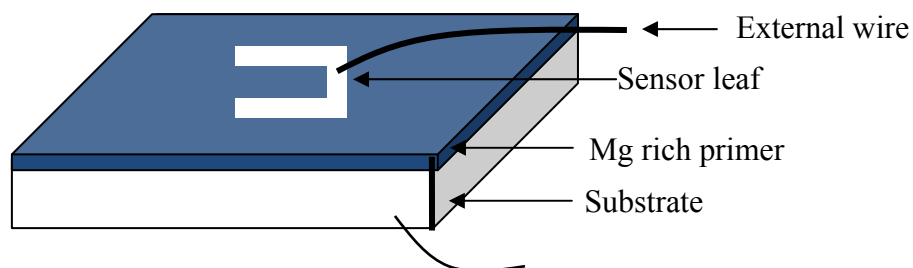
Figure 4.1: Schematic of sensor design.
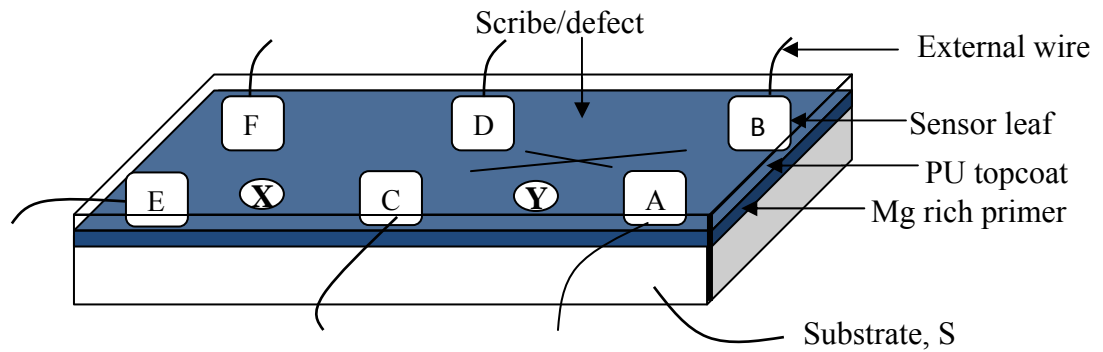
Figure 4.2: Schematic of sensors embedded between primer and topcoat, the scribed/defect region (ABCD), unscribed/intact region (CDEF) and points X and Y where 3-electrode EIS measurements were taken.

4.2.2. Experimental configuration

In-situ EIS measurements were performed using a two electrode setup, with one electrode acting as working electrode and the other electrode acting as counter/reference electrode respectively. However two different configurations were used. In one of the configurations, the substrate is the working electrode and the sensor is the counter/reference electrode (sensor configuration); whereas, in the other configuration, one of the sensors is the working electrode and the other sensor acts as counter/reference electrode respectively (dual configuration).[25] A Gamry Instrument R600 Potentiostat/ Galvanostat/ ZRA in conjunction with Gamry Framework Version 5.20/EIS 300 software was employed for the EIS measurements. The instrument and software were supplied by Gamry Instruments, Inc. of Willow Grove, PA. A frequency range of 0.1Hz to 100 kHz was used for the measurements with an acquisition rate of 10 points per decade. The amplitude of potential perturbation was 10mV with respect to the open circuit potential (OCP).

A configuration named reversed ENM method was used for in-situ ENM measurements.[25] Reversed ENM measurements were performed using two sensors as the

two working electrodes and substrate as the reference electrode. The noise resistance was obtained by dividing the standard deviation of the potential noise by the standard deviation of the current noise. Measurement was made for 15 minutes at a frequency of 5Hz. The first 180 seconds were cut off and the data points for 720 seconds were used. The original ENM data was divided into 7 blocks with each block having 512 points, which is 102.4 seconds of measurement. Therefore each R_n values reported are the averages of 512 data points (102.4 seconds). Moreover the R_n value was obtained after linear detrending of the original ENM data to remove the baseline current shift during the test.[28] Gamry Framework Version 4.21/ESA400 software and a Gamry PCI4/300 potentiostat supplied by Gamry Instruments, under zero resistance ammeters (ZRA) mode were used for the ENM measurements.

In order to monitor the OCP and the sacrificial protection performance of the Mg rich primer, *in-situ* conventional three electrode EIS measurements were performed on the test panel, one in the vicinity of the scribed region at a distance of ~7 cm from the scribe (mark Y in figure 4.2) and other at the unscribed/intact region (mark X in figure 4.2) of the test panel. The substrate was the working electrode, a Pt mesh was the counter electrode and SCE was used as the reference electrode. Perspex cylinders with a surface area of 7.07 cm^2 were mounted on the sample and were clamped with an O-ring insert to facilitate electrochemical measurement. Dilute Harrison's solution was the electrolyte used.

4.2.3. Testing procedure

Prior to the experimental data acquisition scribe (artificial defect) in the form of X was made inside the region ABCD such that the scribe was surrounded by the four sensors and the nearest distance of the scribe from the sensors was 7 cm. The other region CDEF

106

was unscribed, defect free region. The test panel was then placed inside glove box, #890-THC, supplied by Plas labs, Inc. of Lansing, MI, USA. The glove box is designed to control temperature and humidity. A very good control of humidity could be achieved inside the glove box to an accuracy of ±1%. Wires attached to sensors and the substrate was connected out of the glove box to the measurement site to facilitate in situ EIS and ENM experiments. The measuring instruments were placed outside the glove box and all the measurements were made externally.

EIS and ENM measurements were performed at humidity levels of 50%, 60%, 70%, 80% and 90 %. Figures 4.3a and 4.3b are the humidity controlling glove box and the substrate with sensors embedded between primer and topcoat respectively used for the experiment. The panel was exposed at each humidity level for three days prior to any EIS or ENM measurements. The variation of humidity was cyclic beginning with ascending order of 50% to 90% and then descending order of 90 % to 50 % and so on. After 75 days of exposure the sample was exposed for 5 days each in a particular humidity prior to EIS/ENM measurements with the exception at day 110. The 135 day duration of humidity exposure variation is shown in Figure 4.4. Each dot in the figure represents the day of EIS and ENM measurement. For the entire experimental period the temperature was maintained at 25°C. After day 90, scribe similar to the one between ABCD was introduced on the initially unscribed region, CDEF.
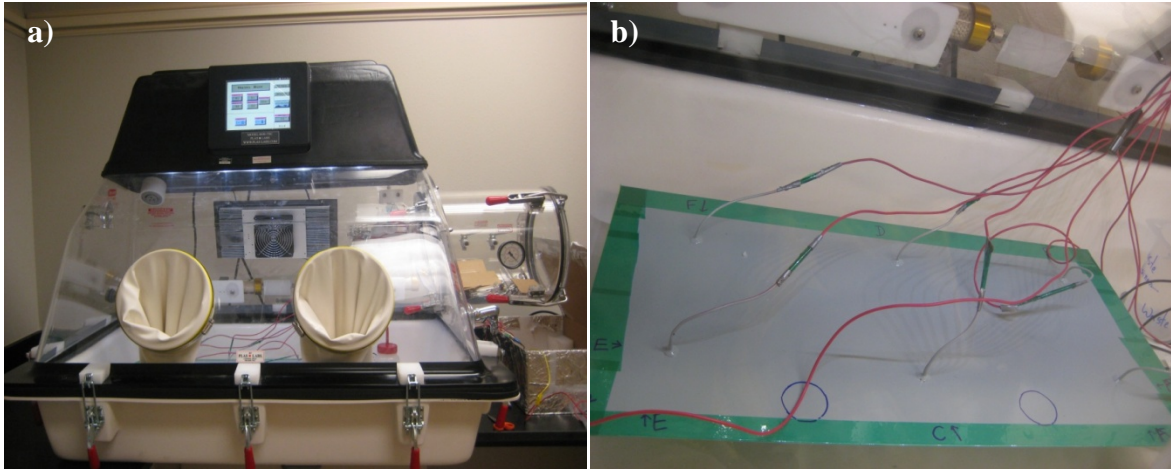
Figure 4.3: a) Humidity controlling glove box where the test panel was kept during the experiment and b) substrate with sensors embedded between primer and topcoat.
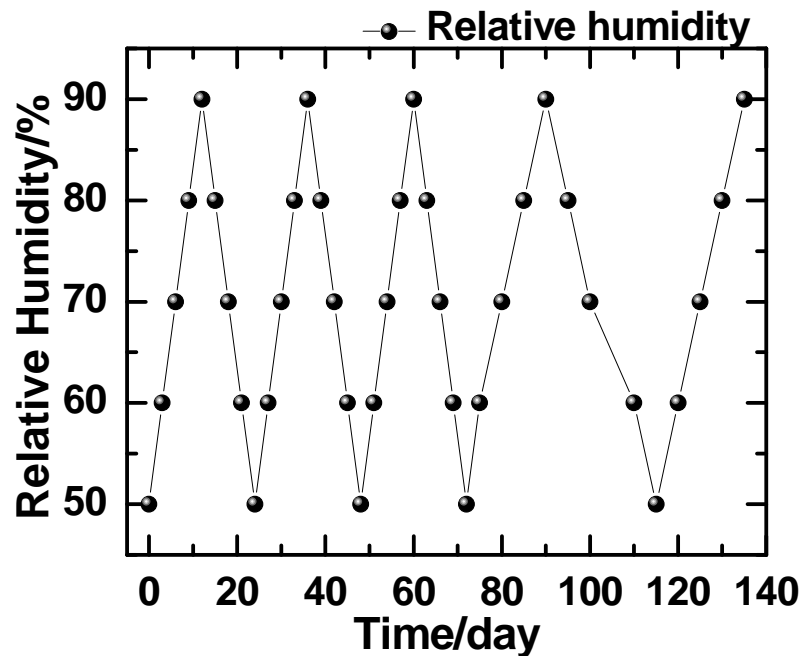
Figure 4.4: Variation of humidity as a function of time during the experiment. At each points EIS and ENM data were acquired.

4.3. Results and discussions

4.3.1. Open circuit potential (OCP)

The open circuit potential is an important parameter for monitoring the sacrificial effect of Mg pigments in primer. The OCP of magnesium in immersed DHS is ~ -1.8V (vs. SCE) whereas the OCP of the bare Al alloy (Al 2024) is ~ -0.5V (vs. SCE).[17] In this

work, the OCP measurements were performed in-situ at point X (a distance of 7 cm from the defect region) and point Y (intact region), as depicted in Figure 4.2, using a three electrode set up with the metal substrate as the working electrode, a Pt mesh as the counter electrode and a saturated calomel electrode as the reference electrode. DHS was the electrolyte used.
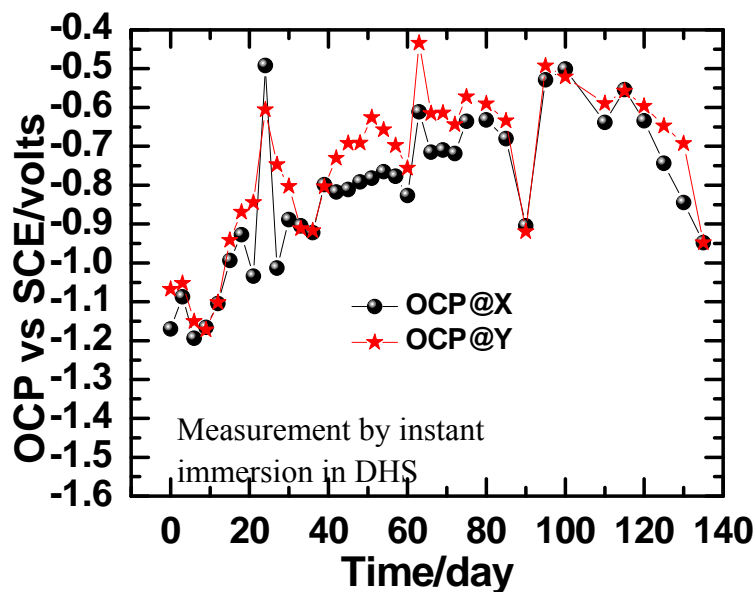
Figure 4.5: Evolution of OCP at the intact region (point X in figure 4.1) and scribed/defect region (point Y in figure 4.1) as a function of exposure time.

The open circuit potential value measured at the intact region (point X in figure 4.2) and in the vicinity of the scribed/defect region (point Y in figure 4.1) follows almost similar trend and displays a mixed potential value that is between the OCP of pure Al AA 2024 T3 alloy substrate and pure Mg.[17] This suggests that the substrate is cathodically polarized by Mg pigment particles throughout the duration of the experiment. Mg pigments particles are in electrical contact and are acting as sacrificial anode throughout the time of measurements. After day 100, gradual decrease in the OCP values were observed. This could probably be due to Mg oxide/hydroxide layer accumulating at the surface of Mg.

However, the OCP measured near the defect region was similar to the OCP measured at the intact region, indicating no influence of the defect on OCP.

4.3.2. EIS results

4.3.2.1. Sensor-substrate configuration

4.3.2.1.1. Low frequency EIS

The humidity was varied from 50% and above due to the fact that the average relative humidity in USA for the entire year is above 50% according to the National Oceanic and Atmospheric Administration (NOOA), United States Department of Commerce.[29] Therefore working at 50% RH and above seemed appropriate. A total of four and half cycles were run as observed from the Figure 4.6. They consisted of cycle 1 (1-24 days), cycle 2 (25-48 days), cycle 3 (49 to 72 days), cycle 4 (day 73 to day 115) and cycle 5 (day 116 to 135). The first four cycles consisted of relative humidity ranging from 50% to 90% and back to 50% whereas the fifth cycle had relative humidity from 50% to 90% only.
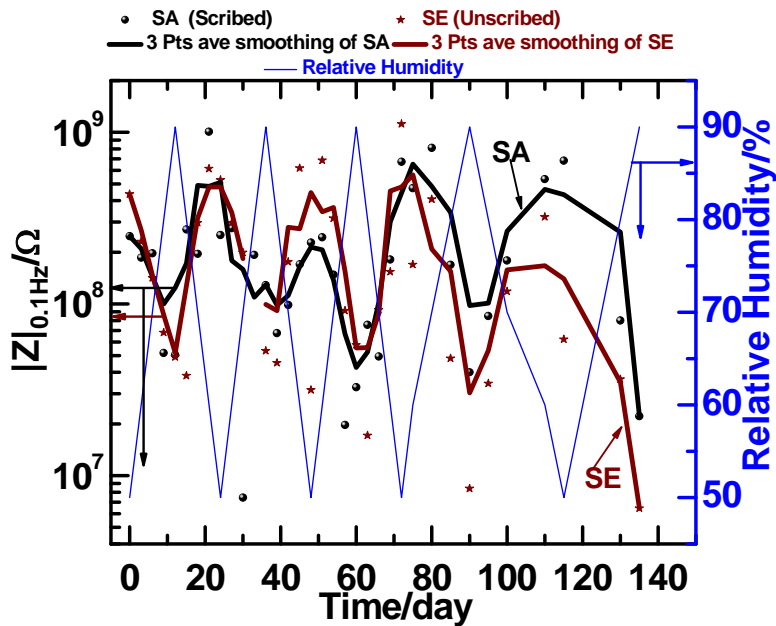
Figure 4.6: Low frequency impedance $|Z|_{0.1Hz}$ (left) and relative humidity (right) as a function of exposure time for SA and SE sensor-substrate configurations.

110
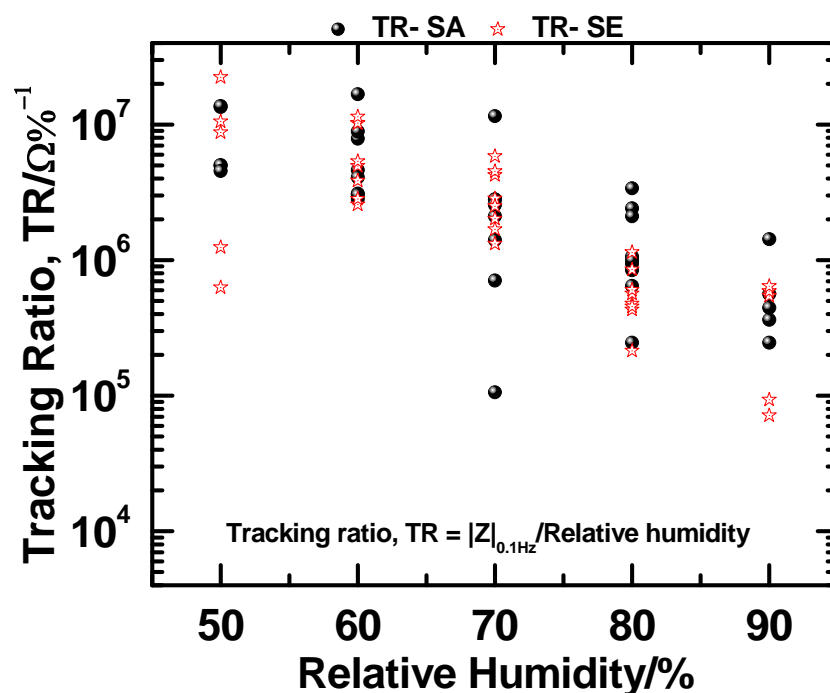
Figure 4.7: Tracking ratio, TR, defined by $|Z|_{0.1Hz}$/Relative Humidity (RH) as a function of Relative Humidity for SA and SE, sensor-substrate configurations.

As shown in the Figure 4.6 EIS measurement of the primer with the sensor-substrate configuration was possible at all the humidity levels. A clear correlation in the humidity level and the low frequency impedance $|Z|_{0.1Hz}$ of the primer is observed. The impedance values varied depending on the relative humidity the panel was exposed to during the time of measurements. Measurements using both the sensor-substrate configurations, SA and SE responded to humidity changes with higher humidity resulting in lower impedance and vice versa, respectively. Minor unexpected behaviors were also observed for both of them. For instance during cycle 1 (day 0-24), SA displayed maximum impedance at 60% RH whereas SE displayed lowest impedance at 80%. During cycle 2 day 30 SA displayed lower impedance at 70% RH whereas SE displayed impedance greater than 10^{12} Ω cm^2 at day 33 (80% RH, removed considering it as a bad data) and at day 45(50% RH) it displayed much lower impedance. Cycle 3, 4 and 5 also had some minor

erratic impedance observation. Smoothing of the acquired data was performed to obtain trend in the data using 3 points average smoothing for both SA and SE measurements. It is observed that a trend consistent with the humidity is observed. Higher humidity resulted in low impedance and vice versa. Overall, the trend in the $|Z|_{0.1Hz}$ was inversely related to the humidity variation. This is also further verified by the plot of tracking ratio, TR, given by $|Z|_{0.01HZ}$/RH as a function of humidity, as shown in figure 4.7. The plot displays higher TR values at low humidity and vice versa.

4.3.2.1.2. High frequency capacitance

The capacitance of a coating can be written as C =$\varepsilon\varepsilon_o$A /d, where ε is the dielectric of the coating, ε_o is the dielectric of vacuum, A is the area and d is the coating thickness.[30-32]Changes in these properties will change the capacitance of the coating. Epoxy films have a dielectric constant of around 2-4 whereas the dielectric constant of water is around 80 at room temperature.[33, 34] Therefore depending upon the amount of water absorbed by the coating the dielectric of the coating will also increase, thereby increasing its capacitance. This is manifested as an increase in the imaginary impedance during EIS measurement since capacitance is related to the imaginary impedance according to equation 1.25. The imaginary (out of phase) impedance value corresponding to the frequency of 10 kHz was used to calculate and obtain the capacitance plot of Figure 4.7. A frequency of 10 kHz is often used for capacitance measurement,[35, 36] since the response of coating to EIS at high frequency is dominated by capacitive behavior.
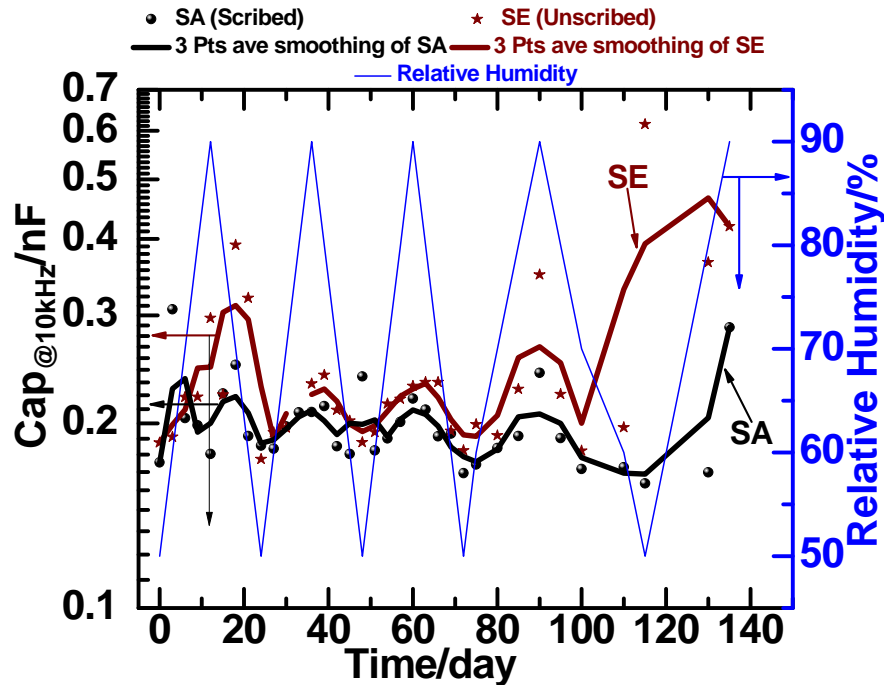
Figure 4.8: Capacitance at 10 kHz (left) and relative humidity (right) as a function of exposure time for SA and SE configuration.

The plot observed in Figure 4.7 reveals that the capacitance profile for measurements made with both the SA and SE configuration, mostly, resembles the relative humidity profile, with increase in humidity resulting in an increase in capacitance and vice versa. Cycle 1 (day 0-24) for both the SA and SE however displayed few erratic behavior. Capacitance of SA at 70-90% humidity (day 6-12) displayed lower capacitance value. Barring first cycle, the capacitance behavior of cycle 2, cycle 3, cycle 4, and cycle 5 were fairly smooth and had trend similar to the humidity except for day 48. SE also displayed some erratic behavior on day 12, 15, 33 and 115. Three points average smoothing of the data displays that the overall trend in capacitance tracked humidity content, indicating that the sensor-substrate configuration can monitor the changing capacitance under changing humidity condition.

4.3.2.1.3. EIS Bode plots

Figure 4.8a and 4.8b displays the EIS bode plots of sensor-substrate configurations SA and SE respectively. Plots of 50% RH and 90% RH are only shown in order to facilitate easy distinction of plots. For measurement made using SA configuration, a clear distinction in the low frequency region is observed with high impedance values corresponding to measurement made at 50% RH and a lower impedance value corresponding to measurement made at 90% RH. A graph of SE also displays high impedance for measurements made at 50% RH. For measurement made at 90% RH the impedance is higher for day 12, 36 and 60. For day 90 and day 135 the impedance further decreases. However a clear trend of high and low impedance at low and high relative humidity is observed indicating the ability of the sensor in a sensor-substrate configuration to discriminate humidity level.
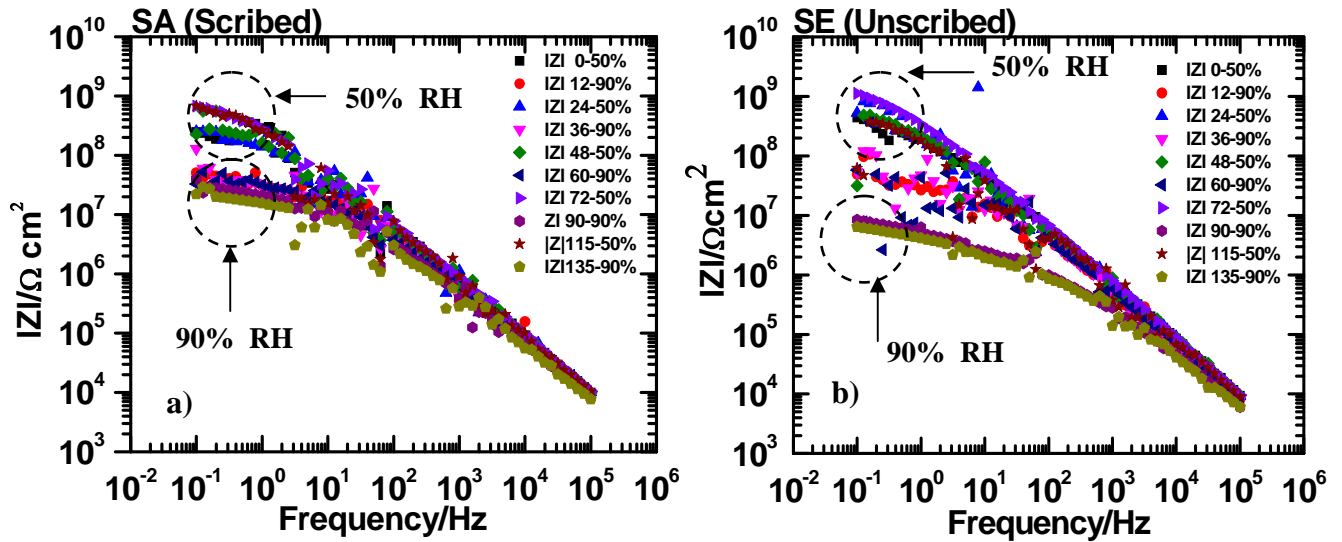
Figure 4.9: Bode modulus plot EIS results of measurements made with the sensor-substrate configuration a) SA and b) SE.

4.3.2.2. Sensor-sensor EIS results

4.3.2.2.1. Low frequency impedance results

Figure 4.9a and 4.10a displays the results of low frequency EIS measurements made using sensor-sensor configuration across the scribed/defect and the unscribed/intact region respectively. EIS measurement made across A-D and B-C represents scribed/defect region measurement whereas EIS measurement made across D-E and F-C represents unscribed/intact region measurements.

Examination of the $|Z|_{0.1Hz}$ vs. time plot of the measurement made at the scribed region reveals a consistency in variation of $|Z|_{0.1Hz}$ with varying humidity, barring few exceptions. Increase in humidity results in decrease in $|Z|_{0.1Hz}$ and vice versa. Measurement made with B-C configuration displayed more consistency with exceptions on day 33, 42 and 75 compared to A-D. A-D displayed few more erratic $|Z|_{0.1Hz}$ values compared to B-C. The trends in the plots are more conspicuous after smoothing the plots using 3 points average smoothing. An inverse relationship with changing humidity was observed. This observation is also further reinforced by the tracking ratio as observed in Figure 4.9b. An increase the tracking ratio at low humidity and a decrease at high humidity content is observed.

An examination of the $|Z|_{0.1Hz}$ vs. time plot of the unscribed /intact region obtained from EIS measurement across D-E and F-C also displays trend similar to the one observed for the defect region. Higher humidity results in low $|Z|_{0.1Hz}$ and vice versa. Increase in humidity results in decrease in resistance of the primer resulting in decrease in $|Z|_{0.1Hz}$ value. Few erratic $|Z|_{0.1Hz}$ were observed for both the measurements. However the overall trend displayed an inverse relationship of $|Z|_{0.1Hz}$ with humidity when observed using the 3

points average data smoothing. After 90 days scribed were made between CDEF similar to

the scribe made between ABCD. However no change in the trend was observed.
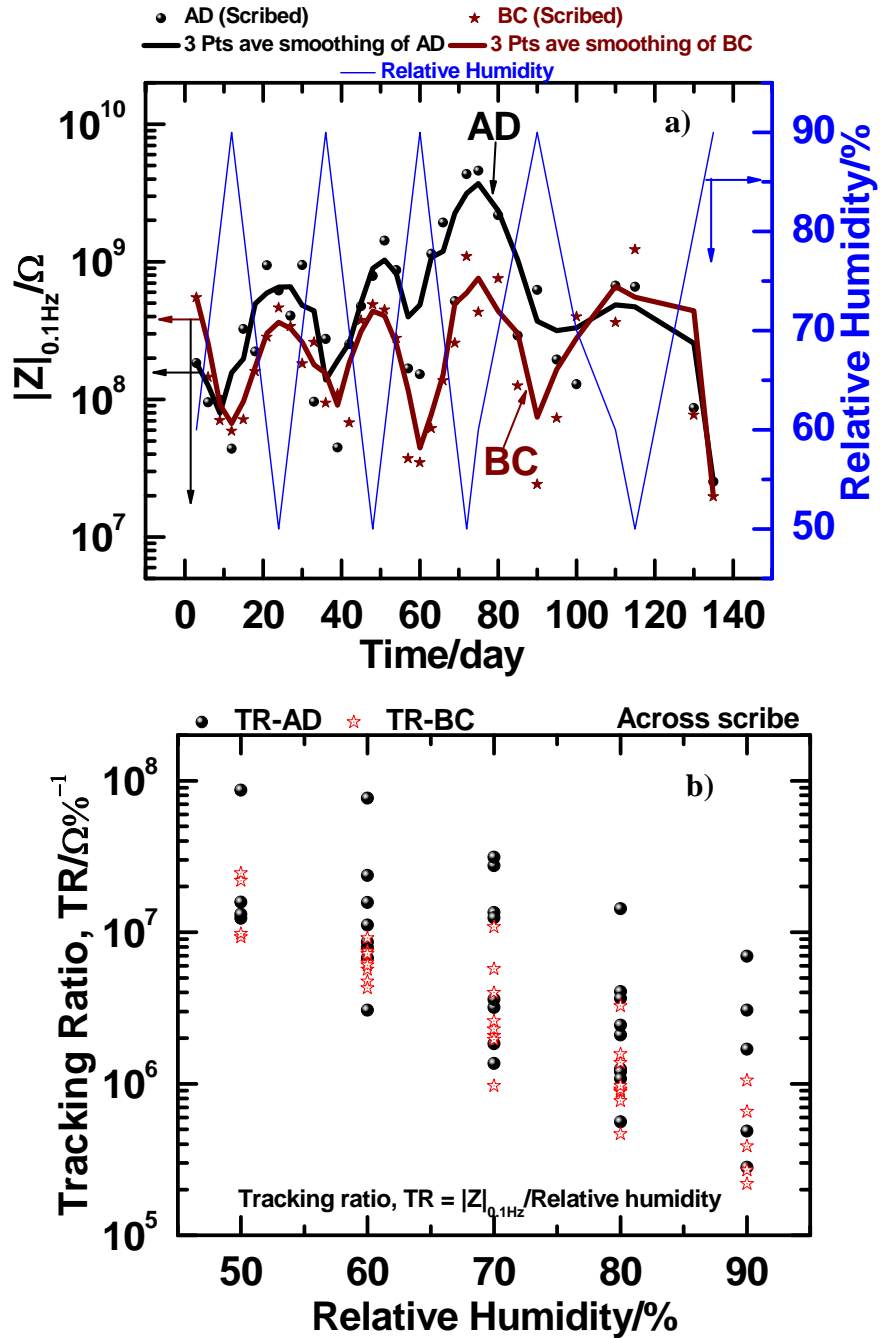
Figure 4.10: a) Low frequency impedance $|Z|_{0.1Hz}$ (left) and relative humidity (right) as a function of exposure time for b) tracking ratio as a function of relative humidity, for AD and BC (scribed region).
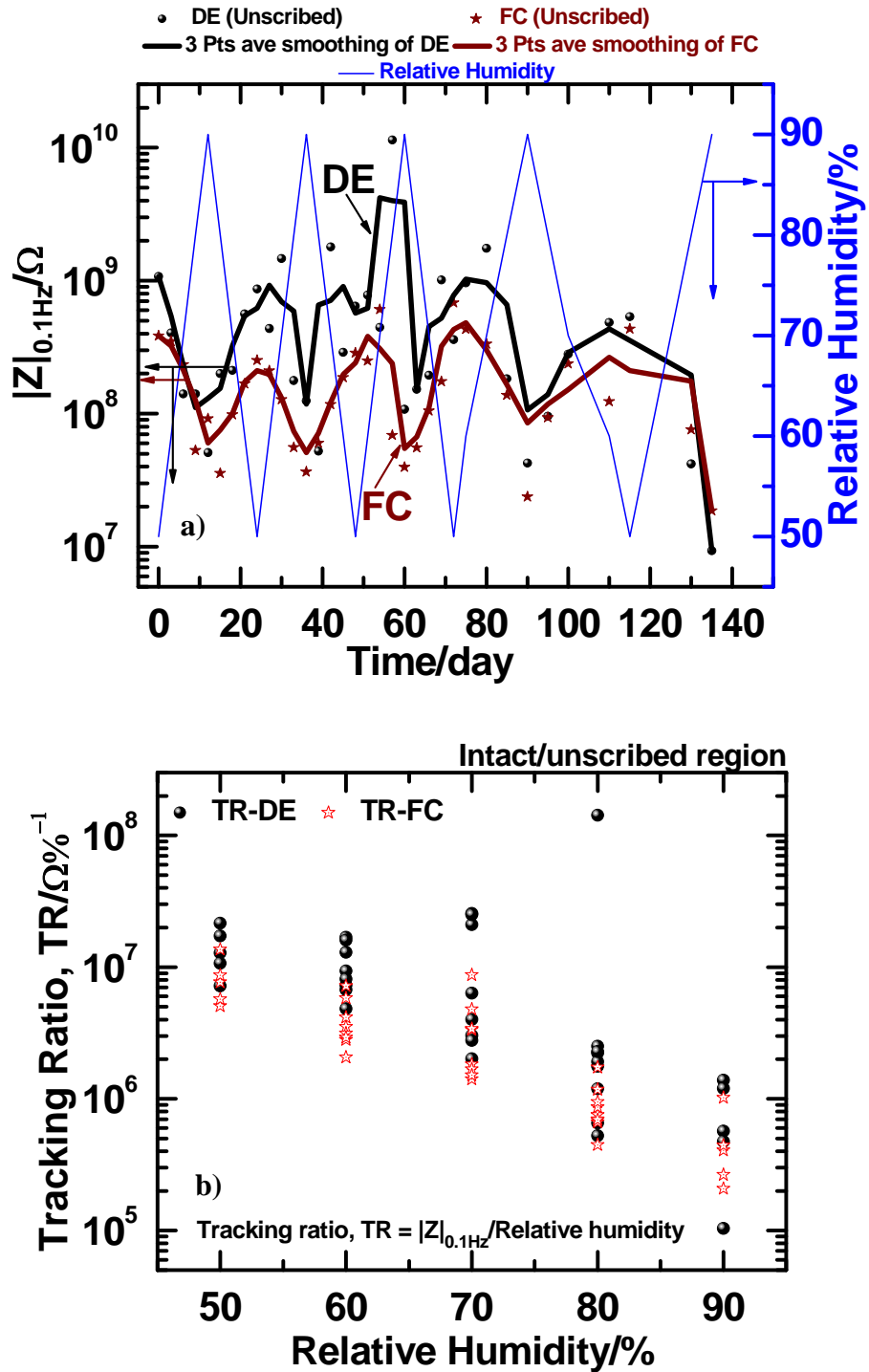
Figure 4.11: a) Low frequency impedance $|Z|_{0.1Hz}$ (left) and relative humidity (right) as a function of exposure time and b) tracking ratio as a function of relative humidity, for DE and FC (unscribed region).

A comparison between the plots 4.9a and 4.10a corresponding to the measurement

made across the defect and intact region reveals no influence of defect on the $|Z|_{0.1Hz}$ value

under the condition of experiment. The $|Z|_{0.1Hz}$ values of both plots revealed similar values ranging between 10^7-10^9 ohm.cm^2, with most of the values between 10^8-10^9 Ω.cm^2. However a clear influence of humidity on the measured value of $|Z|_{0.1Hz}$ is observed and the EIS measurement made by the sensor-sensor configuration is able to track the varying humidity condition.

4.3.2.2.2. High frequency capacitance results

Figure 4.11a and 4.11b display the capacitance plots obtained from EIS measurement at 10 kHz using the sensor-sensor configurations across the defect region and the intact region respectively. EIS measurement made across A-D and B-C represents defect region (Figure 4.11a) whereas measurement made across D-E and F-C represents intact region (Figure 4.11b). A comparison of the capacitance plots of the defect region and the intact region reveals that the measurement made across the intact region displays comparatively smoother plot compared to the measurement made across the defect region, indicating that the defect region has a different water uptake behavior compared to the intact region.
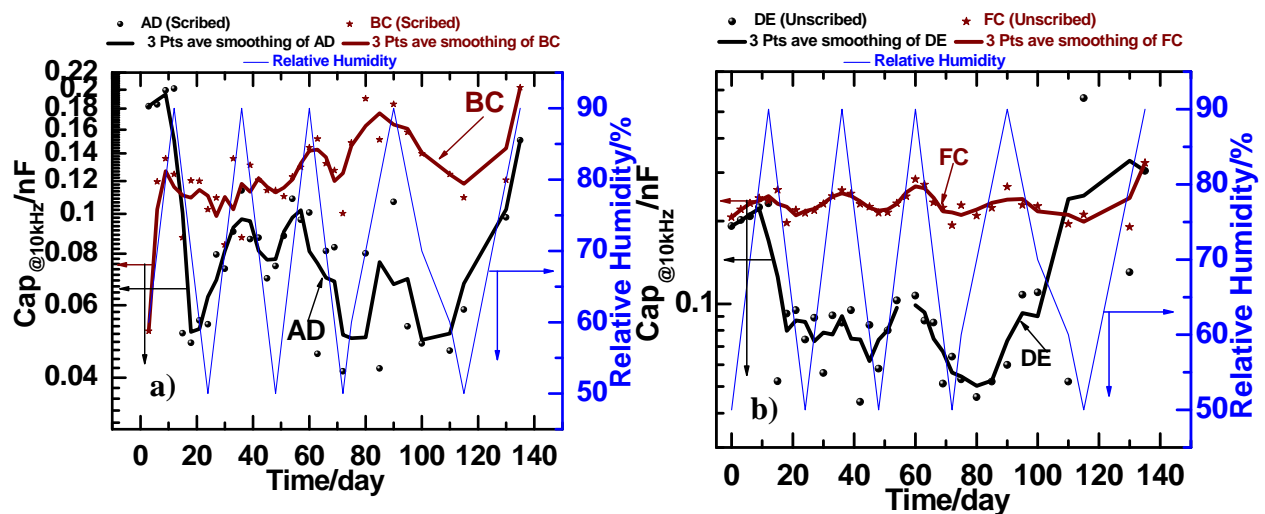
Figure 4.12: Capacitance at 10 kHz (left) and relative humidity (right) as a function of exposure time for measurement made across a) defect/scribed region b) intact region.

4.3.3. ENM results

4.3.3.1. Noise resistance of the defect and intact region

Figure 4.12a and 4.12b are the noise resistance plot of measurements made at the defect region and the intact region respectively. Sensor A-sensor D-Substrate (ADS) and sensor B-sensor C-Substrate (BCS) correspond to scribed/defect region whereas sensor D-sensor E-Substrate (DES) and sensor F-sensor C-Substrate (FCS) corresponds to unscribed/intact region. The noise resistance value of ADS displayed a low value up to day 12 owing to the low value of standard deviation of potential noise. Barring this the R_n value for both the configurations of the scribed region displayed trend with an inverse relationship to the changing humidity. Similarly the intact region measurement with DES configuration displayed trend similar to the scribed region. FCS displayed a low noise resistance value compared to DES. The trend in R_n value however displayed an inverse relationship to changing humidity.

A comparison between the measurements made at the defect and the intact region reveals that ENM measurements made with the embedded sensors can track humidity change. However it could not distinguish between the defect and the intact region under the condition of our experiment.
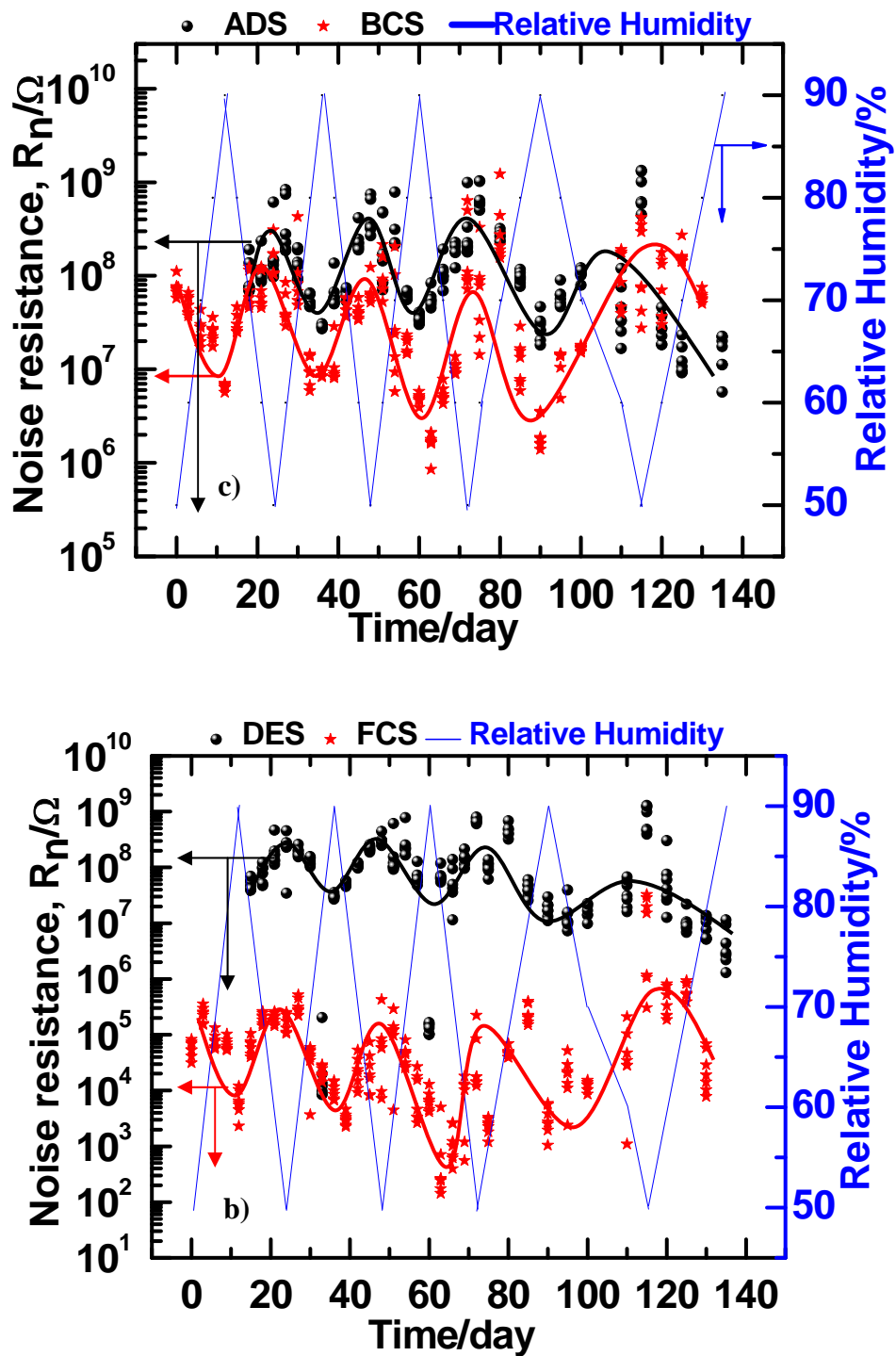
Figure 4.13: Noise resistance as a function of exposure time for ENM measurement made with ADS and BCS (representing the defect region) and b) DES and FCS (representing the intact region). Solid lines are the trend lines.

4.4. Conclusions

Embedded sensors were successfully deployed in Mg rich primer/topcoat epoxy system. Based on the EIS and ENM measurements made using embedded sensors across the defect and the intact region under varying humidity conditions and the 3 electrode EIS measurement at the defect and the intact region the following conclusions were made;

1) OCP revealed sacrificial protection offered by Mg rich pigments throughout the time of experiment. However similar OCP were measured at the intact region and near the defect region.

2) With the sensor-substrate configuration both the low frequency impedance and the high frequency capacitance was influenced by varying humidity condition. Higher humidity resulted in lower impedance and high capacitance and vice versa. Sensor in sensor-substrate configuration was successful in tracking changing humidity.

3) The non substrate sensor-sensor configuration also could detect changes in humidity. $|Z|_{0.1Hz}$ displayed an inverse relationship to changing humidity similar to sensor substrate configuration. However discrimination between defect and intact region could not be observed. Some changes in the trend in high frequency capacitance measured in the defect region compared to that of the intact region was observed. However it was not significant.

4) R_n measurement using reverse ENM configuration could successfully monitor humidity change. R_n varies inversely with humidity level. A distinction between defect and the intact region however could not be made.

No other such data system on electrochemical response to varying humidity as measured by embedded sensor is available as yet. This is the first such experiment.

4.5. References

[1] J.J. Grebe, Cored magnesium anode in galvanic protection, in, US, 1949.

[2] R.A. Gummow, P. Eng, GIC effects on pipeline corrosion and corrosion control systems, Journal of Atmospheric and Solar-Terrestrial Physics, 64 (2002) 1755-1764.

[3] R.D. Taylor, Sacrificial anode, in, US, 1953.

[4] H. Karimzadeh, T.E. Wilks, Composite sacrificial anodes, in, US, 2008.

[5] H.A. Robinson, Cathodic Protection of Underground Metals, in, US, 1952.

[6] J.E.O. Mayne, The use of metallic pigments in the preparation of protective paints, Journal of the Society of Chemical Industry, 66 (1947) 93-95.

[7] H. Marchebois, S. Touzain, S. Joiret, J. Bernard, C. Savall, Zinc-rich powder coatings corrosion in sea water: influence of conductive pigments, Progress in Organic Coatings, 45 (2002) 415-421.

[8] O.Ø. Knudsen, U. Steinsmo, M. Bjordal, Zinc-rich primers--Test performance and electrochemical properties, Progress in Organic Coatings, 54 (2005) 224-229.

[9] J.E.O. Mayne, Corrosion inhibitive action of zinc compounds, Journal of the Society of Chemical Industry, 68 (1949) 272-274.

[10] U. Evans, J. Mayne, Protection by Paints Richly Pigmented with Zinc Dust, Society of Chemical Industry Journal, 22 (1944) 109-110.

[11] T. Franz, The rust preventing mechanism of zinc dust paints, Corrosion Science, 14 (1974) 405-414.

[12] M. Nanna, G. Bierwagen, Mg-rich coatings: A new paradigm for Cr-free corrosion protection of Al aerospace alloys, Journal of Coatings Technology and Research, 1 (2004) 69-80.

[13] M.E. Nanna, G.P. Bierwagen, D. Battocchi, Magnesium rich coatings and coating systems, App.10/579,148, in, US, 2004.

[14] R.L. Twite, G.P. Bierwagen, Review of alternatives to chromate for corrosion protection of aluminum aerospace alloys, Progress in Organic Coatings, 33 (1998) 91-100.

[15] M. Darrin, Chromate Corrosion. Inhibitors in Bimetallic Systems, Industrial & Engineering Chemistry, 37 (1945) 741-749.

[16] D. Battocchi, A.M. Simões, D.E. Tallman, G.P. Bierwagen, Electrochemical behaviour of a Mg-rich primer in the protection of Al alloys, Corrosion Science, 48 (2006) 1292-1306.

[17] D. Battocchi, A.M. Simões, D.E. Tallman, G.P. Bierwagen, Comparison of testing solutions on the protection of Al-alloys using a Mg-rich primer, Corrosion Science, 48 (2006) 2226-2240.

[18] N. LeBozec, N. Blandin, D. Thierry, Accelerated corrosion tests in the automotive industry: a comparison of the performance towards cosmetic corrosion, Materials and Corrosion, 59 (2008) 889–894.

[19] G. Davis, L. Krebs, C. Dacres, Coating evaluation and validation of accelerated test conditions using an in-situ corrosion sensor, Journal of Coatings Technology, 74 (2002) 69-74.

[20] G. Bierwagen, X. Wang, D. Tallman, In situ study of coatings using embedded electrodes for ENM measurements, Progress in Organic Coatings, 46 (2003) 163-175.

[21] B.E. Merten, D. Battocchi, D.E. Tallman, G.P. Bierwagen, Embedded Reference Electrode for Potential-Monitoring of Cathodic Protective Systems, Journal of The Electrochemical Society, 157 (2010) C244.

[22] D. Wang, D. Battocchi, K.N. Allahar, S. Balbyshev, G.P. Bierwagen, In situ monitoring of a Mg-rich primer beneath a topcoat exposed to Prohesion conditions, Corrosion Science, 52 (2010) 441-448.

[23] K.N. Allahar, D.N. Wang, D.N. Battocchi, G.P. Bierwagen, S.N. Balbyshev, Real Time Monitoring of An Air Force Topcoat/Mg-Rich Primer System in B117 Exposure by Embedded Electrodes, CORROSION 2009, (2009).

[24] Q.S. Kerry N. Allahar, Gordon P. Bierwagen, In-situ monitoring of organic coatings under QUV/Prohesion exposure by embedded sensors, in: In-situ monitoring of organic coatings under QUV/Prohesion exposure by embedded sensors,CORROSION 2008

NACE International, New Orleans LA, 2008.

[25] K.N. Allahar, V. Upadhyay, G.P. Bierwagen, V.J. Gelling, Monitoring of a military vehicle coating under Prohesion exposure by embedded sensors, Progress in Organic Coatings, 65 (2009) 142-151.

[26] Q. Su, K.N. Allahar, G.P. Bierwagen, Application of embedded sensors in the thermal cycling of organic coatings, Corrosion Science, 50 (2008) 2381-2389.

[27] Q. Su, K. Allahar, G. Bierwagen, Embedded electrode electrochemical noise monitoring of the corrosion beneath organic coatings induced by ac-dc-ac conditions, Electrochimica Acta, 53 (2008) 2825-2830.

[28] R.A. Cottis, Interpretation of Electrochemical Noise Data, Corrosion, 57 (2001) 265.

[29] http://lwf.ncdc.noaa.gov/oa/climate/online/ccd/avgrh.html (09/15/2011), in.

[30] F. Bellucci, L. Nicodemo, Water Transport in Organic Coatings, Corrosion, 49 (1993) 235-247.

[31] S. Lindqvist, Theory of dielectric-properties of heterogeneous substances applied to water in a paint film, Corrosion 41 (1985) 69–75.

[32] D.M. Brasher, A.H. Kingsbury, Electrical measurements in the study of immersed paint coatings on metal. I. Comparison between capacitance and gravimetric methods of estimating water uptake, Journal of Applied Chemistry, 4 (1954) 62-72.

[33] Y. Rao, S. Ogitani, P. Kohl, C. Wong, Novel polymer–ceramic nanocomposite based on high dielectric constant epoxy formula for embedded capacitor application, Journal of Applied Polymer Science, 83 (2002) 1084-1090.

[34] D. Bogdal, A. Prociak, Microwave-enhanced polymer chemistry and technology, John Wiley and Sons, 2007.

[35] K.N. Allahar, B.R. Hinderliter, A.M. Simoes, D.E. Tallman, G.P. Bierwagen, S.G. Croll, Simulation of Wet-Dry Cycling of Organic Coatings Using Ionic Liquids, Journal of The Electrochemical Society, 154 (2007) F177-F185.

[36] K.N. Allahar, B.R. Hinderliter, G.P. Bierwagen, D.E. Tallman, S.G. Croll, Cyclic wet drying of an epoxy coating using an ionic liquid, Progress in Organic Coatings, 62 (2008) 87-95.

CHAPTER 5. ATTEMPTING TO LOCATE DEFECTS IN COATINGS USING EMBEDDED ELECTRODES

5.1. Introduction

Embedded sensors in coating provide an intelligent and convenient approach to remotely monitor the performance of a coating system. Such sensors can not only track coating performance and monitor changes in real time but also facilitate electrochemical measurements such as EIS and ENM that can detect coating degradation and substrate corrosion at a very early stage allowing sufficient time for maintenance and repair.[1-4] Embedded sensors can also increase safety, reliability and reduce maintenance cost. Moreover their influence on the performance of coating system is insignificant.[5] Embedded sensors have been used to study the behavior of coating system under stressed conditions of AC-DC-AC and thermal cycling. It has also been used to study the interlayer adhesion between the layers.[6-10] A significant advantage of embedded sensors is that they facilitate non-substrate electrochemical monitoring of coating system.[11]

The use of embedded sensors to locate defects in coating or identify sites of significant corrosion of the substrate has not yet been studied. Location of defects in coating or corrosion of the substrate by embedded sensors would aid in identifying areas needing repair and facilitating timely maintenance. In an effort towards this end, this work investigates the use of embedded sensors to locate defect in coating in-situ. Six sensors were embedded between an epoxy primer pigmented with Mg particles and a low gloss polyurethane topcoat. The substrate was a 30 cm x 30 cm AA 2024-T3 Al alloy sheet. Defects in the form of X were scribed across the sensor configurations. The panel was then exposed to ASTM B117 salt fog chamber and leads were attached to sensors from outside

the chamber to facilitate in-situ EIS measurements. EIS and ENM measurements were performed across the defect and intact region. EIS was performed using the sensor-sensor configuration using two electrode set-up whereas ENM was performed using the "reverse" configuration.[12, 13] Analysis of the data obtained from EIS and ENM measurements was made. The data was carefully examined for any differences in the electrochemical behavior obtained from measurements made across the defect and intact region.

5.2. Experimental procedure

The coatings used in this work comprised of an epoxy primer and a low gloss polyurethane topcoat. The substrate used was a large aluminum AA 2024-T3 sheet with dimensions of 30 cm x 30 cm. It was sand blasted and cleaned with n-hexane before the application of primer. The primer was formulated using Epon 828 crosslinked with Epikure 3164, both procured from Hexion Specialty Chemicals™. Epoxy equivalent to amine hydrogen equivalent ratio was 1:1. Xylene procured from Sigma-Aldrich® was the solvent used. The primer contained Mg particles as pigments (supplied by Ecka Granules®) with a mean diameter of 20 µm at 45% pigment volume concentration (PVC). It was applied by an air spray gun and cured for a week at room temperature before sensors were adhered on them. It had a thickness of approximately 60 microns.

Six square shaped platinum leaves 130nm thick with the dimensions of ~1.5 cm x ~1.5 cm were designed as sensors and adhered on the primer surface. The sensor leaves were supplied by Wrights of Lymm Ltd., Manchester, England. These sensors were designated as A, B, C, D, E and F. Supported by tissue paper they were cut into the designed sensor shape such that the surface area of the sensors was ~2.2 cm^2. A schematic of sensor diagram is depicted in Figure 5.1. Sensors were adhered to the primer surface by

a thin layer of non-conductive epoxy resin formulated using D.E.R 331, Ancamide 2353 and methyl ethyl ketone in the ratio 5:3:5 by weight. Adherence was achieved after solvent flash off and cure. The supporting tissue paper was then detached leaving the sensors adhered to the primer for a day. The sensors were then attached to a copper core electrical conducting wire to facilitate remote connection to the measuring instruments. Sealing of the sensor-wire joint was performed using D.E.R 331 and ancamide 2353 in the ratio 5:3 by weight. This was cured one day under ambient conditions. A Topcoat, 2K polyurethane PU 03-GY-277 procured from Deft was then sprayed on the primer. The dry film thickness of the topcoat was approximately 40 microns. The back side and the edges of the substrate was sealed using plastic tape in order to isolate it from the exposure conditions.
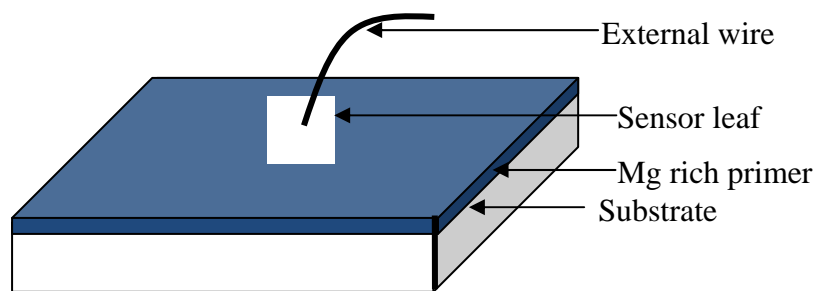
Figure 5.1: Schematic of sensor design.
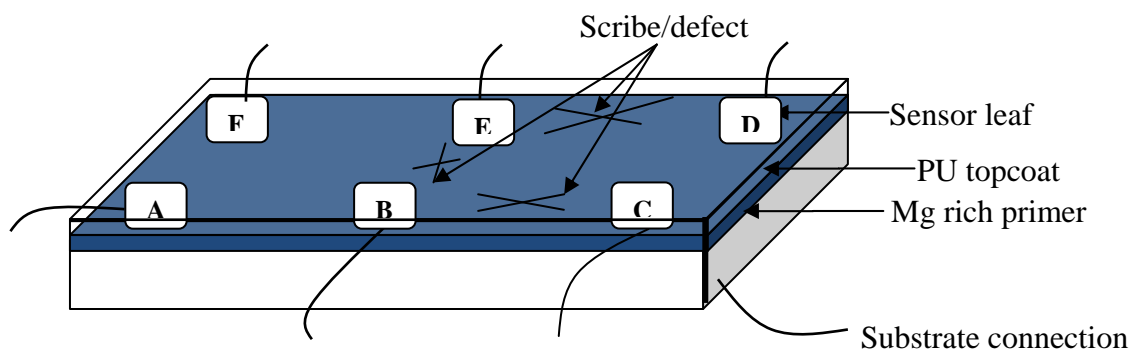
Figure 5.2: Schematic of sensors embedded between primer and topcoat and the scribe/defect and the intact region.

In-situ EIS measurements were performed using a two electrode setup with one sensor acting as working electrode and the other sensor acting as counter/reference electrode. For EIS measurements across Sensor A-Sensor F and across Sensor A-Sensor B, Sensor A was the working electrode and the other sensor was the counter/reference electrode, whereas for EIS measurements across Sensor B-Sensor C and across Sensor B-Sensor E, Sensor B was the working electrode and the other sensor was the counter/reference electrode. A Gamry Instrument R600 Potentiostat/ Galvanostat/ ZRA in conjunction with Gamry Framework Version 5.20/EIS 300 software was used for the EIS measurements. The instrument and software was supplied by Gamry Instruments, Inc. of Willow Grove, PA. A frequency range of 0.1Hz to 100 kHz was used for the measurements with an acquisition rate of 10 points per decade. A potential perturbation of 10mV with respect to the open circuit potential (OCP) was applied during measurement.

ENM method described in reference [12, 13] was used for the in-situ ENM measurements. Measurements were performed using two sensors as the two working electrodes and substrate as the reference electrode. The noise resistance was obtained by dividing the standard deviation of the potential noise by the standard deviation of the current noise. Measurement was performed for 12 minutes at a frequency of 10Hz. The first 180 seconds were cut off and the data points for 540 seconds were used. The original ENM data was divided into 10 blocks with each block having 512 points, which is 51.2 seconds of measurement. Therefore each R_n values reported are the averages of 512 data points (51.2 seconds). Moreover the R_n value was obtained after linear detrending of the original ENM data to remove the baseline shift during the test.[14] Gamry Framework Version 4.21/ESA400 software and a Gamry PCI4/300 potentiostat under zero resistance

129

ammeters (ZRA) mode, supplied by Gamry Instruments was used for the ENM measurements.

Prior to the experimental process defects in the form of artificial X shaped scribe were introduced between sensor B-sensor C, sensor D-sensor E and sensor B-sensor E. Figure 5.2 gives a visual description of the sensors and the scribes. The panel was placed inside ASTM B117 salt fog chamber. Wires attached to sensors and the substrate was connected out of the chamber to the measurement site to facilitate in-situ EIS and ENM experiments. All measurements were made externally.

5.3. Results and discussions

5.3.1. EIS results from sensor-sensor configuration

5.3.1.1. Bode plot

EIS measurements were made at day 1, 2, 3, 4, 5, 8, 10, 12 and 15. Day 1 corresponds to the first day after 5 hours of exposure to the B117 condition. Figure 5.3 depicts plots of EIS measurements made across the defect region and across the intact region. Figure 5.3a (Sensor A- Sensor F) and 5.3c (Sensor A-Sensor B) corresponds to measurements made across the intact region whereas Figure 5.3b (Sensor B-Sensor E) and 5.3d (Sensor B-Sensor C) corresponds to measurements made across the defect region. The number suffixed to |Z| on the graphs corresponds to the day of EIS measurement. For example |Z| 1 corresponds to |Z| plot of the first day of measurement whereas |Z| 5 corresponds to |Z| plot of measurement at day 5 and so on.

On exposure to ASTM B117 salt fog condition, a difference in impedance behavior as measured by EIS is observed for the measurement made across the defect region as compared to intact region. The impedance corresponding to the initial days of measurement

were higher for measurements made across the intact region. Figure 5.3a and 5.3c display higher impedance values during the initial days of measurements as opposed to relatively low impedance values as observed in Figure 5.3b and 5.3d (corresponding to the defect region). This suggests that a different route of current passage exists across the sensors in the intact region as compared to the sensors across the defect region when measurement was made under the exposure condition. The scale at the abscissa and the ordinate is similar in all the graphs to facilitate comparison.

Measurements across <u>intact</u> region   **Measurements across <u>defect</u> region**
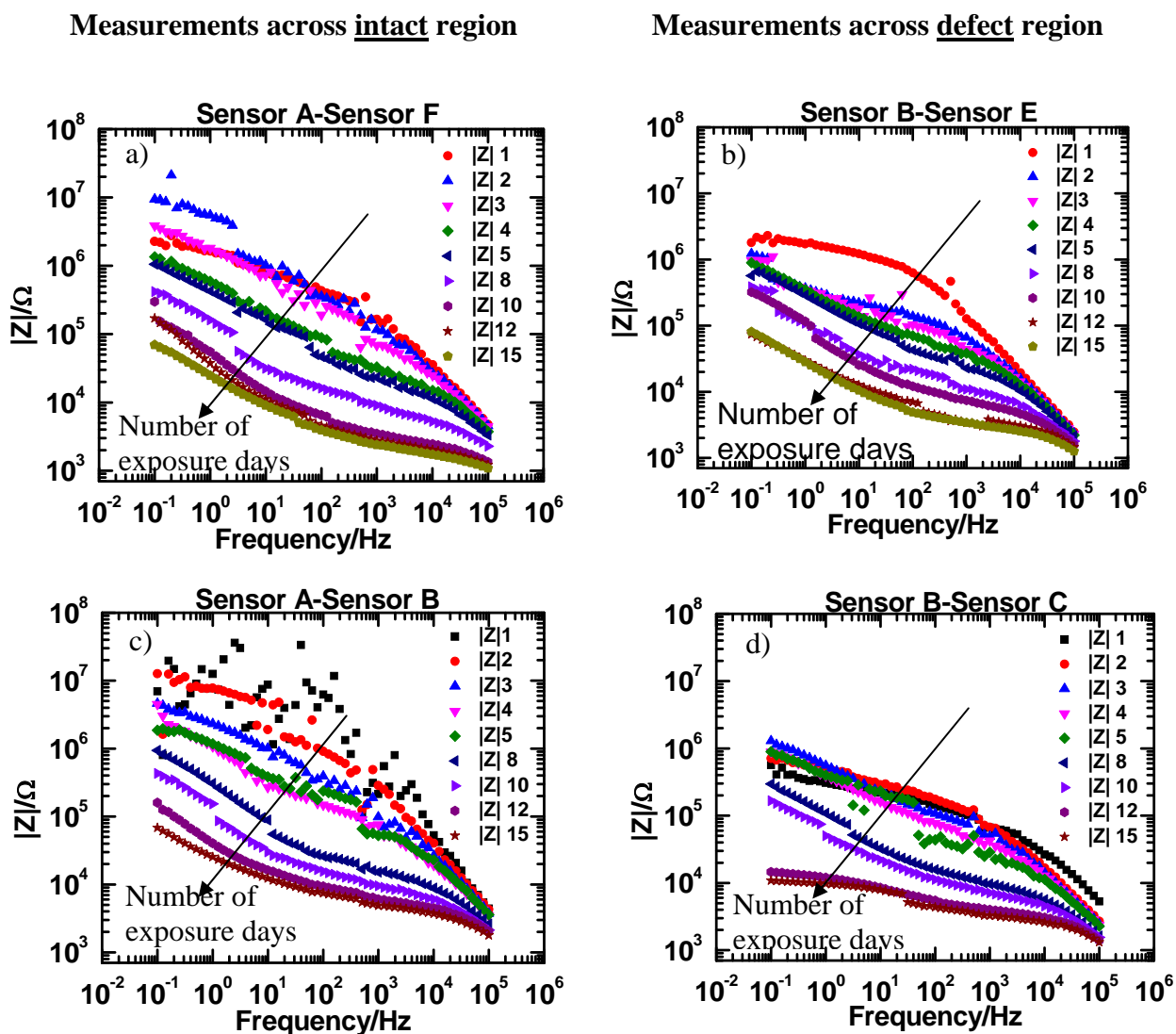
Figure 5.3: Bode modulus plots of EIS measurements made between a) Sensor A-Sensor F, b) Sensor B-Sensor E, c) Sensor A-Sensor B and d) Sensor B-Sensor C.

5.3.1.2. Low frequency impedance (Barrier) measurement

Low frequency impedance, $|Z|_{0Hz}$, is a measure of DC resistance and hence is a measure of barrier property of the coating. In this work $|Z|_{0.1Hz}$ was used as a measure of barrier properties of the coating. The barrier response of the coating as observed from the plots corresponding to the EIS measurements made across the intact region, Sensor A-Sensor B and Sensor A-Sensor F (Figure 5.4a and 5.4c) and across the defect region, Sensor B-Sensor C and Sensor B-Sensor E (Figure 5.4b and 5.4d) also reveals differences between the defect and the intact region. Sensor A-Sensor B and Sensor A-Sensor F displays high initial barrier in contrast to Sensor B-Sensor C and Sensor B- Sensor E. Analysis of the figures indicates that barrier property of the coating can be affected by defects and can be differentiated by sensors. This also suggests that using non-substrate sensor-sensor EIS measurement defects in coatings could be differentiated by low frequency impedance values.

5.3.2. Noise resistance measurement at the defect and the intact region

Figure 5.5a-5.5d depicts the noise resistance, R_n, as a function of exposure time for ENM measurements made at the defect region and the intact region. Figure 5.5a and 5.5c corresponds to R_n measurement made at the intact region whereas Figure 5.5b and 5.5d corresponds to R_n measurement made at the defect region. ENM was measured using the reversed configuration where two sensors were the two working electrodes and the substrate was the reference electrode. For measurement made at the defect region the scribe was between the two working electrodes, whereas for measurement made at the intact region no scribe was present between the working electrodes.
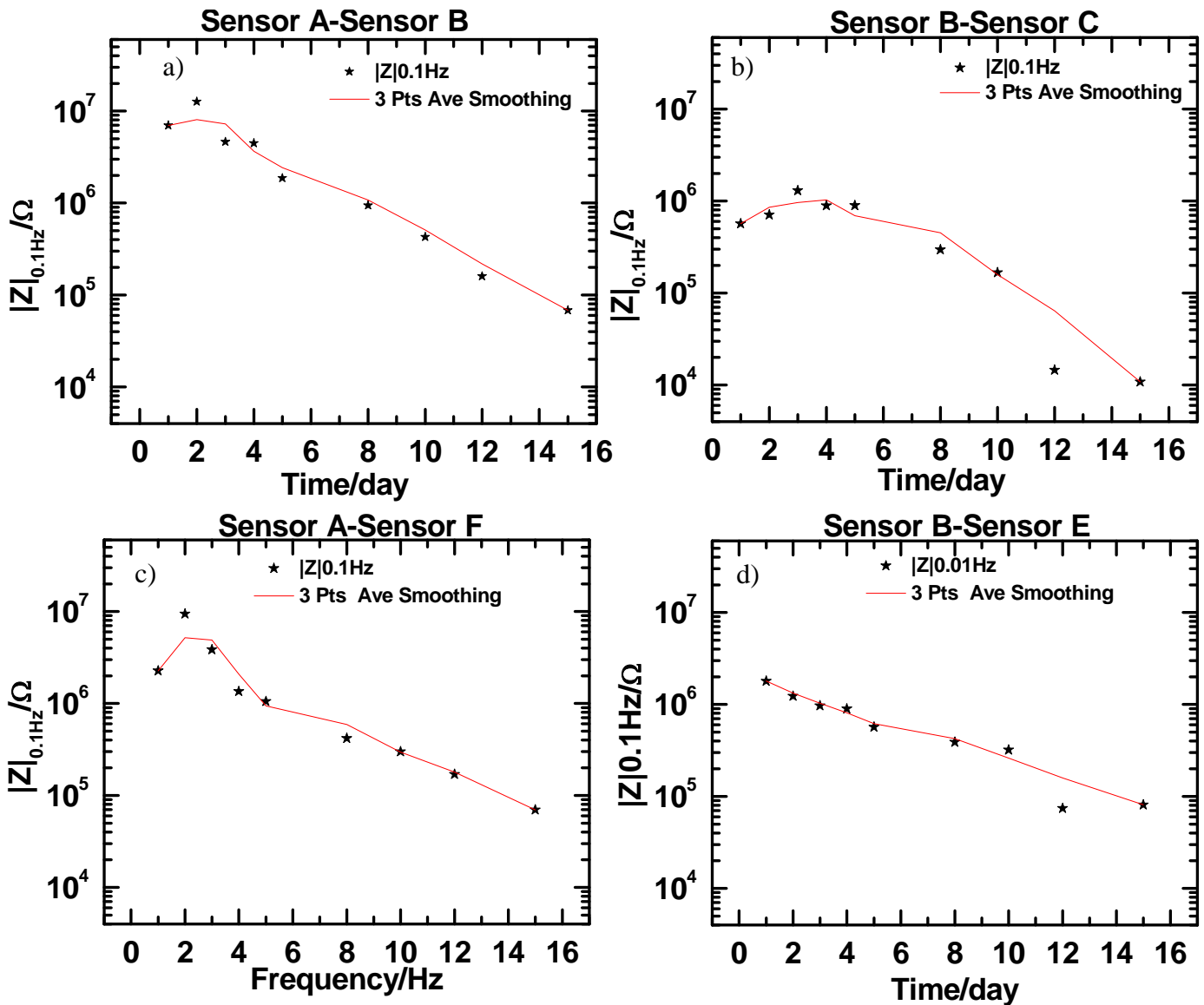
Figure 5.4: Modulus plots at 0.1 Hz ($|Z|_{0.1Hz}$) as a function of exposure time as obtained by EIS measurements made between a) Sensor A-Sensor B, b) Sensor B-Sensor C, c) Sensor A-Sensor F and d) Sensor B-Sensor E.

Out of the 15 days experiment, R_n data of only 5 days could be retrieved from the ENM measurement. Post day 5 the standard deviation of current noise displayed 0 value and hence R_n could not be measured. With only 5 data points obtained from ENM measurement it was not enough to distinguish trend in noise behavior between the defect region and the intact region. Also for R_n measured for Sensor A-Sensor F-Substrate, data

could not be obtained at day 4. From the plots it is observed that R_n corresponding to the intact region decreased constantly whereas R_n corresponding to the defect region decreased and then started to increase. However, with the limited data obtained it is difficult to come to any conclusion. More data collection at closer interval might be required to obtain a distinguishing trend, if any, between the intact region and the defect region.
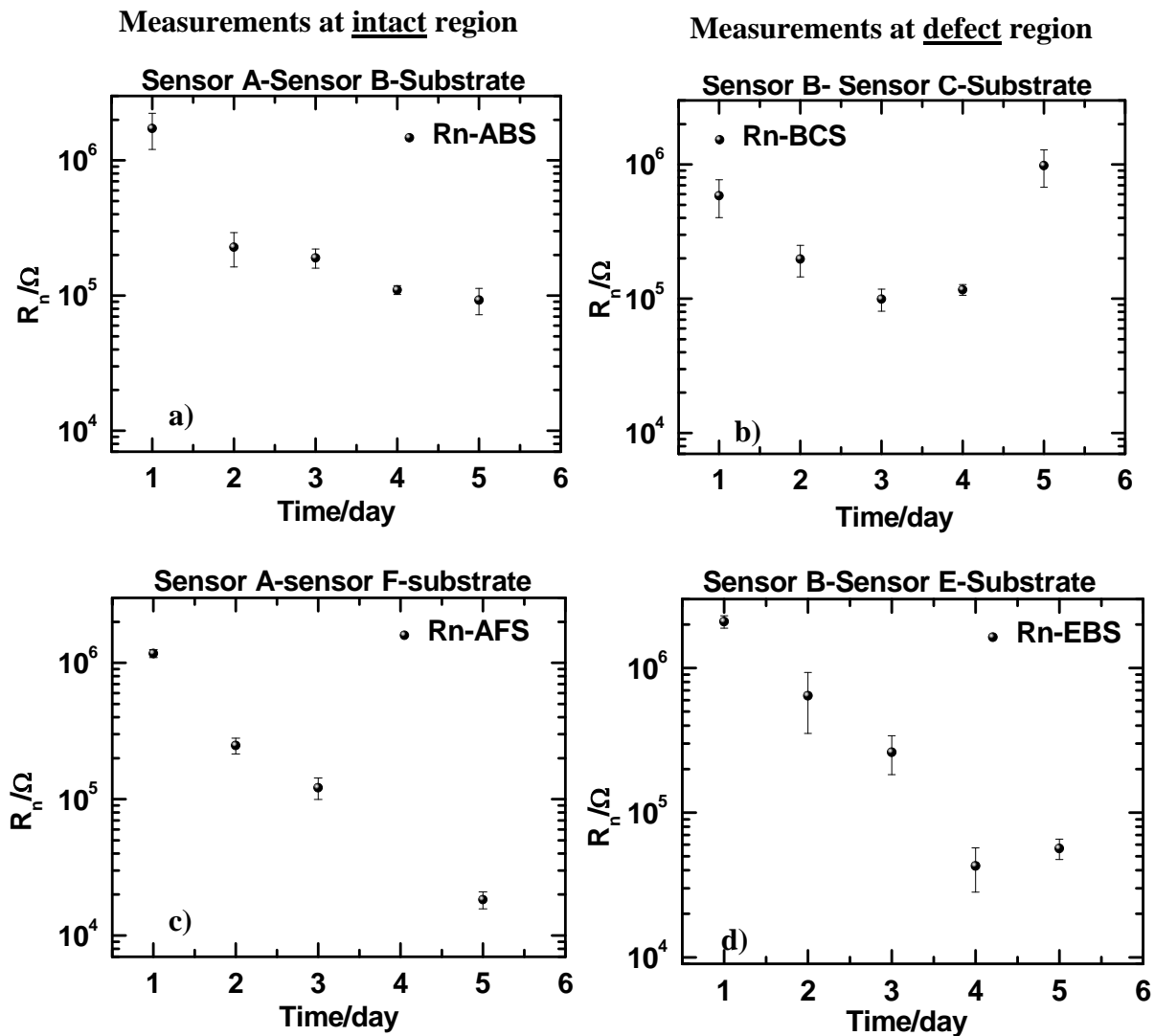
Figure 5.5: Noise resistance, R_n, measured as a function of exposure time for configurations   a) Sensor A-Sensor B-Substrate (ABS), b) Sensor B-Sensor C-Substrate (BCS) c) Sensor A-Sensor F-Substrate (AFS), and d) Sensor B-Sensor E-Substrate (BES). ABS and AFS corresponds to measurement made at intact region whereas BCS and BES correspond to measurement made at the defect region.

5.4. Conclusions

An attempt was made to investigate the ability of Pt leaf embedded sensors to locate scribed defect in coating. Sensor-sensor EIS measurements made across the defect region displayed differences in impedance behavior compared to measurement made across the intact region. Both the Bode modulus plots and barrier plots displayed initial differences, indicating that embedded sensors could perhaps differentiate and locate defects in coating. ENM measurements were also performed at the defect region and at the intact region using the reverse ENM configuration. However adequate data during ENM measurement could not be obtained to facilitate any differentiation. Measurements at closer interval could furnish more data points and perhaps be helpful in obtaining differences, if any, between the defect region compared to the intact region.

This experiment is only a first such attempt to investigate if embedded sensors can locate defect in coating via EIS and ENM means. Further investigations are required to come to a more solid conclusion though this initial work shows some promising results.

5.5. References

[1] K.N. Allahar, D. Wang, D. Battocchi, G.P. Bierwagen, S. Balbyshev, Real-Time Monitoring of a United States Air Force Topcoat/Mg-Rich Primer System in ASTM B117 Exposure by Embedded Electrodes, NACE, 2010.

[2] G. Bierwagen, X. Wang, D. Tallman, In situ study of coatings using embedded electrodes for ENM measurements, Progress in Organic Coatings, 46 (2003) 163-175.

[3] K. Allahar, Quan Su, G. Bierwagen, D. Battocchi, V. Johnson Gelling, D. Tallman, "Examination of the Feasibility of the use of In-Situ Corrosion Sensors in Army Vehicles," published in Proc.Tri-Services Corrosion Conference 2005, Orlando FL.

[4] D. Wang, D. Battocchi, K.N. Allahar, S. Balbyshev, G.P. Bierwagen, In situ monitoring of a Mg-rich primer beneath a topcoat exposed to Prohesion conditions, Corrosion Science, 52 (2010) 441-448.

[5] K. Allahar, Quan Su, G. Bierwagen, D. Battocchi, V. Johnson Gelling, D. Tallman, "Further Studies of Embedded Electrodes for In-Situ Measurement of Corrosion Protective Properties of Organic Coatings," Refereed Paper 06675 NACE Corrosion 2006 Conference, San Diego CA.

[6] Q.S. K. N. Allahar, G. P. Bierwagen1, D. H. Lee, Monitoring of the AC-DC-AC Degradation of Organic Coatings Using Embedded Electrodes, Corrosion, 64 (2008) 773.

[7] Q. Su, K.N. Allahar, G.P. Bierwagen, Application of embedded sensors in the thermal cycling of organic coatings, Corrosion Science, 50 (2008) 2381-2389.

[8] Q. Su, K. Allahar, G. Bierwagen, Embedded electrode electrochemical noise monitoring of the corrosion beneath organic coatings induced by ac–dc–ac conditions, Electrochimica acta, 53 (2008) 2825-2830.

[9] Q. Su, K.N. Allahar, G.P. Bierwagen, In Situ Embedded Sensor Monitoring of a United States Air Force Primer beneath a Topcoat Exposed to Atmospheric Humidity and Thermal Conditions, 66 (2010) 066001.

[10] A. Miszczyk, T. Schauer, Electrochemical approach to evaluate the interlayer adhesion of organic coatings, Progress in Organic Coatings, 52 (2005) 298-305.

[11] K. Allahar, Q. Su, G. Bierwagen, Non-substrate EIS monitoring of organic coatings with embedded electrodes, Progress in Organic Coatings, 67 (2010) 180-187.

[12] K.N. Allahar, V. Upadhyay, G.P. Bierwagen, V.J. Gelling, Monitoring of a military vehicle coating under Prohesion exposure by embedded sensors, Progress in Organic Coatings, 65 (2009) 142-151.

[13] K.N. Allahar, Q. Su, G.P. Bierwagen, Electrochemical Noise Monitoring of the Cathodic Protection of Mg-Rich Primers, in: Corrosion(Houston), National Association of Corrosion Engineers, P. O. Box 218340 Houston TX 77084 USA, 2010.

[14] R.A. Cottis, Interpretation of Electrochemical Noise Data, Corrosion, 57 (2001) 265.

CHAPTER 6. ATTEMPTING TO LOCATE DEFECTS IN COATINGS USING EMBEDDED ELECTRODES: EFFECT OF TOPCOAT

6.1. Introduction

The ability of coating to perform its intended role has to be verified before being put to use and hence a reliable evaluation has to be performed. The best way to test coating systems is to expose them to natural environmental conditions. This approach is ideal but impractical since it may require months or even years under such condition for a coating to fail. Conventional test methods such as salt-fog (ASTM B117), Prohesion (ASTM G85 annex A5) and the Prohesion®/QUV® (ASTM D 5894) have been designed for performance evaluation of organic coatings and to test their barrier/corrosion resistance property under accelerated conditions. These methods attempt to simulate worst case weathering conditions in the laboratory such that coating failure is promoted in shorter time as compared to actual service lifetime. The assumption made is that the failure mechanisms promoted by the testing conditions are consistent with that of natural weathering conditions. These test methods however rank coatings based on visual inspection and thus lack quantitative information. The results obtained from such exposure methods are prone to error and have been criticized in the literature.[1-5] Recent unconventional electrochemical test methods such as AC-DC-AC and thermal cycling provides fast ranking with quantitative results.[1, 6-11] AC-DC-AC imposes a direct current to the substrate to force cathodic reactions at the interface whereas thermal treatment is intended to reduce activation barrier and increase diffusion and transport rates of ions and electrolyte to the metal-coating interface by increasing the temperature of the coating. However, these methods have been limited to ranking of coating only.

Embedded sensors in coating provide a direct and convenient approach to remotely monitor the performance of a coating system. Such sensors can not only track coating performance and monitor changes in real time but also facilitate electrochemical measurements such as EIS and ENM that can detect coating degradation and substrate corrosion at a very early stage allowing sufficient time for maintenance and repair.[12-15] Embedded sensors can also increase safety, reliability and reduce maintenance cost. Moreover their influence on the performance of coating system is insignificant.[16] Embedded sensors have been used to study the behavior of coating system under stressed conditions of AC-DC-AC and thermal cycling. They have been used to study the interlayer adhesion between the layers.[17-21] A significant advantage of embedded sensors is that they facilitate non-substrate electrochemical monitoring of coating system.[22]

Investigation on the use of embedded sensors to locate defects in coating or corrosion of the substrate was discussed in chapter 5. This chapter is an extension of works reported in chapter 5. In coatings with embedded sensors, the topcoat provides numerous advantages such as improved isolation between sensors, better adhesion to the underlying films, improved measurement and higher sensitivity to small changes in coating impedance.[13] Most importantly, topcoat protects the sensor from external environmental influence. However the nature of the topcoat may also influence measurements made using embedded sensors. In an effort towards such an attempt this work seeks to investigate the influence of topcoat on the EIS/ENM results measured using embedded sensors. Six sensors were embedded between an epoxy primer pigmented with Mg particles and a high gloss polyurethane topcoat. Substrate was a large 30 cm x 30 cm AA 2024-T3 Al alloy sheet. Defects in the form of X were scribed across some sensor configurations. The panel

was then exposed to ASTM B117 salt fog chamber and wires attached to sensors were protruded out of the chamber to facilitate in-situ EIS measurements. EIS and ENM were performed across the defect and intact region. EIS was performed using the sensor-sensor configuration using two electrode set-up whereas ENM was performed using the reverse configuration. Analysis of the data obtained from EIS and ENM measurements were made and any differences in the electrochemical behavior obtained from measurements made across the defect and intact region were examined and were compared with results obtained in chapter 5.

6.2. Experimental procedure

The experimental procedure for this work is similar to that of chapter 5. The coatings used in this work comprised of an epoxy primer, the difference being a high gloss polyurethane topcoat was used. The substrate used was a large aluminum AA 2024-T3 sheet with dimensions of 30 cm x 30 cm. It was sand blasted and cleaned with n-hexane before the application of primer. The primer was formulated using Epon 828 crosslinked with Epikure 3164, both procured from Hexion Specialty Chemicals™. Epoxy equivalent to amine hydrogen equivalent ratio was 1:1. Xylene procured from Sigma-Aldrich® was the solvent used. The primer contained Mg particles as pigments (supplied by Ecka Granules®) with a mean diameter of 20 μm at 45% pigment volume concentration (PVC). It was applied by an air spray gun and was cured for a week at room temperature before sensors were adhered on them. The primer had a thickness of approximately 70 microns.

Six square shaped platinum leaves 130nm thick with the dimensions of ~1.5 cm x ~1.5 cm were designed as sensors and adhered on the primer surface. The sensor leaves were supplied by Wrights of Lymm Ltd., Manchester, England. These sensors were

designated as A, B, C, D, E and F. Supported by tissue paper they were cut into the designed sensor shape such that the surface area of the sensors was ~2.2 cm^2. A schematic of sensor diagram is depicted in Figure 6.1. Sensors were adhered to the primer surface by a thin layer of non-conductive epoxy resin formulated using D.E.R 331, Ancamide 2353 and methyl ethyl ketone in the ratio 5:3:5 by weight. Adherence was achieved after solvent flash off and cure. The supporting tissue paper was then detached leaving the sensors adhered to the primer for a day. The sensors were then attached to a copper core electrical conducting wire to facilitate remote connection to the measuring instruments. Sealing of the sensor-wire joint was performed using D.E.R 331 and ancamide 2353 in the ratio 5:3 by weight. It was left for a day to harden. A topcoat, eclipse high gloss polyurethane enamel, ECL-G-10, procured from AkzoNobel was then sprayed on the primer. The dry film thickness of the topcoat was approximately 55 microns. The back side and the edges of the substrate was sealed using plastic tape in order to isolate it from the exposure conditions.
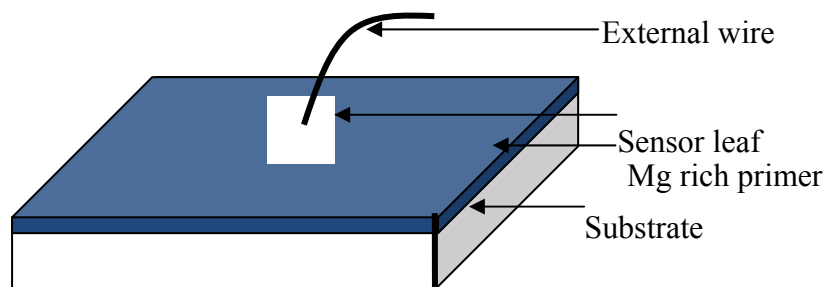
Figure 6.1: Schematic of sensor design.
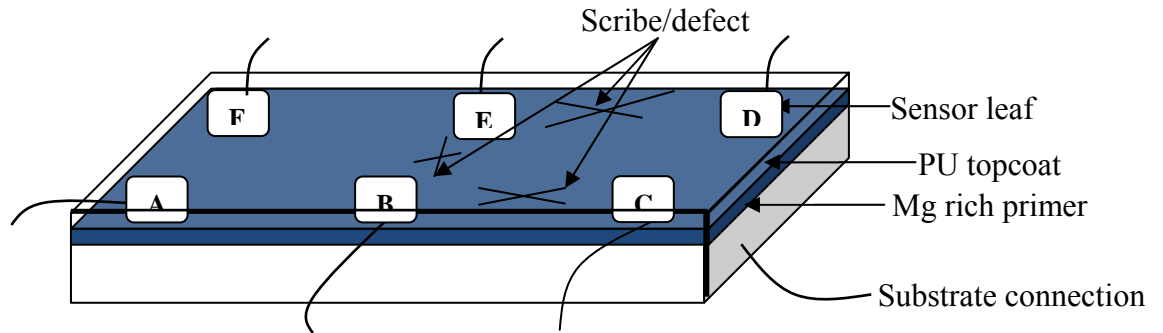
Figure 6.2: Schematic of sensors embedded between primer and topcoat and the scribe/defect and the intact region.

In-situ EIS measurements were performed using a two electrode setup with one sensor acting as working electrode and the other sensor acting as counter/reference electrode. For EIS measurements across Sensor A-Sensor F and across Sensor A-Sensor B, Sensor A was the working electrode and the other sensor was the counter/reference electrode, whereas for EIS measurements across Sensor B-Sensor C and across Sensor B-Sensor E, Sensor B was the working electrode and the other sensor was the counter/reference electrode. A Gamry Instrument R600 Potentiostat/ Galvanostat/ ZRA in conjunction with Gamry Framework Version 5.20/EIS 300 software was used for the EIS measurements. The instrument and software was supplied by Gamry Instruments, Inc. of Willow Grove, PA. A frequency range of 0.1Hz to 100 kHz was used for the measurements with an acquisition rate of 10 points per decade. A potential perturbation of 10mV with respect to the open circuit potential (OCP) was applied during measurement.

Reversed ENM method was used for the in-situ ENM measurements. Measurements were performed using two sensors as the two working electrodes and substrate as the reference electrode. The noise resistance was obtained by dividing the standard deviation of the potential noise by the standard deviation of the current noise.

Measurement was made for 12 minutes at a frequency of 10Hz. The first 180 seconds were cut off and the data points for 540 seconds were used. The original ENM data was divided into 10 blocks with each block having 512 points, which is 51.2 seconds of measurement. Therefore each R_n values reported are the averages of 512 data points (51.2 seconds). The 10 R_n values obtained were further averaged and their standard errors were obtained. Linear detrending of the original ENM data was done to remove the baseline shift during the test.[23] Gamry Framework Version 4.21/ESA400 software and a Gamry PCI4/300 potentiostat under zero resistance ammeters (ZRA) mode, supplied by Gamry Instruments was used for the ENM measurements.

Prior to the experimental process defects in the form of artificial X shaped scribe were introduced between sensor B-sensor C, sensor D-sensor E and sensor B-sensor E. Figure 6.2 gives a visual description of the sensors and the scribes. The panel was placed inside ASTM B117 salt fog chamber. Wires attached to sensors and the substrate, were protruded out of the chamber to the measurement site to facilitate in-situ EIS and ENM experiments. All measurements were made externally.

6.3. Results and discussions

6.3.1. EIS results from sensor-sensor configuration

6.3.1.1. Bode plot

EIS measurements were made at day 2, 3, 4, 5, 8, 10, 12 and 15. An attempt at EIS measurement at day 1 after 5 hours of initial exposure was also made. However highly scattered data were obtained for all measurements and hence have been omitted from the graphs. Figure 6.3 depicts plots of EIS measurements made across the defect region and across the intact region. Figure 6.3a (Sensor A- Sensor F) and 6.3c (Sensor A-Sensor B)

corresponds to measurements made across the intact region whereas Figure 6.3b (Sensor B-Sensor E) and 6.3d (Sensor B-Sensor C) corresponds to measurements made across the defect region. The number suffixed to |Z| on the graphs corresponds to the day of EIS measurement. For example |Z| 2 corresponds to |Z| plot of the second day of measurement whereas |Z| 5 corresponds to |Z| plot of measurement at day 5 and so on.
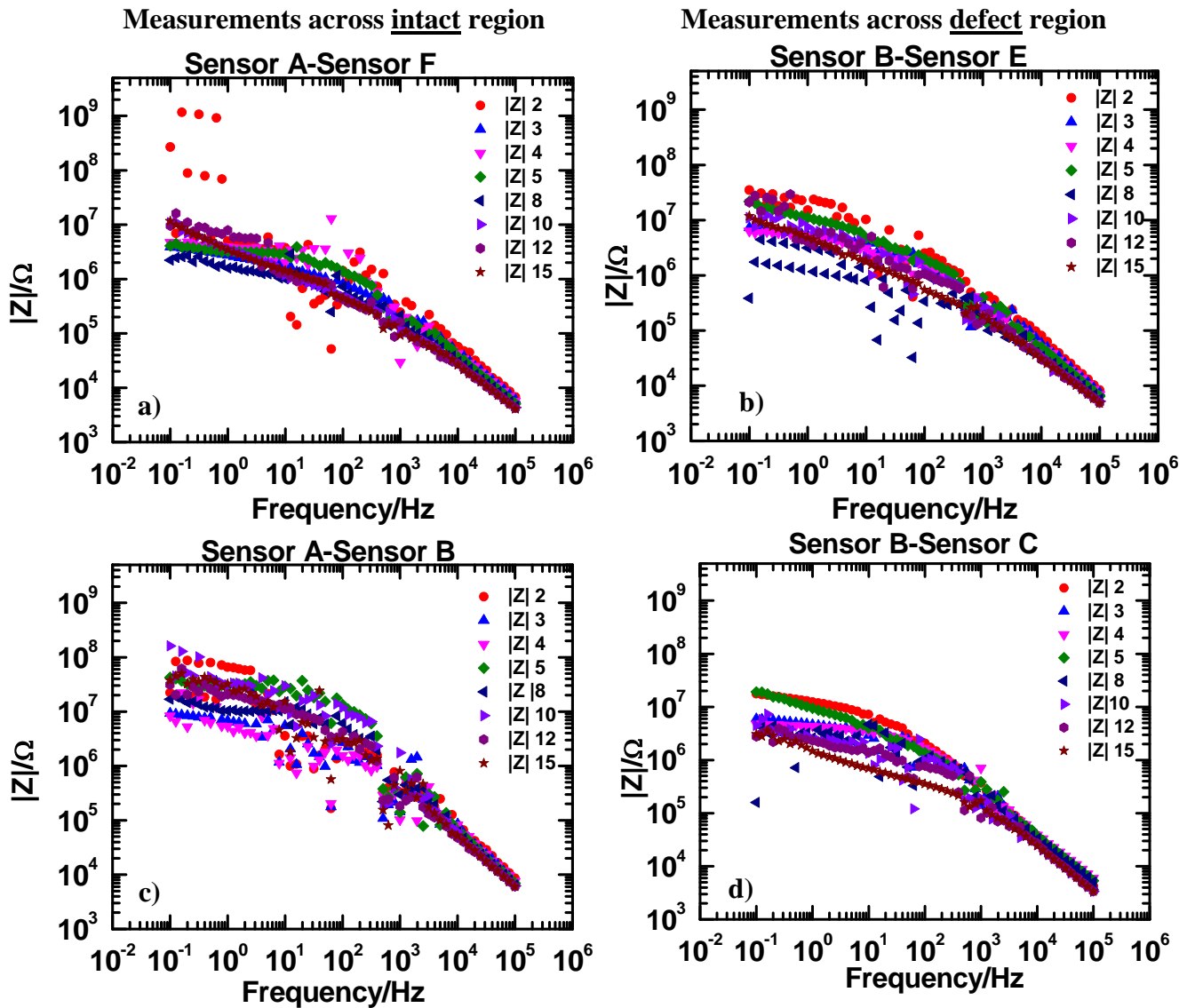

Figure 6.3: Bode modulus plots of EIS measurements made across a) Sensor A-Sensor F, b) Sensor B-Sensor E, c) Sensor A-Sensor B and d) Sensor B-Sensor C.

Measurement across sensor A-sensor F displays highly scattered data on day 2, perhaps due to unstable measurement. Day 3, 4 and 5 displayed similar impedance behavior with a slight reduction in impedance at day 8. Day 10, 12 and 15 then displayed slight increase in impedance, indicating a slight increase in barrier after 8 days of measurements. Sensor B- sensor E on the other hand displayed less scattered data on day 2. Similar to A-F, day 3, 4 and 5 displayed similar behavior whereas day 8 displayed a slight decrease in impedance but data were scattered at day 8. Day 10, 12 and 15 displayed a slight increase in impedance compared to day 3, 4, 5 and 8. Similar impedance behavior was observed for sensor A-sensor F and sensor B-sensor E and the trend in measurements made across defect region were similar to trends observed at the intact region. Sensor A-sensor B displayed low impedance on day 3 and 4 compared to day 2. Post day 4, fluctuations in impedance values were observed with day 5 displaying increase in impedance followed by decrease at day 8, increase at day 10 and again a decrease at day 12 and 15. For sensor B-sensor C, day 3 and 4 displayed a low impedance compared to day 2. An increase in impedance was observed at day 5. Day 8, 10, 12 and 15 then displayed a reduction in impedance. On comparison between sensor A-sensor B and sensor B-sensor C, a distinguishing trend between them was not observed. The scale at the abscissa and the ordinate is similar in all the graphs to facilitate comparison.

Overall, the impedance measured at the defect region could not provide any specific distinguishing trend compared to the impedance measured at the intact region when a high gloss top coat was used. This observation is in contrast to that observed for a low gloss top coated system (in chapter 5) where the initial impedance observed for measurements made

across the defect region was lower compared to the measurement made across the intact region.

6.3.1.2. Low frequency impedance (Barrier) measurement

Low frequency impedance is a measure of DC resistance and hence is a measure of barrier property of the coating. The barrier response of the coating are observed from the $|Z|_{0.01Hz}$ plots corresponding to the EIS measurements made across the intact region, Sensor A-Sensor B and Sensor A-Sensor F (figure 6.4a and 6.4c respectively) and across the defect region, Sensor B-Sensor C and Sensor B-Sensor E (Figure 6.4b and 6.4d respectively). The trend line displayed in the plots is the 3 points average smoothing that was performed for plot smoothing and also to obtain a trend in the plots.

Measurement made across sensor A-sensor B and sensor B-sensor C displays similar initial impedance at around $10 \times 10^7 \Omega$ as observed in day 2. However A-B displays a slight increase in barrier with time. This is in contrast to that observed for sensor B-sensor C, which displays a gradual decrease. Moreover, sensor A-sensor F in contrast to sensor B-sensor E displays a very high initial $|Z|_{0.01Hz}$. However the trend in measurement made across sensor A-sensor F and sensor B-sensor E becomes similar and a distinction based on sensor A-sensor F and sensor B-sensor E could not be made.

Overall, if measurements made at the defect region are compared to the measurements made at the intact region, a trend that can distinguish the intact region with the defect region could not be observed. This is in contrast to that observed for measurement made using embedded sensors with low gloss topcoat, as observed in chapter 5. For embedded sensors with low gloss topcoat, the intact region had displayed higher initial impedance compared to the measurement made at the defect region. This indicates

146

that the nature of the topcoat can influence the electrochemical measurements made using

embedded sensors.

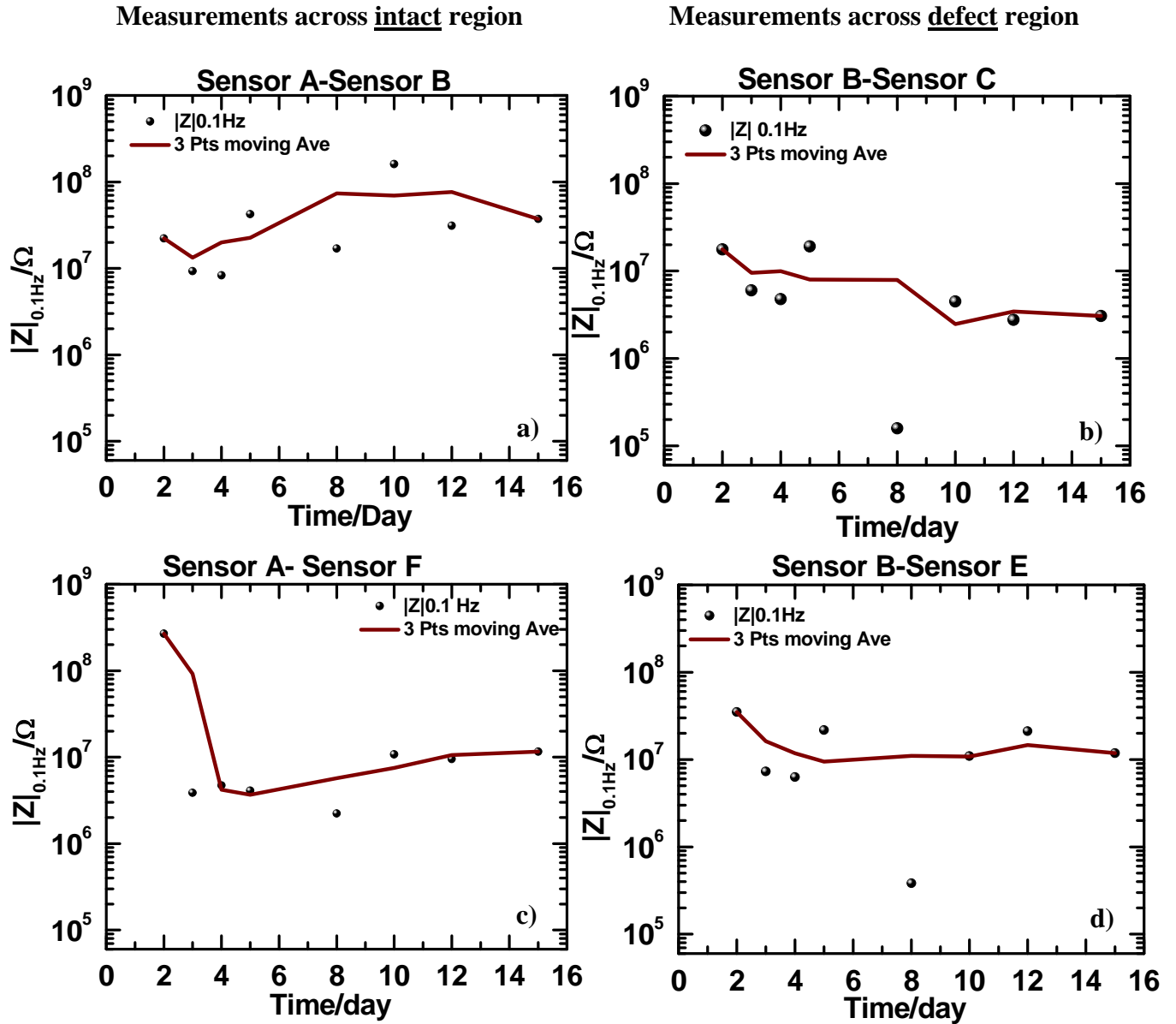Figure 6.4: Modulus plots at 0.1 Hz ($|Z|_{0.1Hz}$) as a function of exposure time as obtained by EIS measurements made across a) Sensor A-Sensor B, b) Sensor B-Sensor C, c) Sensor A-Sensor F and d) Sensor B-Sensor E.

6.3.2. Noise resistance measurement at the defect and the intact region

Figure 6.5 depicts the noise resistance, R_n, as a function of exposure time for ENM measurements made at the defect region and at the intact region. Figure 6.5a and 6.5c corresponds to R_n measurement made at the intact region whereas Figure 6.5b and 6.5d corresponds to R_n measurement made at the defect region. ENM was measured using the reversed configuration where two sensors were the two working electrodes and the substrate was the reference electrode. For measurement made at the defect region the scribe was made between the two working electrodes, whereas measurement made at the intact region had no scribes across the working electrodes.

All the R_n value observed in the plots displays a relatively higher initial R_n. A comparison between measurement made with sensor A-sensor B-Substrate (ABS) and sensor B-sensor C-Substrate (BCS) configuration do not reveal any distinguishing trend between the two. Trend in measurement made with ABS displays a reduced R_n upto day 5 and then levels up to day 10 and then increases again. R_n observed for BCS configuration also decreases initially but displays almost similar values thereafter. A clear distinction between the two cannot be made. On comparison of R_n measurement made between sensor A-sensor F-Substrate (AFS) and sensor B-sensor E-Substrate (BES) (Figure 6.5c and 6.5d) it is observed that for AFS R_n decreases with time and then increases after day 10. However a continuous gradual decrease in R_n is observed for BES. A clear differentiating trend between the two is not observed.

Overallay, on comparison of the R_n measurements made at the intact region with that of the measurement made at the defect region, a trend that can clearly distinguish between the two could not be observed.

Measurements at <u>intact</u> region   **Measurements at <u>defect</u> region**
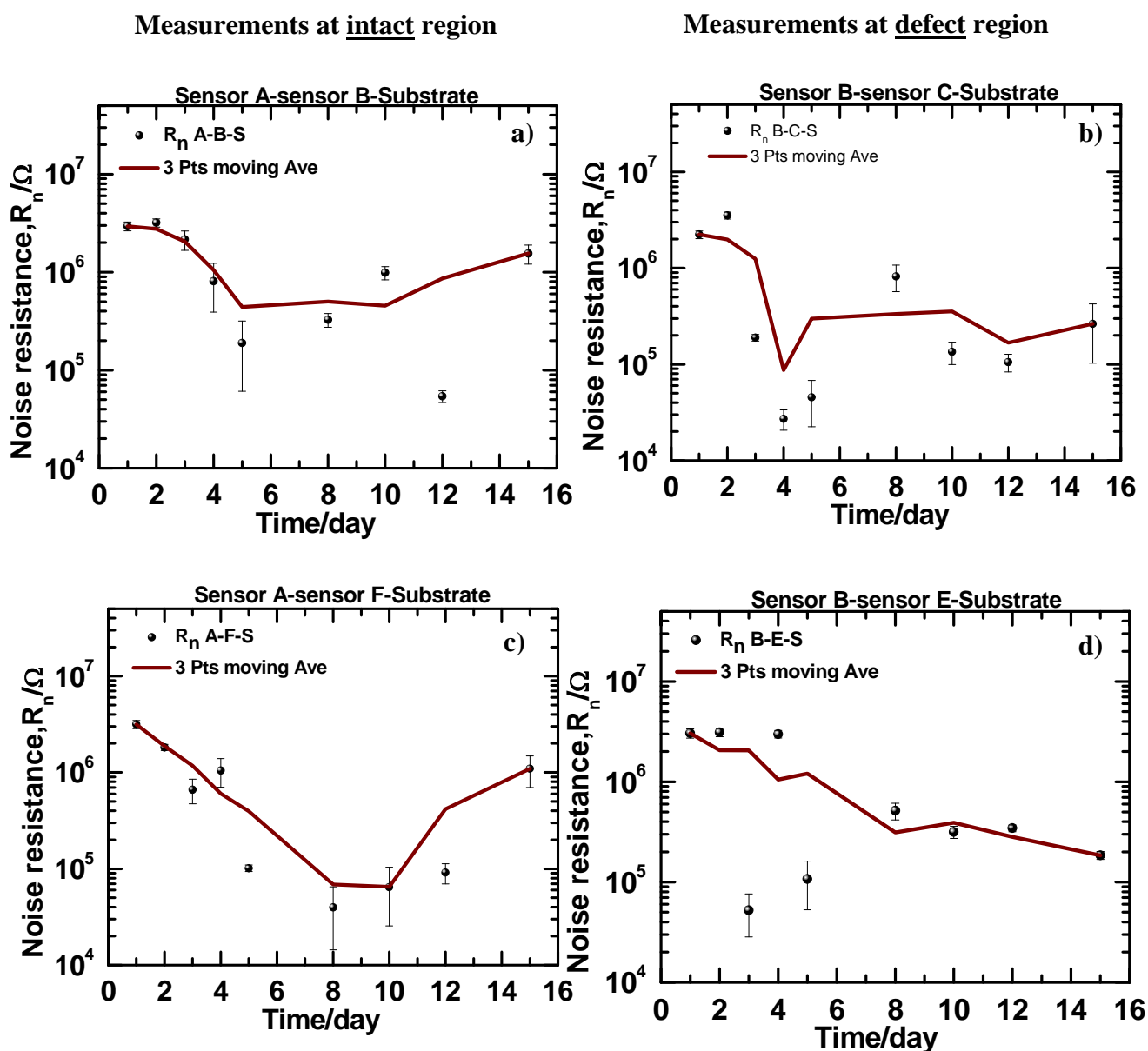
Figure 6.5: Noise resistance, R_n, measured as a function of exposure time for configurations a) Sensor A-Sensor B-Substrate (ABS), b) Sensor B-Sensor C-Substrate (BCS) c) Sensor A-Sensor F-Substrate (AFS), and d) Sensor B-Sensor E-Substrate (BES). ABS and AFS corresponds to measurement made at intact region whereas BCS and BES correspond to measurement made at the defect region.

6.4. Conclusions

As an extension of the work reported in chapter 5, this chapter studied the effect of

topcoat on measurements made using embedded sensors. The ability of the topcoat to

influence the measurement made using embedded sensors was made. It was observed that the topcoat could influence the EIS measurement made using embedded sensors using sensor-sensor configuration as differences were observed in the measurement when results were compared with findings in chapter 5. In contrast to measurements made using low gloss topcoat, measurement made using high gloss topcoat followed a different impedance and noise behavior. However within the high gloss topcoated system, the impedance, barrier and noise resistance measured across the intact region were not very discriminating compared to measurements made across the intact region as any sharp distinguishing features were not observed. This also indicates that the choice of topcoat in the successful use of an embedded sensor could be very important.

6.5. References

[1] G.P. Bierwagen, L. He, J. Li, L. Ellingson, D.E. Tallman, Studies of a new accelerated evaluation method for coating corrosion resistance -- thermal cycling testing, Progress in Organic Coatings, 39 (2000) 67-78.

[2] G. Davis, L. Krebs, C. Dacres, Coating evaluation and validation of accelerated test conditions using an in-situ corrosion sensor, Journal of Coatings Technology, 74 (2002) 69-74.

[3] N. LeBozec, N. Blandin, D. Thierry, Accelerated corrosion tests in the automotive industry: a comparison of the performance towards cosmetic corrosion, Materials and Corrosion, 59 (2008) 889–894.

[4] G.P. Bierwagen, Reflections on corrosion control by organic coatings, Progress in Organic Coatings, 28 (1996) 43-48.

[5] C.G. Oliveira, M.G.S. Ferreira, Ranking high-quality paint systems using EIS. Part I: intact coatings, Corrosion Science, 45 (2003) 123-138.

[6] E.L. J. Hollaender, S. Hillebrand, Proceedings of the Fifth International Tinplate Conference,London, (1992) 300.

[7] K.N. Allahar, G.P. Bierwagen, V.J. Gelling, Understanding ac-dc-ac accelerated test results, Corrosion Science, 52 (2010) 1106-1114.

[8] M.T. Rodríguez, J.J. Gracenea, S.J. García, J.J. Saura, J.J. Suay, Testing the influence of the plasticizers addition on the anticorrosive properties of an epoxy primer by means of electrochemical techniques, Progress in Organic Coatings, 50 (2004) 123-131.

[9] K.N. Allahar, V. Upadhyay, G.P. Bierwagen, Characterizing the Relaxation of the Open-Circuit Potential during an AC-DC-AC Accelerated Test, Corrosion, 66 (2010) 095001.

[10] G.P. Bierwagen, K.N. Allahar, Q. Su, V.J. Gelling, Electrochemically characterizing the ac-dc-ac accelerated test method using embedded electrodes, Corrosion Science, 51 (2009) 95-101.

[11] B.R.H. K. N. Allahar, G. P. Bierwagen, and D. E. Tallman, Army Vehicle Primer Properties during Wet-Dry Cycling, Corrosion, 65 (2009) 126.

[12] K.N. Allahar, D. Wang, D. Battocchi, G.P. Bierwagen, S. Balbyshev, Real-Time Monitoring of a United States Air Force Topcoat/Mg-Rich Primer System in ASTM B117 Exposure by Embedded Electrodes, NACE, 2010.

[13] G. Bierwagen, X. Wang, D. Tallman, In situ study of coatings using embedded electrodes for ENM measurements, Progress in Organic Coatings, 46 (2003) 163-175.

151

[14] K. Allahar, Quan Su, G. Bierwagen, D. Battocchi, V. Johnson Gelling, D. Tallman, "Examination of the Feasibility of the use of In-Situ Corrosion Sensors in Army Vehicles," published in Proc.Tri-Services Corrosion Conference 2005, Orlando FL.

[15] D. Wang, D. Battocchi, K.N. Allahar, S. Balbyshev, G.P. Bierwagen, In situ monitoring of a Mg-rich primer beneath a topcoat exposed to Prohesion conditions, Corrosion Science, 52 (2010) 441-448.

[16] K. Allahar, Quan Su, G. Bierwagen, D. Battocchi, V. Johnson Gelling, D. Tallman, "Further Studies of Embedded Electrodes for In-Situ Measurement of Corrosion Protective Properties of Organic Coatings," Refereed Paper 06675 NACE Corrosion 2006 Conference, San Diego CA.

[17] Q.S. K. N. Allahar, G. P. Bierwagen1, D. H. Lee, Monitoring of the AC-DC-AC Degradation of Organic Coatings Using Embedded Electrodes, Corrosion, 64 (2008) 773.

[18] Q. Su, K.N. Allahar, G.P. Bierwagen, Application of embedded sensors in the thermal cycling of organic coatings, Corrosion Science, 50 (2008) 2381-2389.

[19] Q. Su, K. Allahar, G. Bierwagen, Embedded electrode electrochemical noise monitoring of the corrosion beneath organic coatings induced by ac–dc–ac conditions, Electrochimica acta, 53 (2008) 2825-2830.

[20] Q. Su, K.N. Allahar, G.P. Bierwagen, In Situ Embedded Sensor Monitoring of a United States Air Force Primer beneath a Topcoat Exposed to Atmospheric Humidity and Thermal Conditions, 66 (2010) 066001.

[21] A. Miszczyk, T. Schauer, Electrochemical approach to evaluate the interlayer adhesion of organic coatings, Progress in Organic Coatings, 52 (2005) 298-305.

[22] K. Allahar, Q. Su, G. Bierwagen, Non-substrate EIS monitoring of organic coatings with embedded electrodes, Progress in Organic Coatings, 67 (2010) 180-187.

[23] R.A. Cottis, Interpretation of Electrochemical Noise Data, Corrosion, 57 (2001) 265.

CHAPTER 7. IMPACT OF POLYMER COMPOSITION ON ELECTROCHEMICAL PROPERTIES OF COATINGS AS DETERMINED BY ELECTROCHEMICAL IMPEDANCE SPECTROSCOPY (EIS)

7.1. Introduction

Organic coating films are ubiquitous and most often they are the first thing that we observe around us. They are widely used as barriers to the transport of oxygen, ions and electrolytes from the environment to prevent materials from corrosion, as well as imparting aesthetic appearances and specialty functions.[1] End uses of organic coatings include buildings, bridges, aircrafts, transportation, wood flooring, plastic and metal coil stock. Organic coatings in their final film form consist primarily of a polymeric binder in addition to pigments and additives. The binder in an organic coating system may be natural or synthetic polymers and to a large extent govern the properties of the coatings. They form a continuous film, adhere to the substrate surface and bind together other constituents of the coatings. Various binders such as polyurethanes, epoxies, acrylics, drying oils, alkyds, polyesters, silicones, phenolic and amines are used in the coating industries.[2] Current coating technology research is focused on the design of novel polymers, crosslinkers and additives to meet various functional, environmental and economic objectives for several applications.

Two of the most important high performance coating systems currently in use are polyurethanes (PU) and epoxies. Polyurethanes have gained wide acceptance and are used extensively in the coating market due to their superior properties such as high gloss, chemical resistance and acid etch resistance. An added advantage of PU coatings is their ability to form strong hydrogen bonds thus enhancing coating film performance and

physical properties such as abrasion resistance and film toughness. Films formed from epoxy systems exhibit good corrosion performance, adhesion, chemical resistance, strength and toughness.[3, 4] A novel way of achieving the advantage of both PU and epoxy systems is to unite them by the use of glycidyl carbamate chemistry which utilizes both urethane linkages and reactive epoxy groups. [5-7]

The variation in the polymer structure as well as the composition is expected to change the final properties of the coating films. Changes can be observed in the form of glass transition temperature, hardness, flexibility, toughness, barrier and diffusion properties of the coating among others. In a recent work Deveci et al., [8] has chemically modified polystyrene with succinic anhydride and phthalic anhydride and observed that the modified polymer displayed better thermal, mechanical, elastic and corrosion resistance properties. The corrosion performance, however, was only characterized by visual analysis. Studies on the influence of polymer structure and composition variation on the electrochemical properties of coating films are rare. A study on the influence of plasticizer composition variation on the performance of an epoxy coating as measured by electrochemical impedance spectroscopy (EIS) has been reported.[9] It is also well known that up to 6% water can be absorbed/dissolved in epoxy coatings, and this drastically affects their thermal behavior and their electrochemical barrier properties. Li et al.,[10] have written an extensive analysis of thermal (and aqueous) effects on electrochemical properties of organic coatings that reviewed the literature through 1997. They extensively surveyed the effects of water and temperature especially on epoxy-based corrosion protective coatings. This work came out of studies of FBE (fusion bonded epoxy) pipeline coatings, an especially important use of epoxy polymers, as well as studies of naval ship

155

coatings.[11, 12] Further work on the water and thermal effects on coatings has also been published.[13-15]

These studies outline the manner in which electrochemical properties are affected by polymer variations and the variations in temperature and water content in the polymer. However, investigation of the influence of systematic polymer structural and compositional variations on the EIS response of coated systems are at best incomplete or entirely absent. EIS is a very powerful technique and is widely used to study the protective properties of organic coatings on corrodible materials.[16-20] This technique can also allow for determination of failure mechanism and water uptake behavior of the coating. Moreover, proper use of circuit modeling of the EIS data can also allow qualitative insight as well as quantitative estimation of the various processes occurring at the coating as well as the metal-coating interface.[21-24]

The aim of this work is to investigate the influence of systematic polymer structural and compositional variations on the electrochemical properties of unpigmented coating films as measured by EIS. Novel thermosetting glycidyl carbamate (GC) functional polymers were designed with structure (branching) as well as composition (monomer and concentration) variations. The designed polymers were then mixed with amine, oligomers coated on steel substrates, and cured. EIS measurements were performed on the coating formulations and the influence of polymer structural and compositional variation on the EIS response was investigated. The effect of such changes on the absorption and desorption behavior of water was also studied.

7.2. Experimental

Of the twelve coatings studied in this work, five were based on modified branched GC polymers, termed *M series GC polymers,* and were synthesized using hexamethylenediisocyanate biuret (HDB) polyisocyanate, alcohols and glycidol. Three coatings were based on linear GC polymers and were labeled *L series GC polymers*. Both M and L were solvent based systems. The remaining four coatings were based on water dispersible GC polymers, termed *W series GC polymers*, and were synthesized using hexamethylenediisocyanate isocyanurate (HDI) polyisocyanate, methoxypoly(ethylene glycol) (mPEG) and glycidol.

7.2.1. Materials and polymer formulations

Glycidyl carbamate (GC) polymers are obtained by the reaction of a glycidol with an isocyanate functional compound as shown in Figure 7.1. This polymer system has a unique property of having both epoxy and urethane functional groups in its structure thereby providing reactivity of epoxide and performance of urethane in a single polymer structure.[5-7]
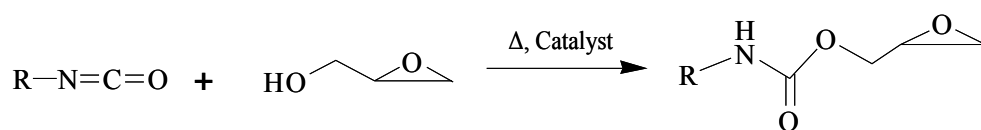

Figure 7.1: Schematic representation of the synthesis of GC polymers.

7.2.1.1. M series GC polymers

The details of the synthesis and characterization of the M series GC polymers has been reported in prior work by Harkal et al.[7] Hexamethylene diisocyanate biuret (HDB) polyisocyanate, procured from Rhodia Inc. was reacted with equivalent amount of only glycidol or both glycidol and alcohol/ether alcohol to obtain *M series GC polymers*. Figure

7.2 is a schematic representation of the reaction to obtain *M series GC polymers*. Among the five *M series GC polymer* compositions, one composition was based on HDB and glycidol at stoichiometric equivalents of isocyanate to hydroxyl at the ratio 1:1 (-NCO : -OH) and was named as biuret glycidyl carbamate (BGC) polymer. Three compositions were obtained by replacing 33 mol % of glycidol by an alcohol or an ether alcohol keeping the equivalent ratio of isocyanate, glycidol and alcohol/ether alcohol at 1:0.66:0.33 (NCO: glycidol: alcohol/ether alcohol). These formulations were termed as BGC-2 ethyl hexanol (BGC-2EHA), BGC-diethyleneglycol butylether (BGC-DB), and BGC-ethyleneglycol propylether (BGC-EP) depending upon the alcohol/ether alcohol used to replace 33 mol % glycidol. The remaining fifth composition was obtained by replacing 15 mol % glycidol by ethyleneglycol propylether and was labeled as BGC-EP 15%. The overall equivalent of -NCO to -OH was maintained at 1:1 during the synthesis of all the five GC polymers. Table 1 lists the details of the *M series GC polymers*. Glycidol was procured from Dixie Chemicals whereas 2-Ethyl Hexanol (2EHA) was supplied by Alfa Aesar. Diethyleneglycol Butylether (DB) and Ethyleneglycol Propylether (EP) were obtained from Aldrich and Fluka-Aldrich respectively.
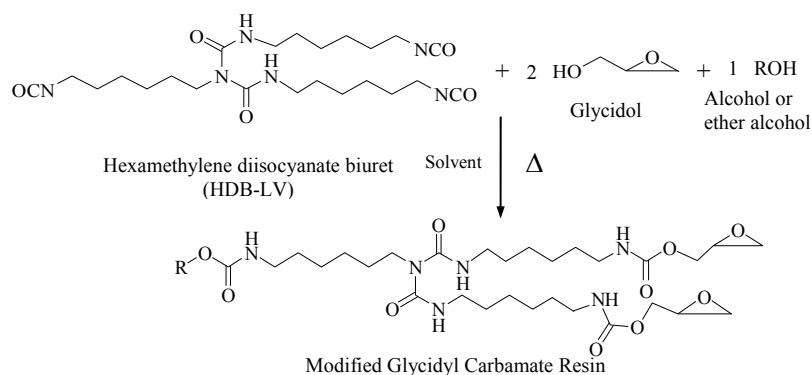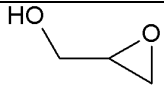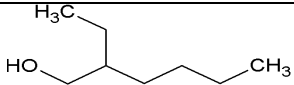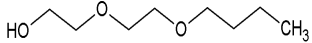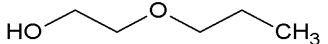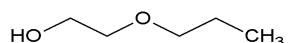

Figure 7.2: Schematic of M series polymer synthesis.

Table 7.1: Chemicals used along with HDB, their structures, EEW and their molar ratio to form the five *M series GC polymers.*

Name of R'OH	Structure of R'OH	Corresponding GC Polymer	NCO:glycidol:alc ohol/ether alcohol (Molar ratio)	EEW (gm/eq)
Glycidol		BGC	1:1:0	255
2 Ethyl Hexanol (2EHA)		BGC-2EHA	1:0.66:0.33	450
Diethylenegyycol Butylether (DB)		BGC-DB	1:0.66:0.33	384
Ethyleneglycol Propylether (EP)		BGC-EP	1:0.66:0.33	355
Ethyleneglycol Propylether (EP)		BGC-EP (15%)	1:0.85:0.15	336

7.2.1.2. L series GC polymers

All the three *L series GC polymer* formulations were diisocyanate, diols and glycidol based linear polymers. The synthesis of these polymers was a two-step reaction process as seen in Figure 7.3. In the first step, a diisocyanate terminated urethane intermediate was formed by the reaction of a diisocyanate and diol(s) and in the second step glycidol was added to the product of the first step to obtain glycidyl carbamate polymer. Details of synthesis and characterization are mentioned elsewhere.[25] Diisocyanates used for the L series polymer formulations were Hexamethylene

diisocyanate (HDI) and dicyclohexyl diisocyanate (H$_{12}$MDI) procured from Bayer. Diols

used were 2-Butyl-2-ethyl-1,3 propane diol (BEPD) and Neopentyl Glycol (NPG) procured
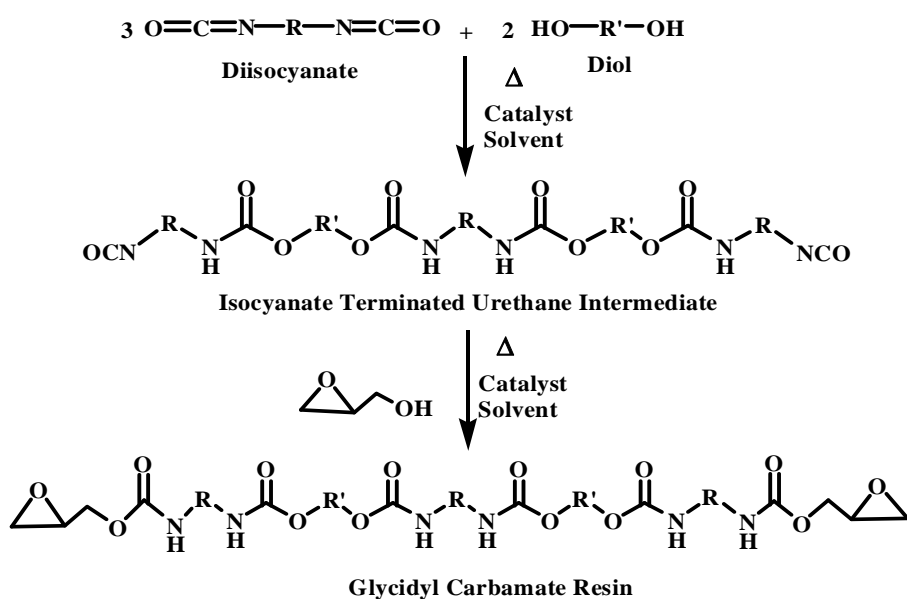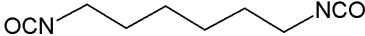
from Aldrich.
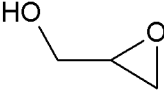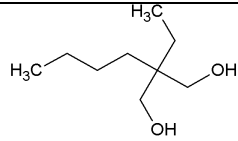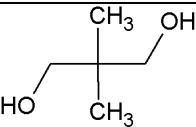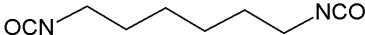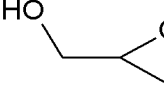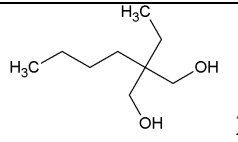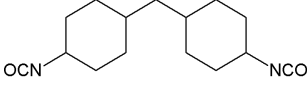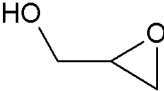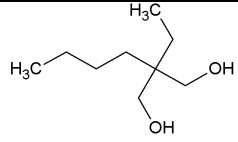
Figure 7.3: Schematic of L series polymer synthesis.

The stoichiometric equivalent of isocyanates and hydroxyl group of diols based on

-NCO and -OH used in the first step of the synthesis to produce diisocyanate functional

urethane intermediate was 1:0.66 (NCO: OH). The reaction was characterized by %NCO

back titration method (ASTM D2572) using di-n-butyl amine and HCl solutions and was

continued until the %NCO value was close to the theoretical expected value. For the

second step of the final GC polymer synthesis the stoichiometric amount of NCO and

glycidol based on total -NCO and -OH groups was 1:1 (NCO : glycidol). Three such GC

polymers were made and were named HDI-BEPD-NPG-GDL, HDI-BEPD-GDL and

H$_{12}$MDI-BEPD-GDL respectively. The reaction was continued until the disappearance of -

NCO peak was observed in the FTIR spectrum. The epoxy equivalent weight (gm/eq) of

the final glycidyl carbamate polymer was determined according to ASTM D 1652.

Table 7.2: Formulation for L based GC polymer, chemicals used along with their structures, molar ratio and EEW.

Polymer (molar ratio)	Composition		EEW
L-A HDI-BEPD-NPG-GDL (1:0.33:0.33:0.33)	Hexamethylene Diisocyanate (HDI)	Glycidol (GDL)	510
	2-Butyl-2-ethyl-1,3 propane diol (BEPD	Neopentyl Glycol (NPG)	
L-B HDI-BEPD-GDL (1:0.66:0.33)	Hexamethylene Diisocyanate (HDI)	Glycidol (GDL)	502
	2-Butyl-2-ethyl-1,3 propane diol (BEPD		
L-C H$_{12}$MDI-BEPD-GDL (1:0.66:0.33)	Dicyclohexyl diisocyanate (H$_{12}$MDI)	Glycidol (GDL)	681
	2-Butyl-2-ethyl-1,3 propane diol (BEPD		

The three *L series GC polymer* were labeled as L-A, L-B and L-C and had epoxy equivalent weights of 510, 502 and 681 respectively. Table 2 lists the properties of the *L series GC polymers* which influenced electrochemical behavior, barrier and diffusion properties of the coatings.

Table 7.3: Properties of L series GC polymers.

L series GC Polymers	EEW (gm/eq)	Wt. % Non-Polar Hydrocarbon in Polymer Composition
L-A	510	58.0
L-B	502	57.8
L-C	681	65.0

7.2.1.3. W series GC polymers

The synthesis and characterization of water dispersible GC polymers used in this work has been previously reported by Harkal et al.[26] The polymers were synthesized in a two-step process as shown in the schematic in Figure 7.4. In the first step partial amount of non-ionic hydrophilic methoxypoly(ethylene glycol) (mPEG), procured from Aldrich, was reacted with hexamethylene diisocyanate isocyanurate (HDI) and in the second step the remaining NCO groups were reacted with glycidol. The extent of hydrophilic group in the final polymer compositions was varied by varying the molecular weight and molar % of mPEG in the polymer composition. A control GC polymer GC-XP-7165 was also synthesized by the reaction of a commercially available hydrophilic isocyanate (Bayhydur XP 7165, Bayer™) with glycidol. Overall stoichiometric equivalent amount of isocyanate,

mPEG and glycidol based -NCO and -OH was maintained at 1:1.The four *W series GC polymers* were labeled W-A, W-B, W-C and W-D. Table 7.4 shows the variation in mPEG molecular weight and molar % mPEG for *W series GC polymers* along with their EEW.

Table 7.4: Molecular weight of mPEG, amount of mPEG incorporated into HDI and the EEW for water dispersible *W series GC polymer* systems.

W series GC Polymers	mPEG Molecular Weight ($\bar{M}_n$)	Mol % of mPEG	Polymer Composition	EEW (gm/eq)
W-A	350	5%	HDI-mPEG350-5%-GDL	416
W-B (Control)	Made from commercial hydrophilic polyisocyanate		GC-XP-7165-GDL	358
W-C	550	5%	HDI-mPEG550-5%-GDL	369
W-D	350	10%	HDI-mPEG350-10%-GDL	324

7.2.2. Coating preparation and film formation

Details of coating preparation for the *M series GC polymers* based coating system have been described elsewhere.[7] Briefly, the prepared polymers were crosslinked with a polyamide, Ancamide 2353. The ratio of amine active hydrogen to epoxy equivalents was kept at 1:1 for all the coating formulations. The coatings were then drawndown on steel panels (Q-Panel, Q236, 0.5x76x152mm) cleaned with p-xylene and cured at 80°C for 1 hour and 45 minutes and then kept at ambient conditions for 3 days prior to the EIS experiments. Dry film thicknesses of about 80-85 microns were prepared. The coating

films were then labeled M1, M2, M3, M4 and M5 obtained from polymers BGC, BGC-2EHA, BGC-DB, BGC-EP and BGC-EP(15%), respectively.
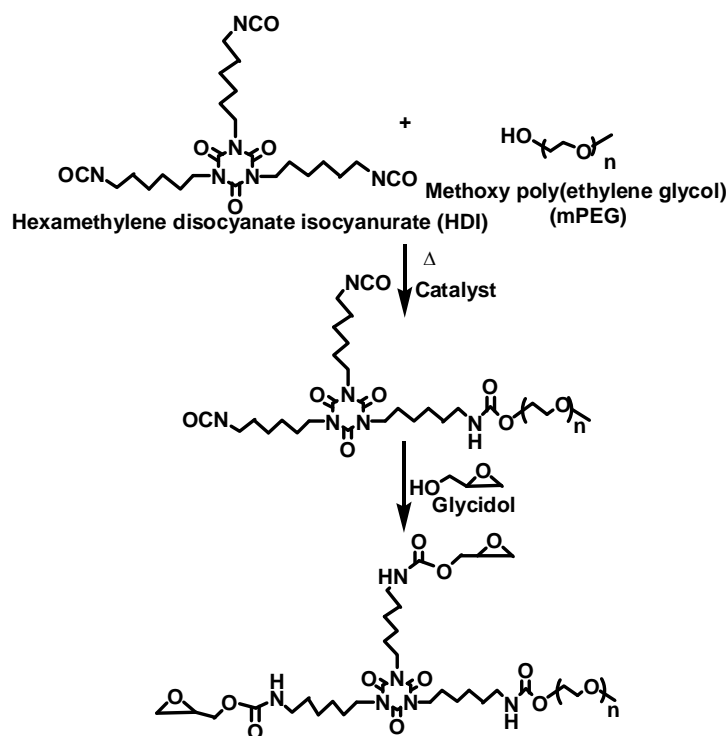
Figure 7.4: Schematic of the W series water dispersible GC polymer synthesis.

For the *L series GC polymers* based coating system Ancamide 2353 was also the crosslinker used. The same ratio of amine active hydrogen to epoxy equivalent of 1:1 was used. The coating were drawndown on steel panels (Q-Panel, Q236, 0.5x76x152mm) cleaned with p-xylene and then cured in an oven for 80°C for one hour. Films with dry film thickness of around 80-85 microns were made. The coatings were kept at room temperature for two weeks before EIS were run on them. Coatings were labeled L1, L2 and L3 based on GC polymers L-A, L-B and L-C, respectively.

Details on the coating preparation from *W series GC polymer* based coating system also has been described elsewhere[26]. The hydrophilic GC polymer was dispersed in

water. W-A and W-B required the addition of 0.7 wt% surfactant for complete dispersion. Anquamine 731, a water based curing agent was used for crosslinking of the *W series GC polymers*. A ratio of 1:1 of amine active hydrogen to epoxy equivalent was used for all the formulations. Films were coated on steel panels (Q-Panel, Q236, 0.5x76x152mm) and were cured at room temperature for two weeks before the evaluation of their electrochemical properties. Dry film thickness of about 80-85 microns was obtained. Coatings were then labeled W1, W2, W3 and W4 based on GC polymers W-A, W-B, W-C and W-D, respectively.

7.2.3. Electrochemical Impedance Spectroscopy (EIS) measurements

A Gamry Instruments R 600 Potentiostat/Galvanostat/ZRA in conjunction with Gamry Framework Version 5.20/EIS 300 software was used for the EIS experiments. The instrument was supplied by Gamry Instruments, Inc. of Willow Grove, PA. A Perspex™ cylinder with a surface area of 7.07 cm^2 was mounted on the samples and was clamped with an O-ring insert to facilitate electrochemical measurements. Sufficient electrolyte was filled in the cylinder to aid EIS measurement.[12, 27, 28]

Two types of EIS measurements were performed. One was multi frequency EIS (MF-EIS). A schematic of MF-EIS set up is shown in Figure 7.5. MF-EIS set up consists of metal substrate as the working electrode (WE) with Platinum (Pt) and saturated calomel electrode (SCE) as counter and reference electrodes respectively. 5 wt. % NaCl, also used in B117 salt spray test was the electrolyte used for the experiment. Information about the coating performance, failure mechanism and various processes involved can be derived via MF-EIS. The impedance response corresponding to the applied frequency of 100 kHz to 0.01 Hz was measured with an acquisition rate of 10 points per decade. A 10mV amplitude

perturbation potential with respect to the open circuit potential was used during the measurement.[28]

The other EIS performed was single frequency EIS (SF-EIS) measurement where the capacitance response of the coating at an applied frequency of 10^4 Hz was monitored every 30 seconds. The equation $C = -\frac{1}{2\pi f Z'}$ was used to calculate the capacitance from the measured impedance data, where C is the capacitance, Z' is the imaginary component of the measured impedance and f is the frequency of measurement. At this frequency of measurement, Z' contains little resistance information and will be stationary[16] with a high signal to noise ratio because of the sampling rate. By SF-EIS capacitance measurements water ingress from an aqueous electrolyte, water egress into a hydrophilic ionic liquid and diffusion behavior of the coating has been studied.[29, 30] Varying polymer structure and composition is expected to vary the SF-EIS response of the coating with certain signatures distinguishing one coating film from the other. SF-EIS measurements were performed in this experiment for both the wetting and the drying stage of the coating. Wetting stage consisted of monitoring the capacitance of the coating for continuous 48 hours in 5 wt % NaCl immersed condition and has the same set up as in Figure 7.5 whereas drying stage was capacitance measured with room temperature ionic liquid (RTIL) as electrolyte. The RTIL used was 1-butyl-1-methylpyrrolidinium trifluoromethanesulfonate ($C_{10}H_{20}F_3NO_3S$), (procured from EMD chemicals, Inc. of Gibbstown NJ). This RTIL is hydrophilic and can cause a coating to dry. Thus the drying process can be followed by SF-EIS. The drying step was also monitored for 48 hours. A two electrode electrochemical cell was used for the drying stage SF-EIS test with substrate as the working electrode and Pt mesh as the counter/reference electrode.[31, 32]

SCE (Reference Electrode)

Pt (Counter Electrode)

Electrolyte (5% NaCl)

Coating

Potentiostat

Metal substrate (Working Electrode)
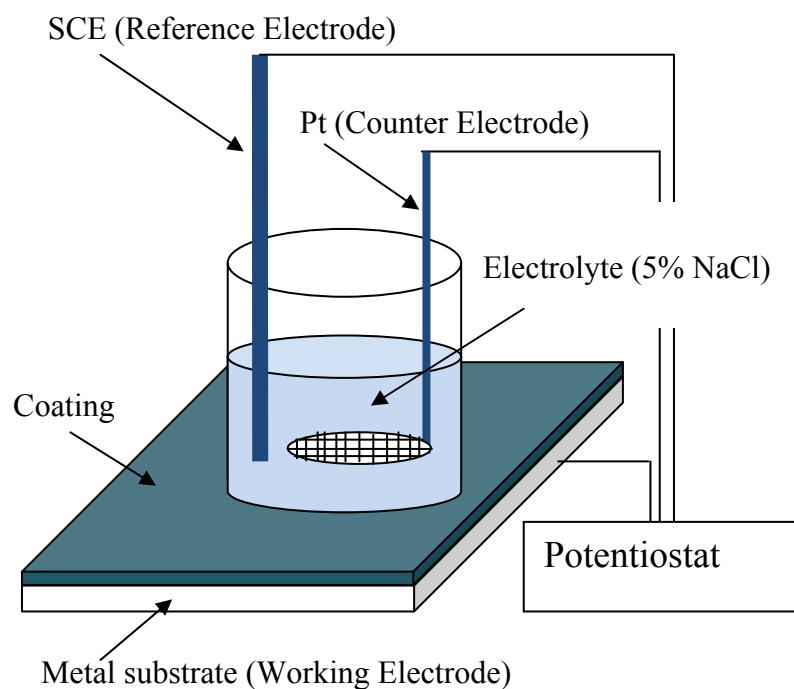
Figure 7.5: Schematic of three electrode EIS set up.

7.3. Results and discussions

7.3.1 M series GC coatings

7.3.1.1 Electrochemical characterization of M series GC coatings

The capacitance measurement of a coating film is based on the assumption that the change in capacitance of the film after immersion of the film in aqueous electrolyte is due to the uptake of water by the film. The Brasher-Kingsbury equation, $\Phi_v = \frac{Log(Ct/C0)}{Log(80)}$ relates the water uptake by a coating to the coating capacitance where Φ_v is the volume fraction of absorbed water, C_t and C_o are the coating capacitance at any time t and at time t=0 respectively and 80 is the dielectric constant of water.[33] The coating capacitance can be written as $C = \frac{\varepsilon \varepsilon_o A}{d}$, where ε is the relative dielectric constant of the coating, ε_o is the dielectric constant of vacuum, A is the area of the coating and d is the coating thickness. Organic coatings have dielectric constants values of around 3-5 whereas the dielectric

constant of free water is around 80.[34] Permeation of water into the organic coating film therefore results in increasing the dielectric constant of the coating film, and in the process, increasing the capacitance of the coating. A change in the relative dielectric value of the coating due to water absorption can be directly measured from change in capacitance of the coating film, if there is no significant change in thickness. The imaginary impedance Z' as measured by EIS can therefore furnish information about the capacitance of a coating and as such furnish information about the water uptake behavior of the coating. Thus using capacitance measurement by EIS, the water uptake behavior of the coating film can be studied. EIS for capacitance measurement was performed at 10^4 Hz to ensure that the system is relatively stationary with respect to the measurement.[16, 35] Capacitance values were obtained from the SF-EIS imaginary impedance data for all the coating films under investigation. Diffusion coefficient or the rate of water diffusion during both the wetting and drying steps were obtained according to the mathematical equation described elsewhere.[36, 37] Other authors also have considered such measurements as applied to coatings.[38-42]

An influence of structural modification as well as polymer composition on the single frequency capacitance behavior of *M series GC polymer* based coatings is observed in Figure 7.6. The trend in capacitance at saturation during wetting stage was observed to be M3>M1>M4>M5>M2. The coating M3 also displayed the fastest water uptake with diffusion coefficient value of 8.88 $\times 10^{-13}$ m^2/sec, whereas M2 with a diffusion coefficient value of 2.66 $\times 10^{-13}$ m^2/sec displayed the slowest diffusion rate. Sample M1, M4 and M5 had a diffusion coefficient value in between sample M2 and M3 and were 3.97 $\times 10^{-13}$ m^2/sec, 4.08 $\times 10^{-13}$ m^2/sec and 4.63 $\times 10^{-13}$ m^2/sec for M1, M4 and M5 respectively.

168

The coating based on BGC-DB (M3) contained two hydrophilic ether groups and displayed the highest affinity for water uptake as seen from Figure 7.6a. The coating based on BGC-2EHA on the other hand contained no hydrophilic group to favor water absorption. Hence BGC-2EHA displayed the lowest capacitance value. BGC-EP (M4) system with NCO: glycidol: OH (ether alcohol) of 1:0.66:0.33 had a higher amount of hydrophilic ether group compared to BGC-EP 15% (M5) system with NCO: glycidol: OH (ether alcohol) of 1:0.85:0.15. This might have led to an increase in the capacitance value for the M4 coating system.
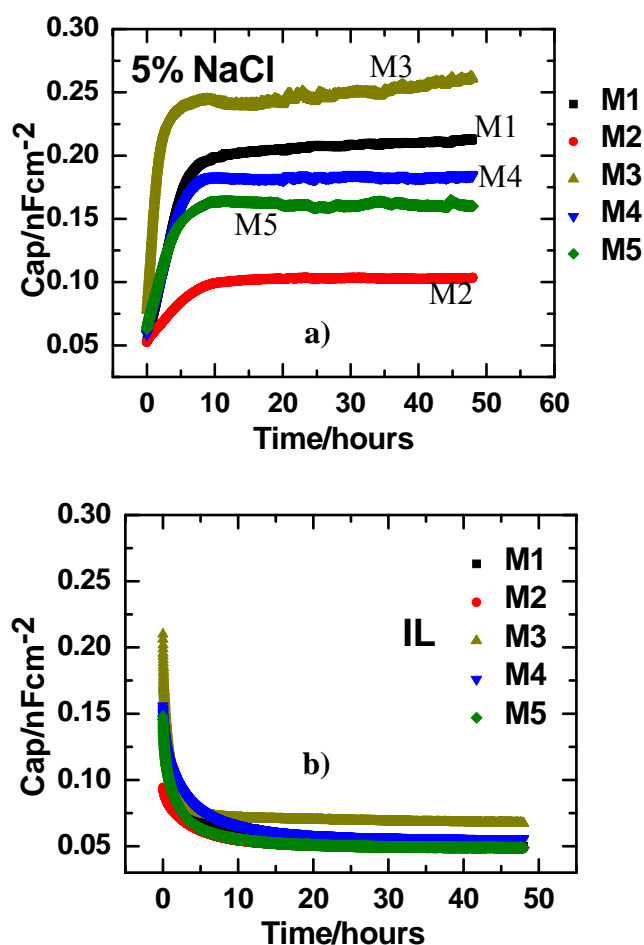

Figure 7.6: Capacitance results for M series GC based coatings as a function of immersion time for samples M1, M2, M3, M4 and M5 in a) 5 wt % NaCl and b) in room temperature ionic liquid.

Plot of capacitance measured during RTIL assisted water desorption is shown in Figure 7.6b. Diffusion coefficient values obtained using the methods of Allahar et al.,[36] for M1, M2, M3, M4 and M5 were 1.41 $\times 10^{-13}$ m^2/sec, 1.31 $\times 10^{-13}$ m^2/sec, 4 .0 $\times 10^{-13}$ m^2/sec, 1.24 $\times 10^{-13}$ m^2/sec and 1.78 $\times 10^{-13}$ m^2/sec respectively. Similar to the wetting cycle, D was highest for M3 indicating that the rate of water desorption was highest for M3 as observed in Figure 7.7. Capacitance values for M3 during drying was higher compared to other coatings which might be due to incomplete desorption or accumulation of water at the coating or metal coating interface.[43]
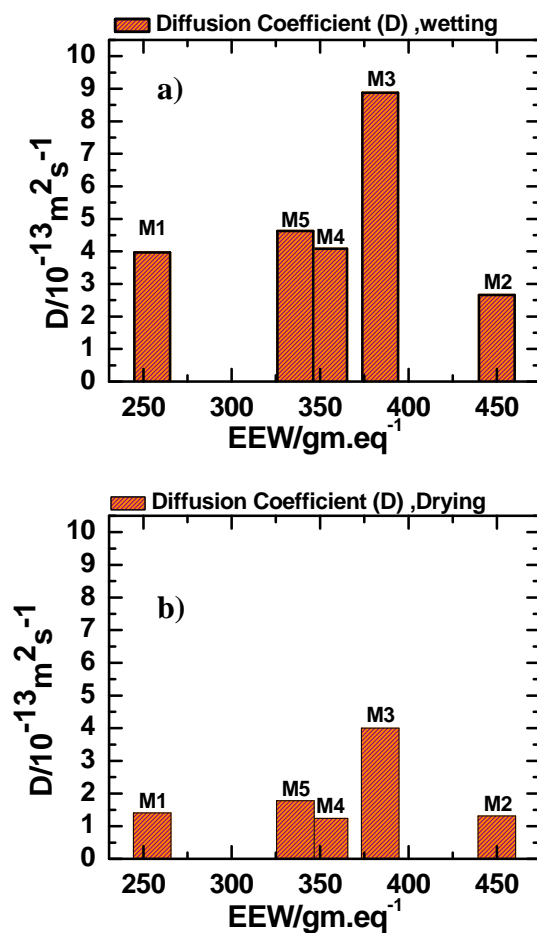

Figure 7.7: Diffusion coefficient as a function of EEW for W coatings during a) wet cycle and b) dry cycle.

Multi frequency EIS measurement performed for the M series samples are shown in Figure 7.8. An initial EIS was run just after immersion to ensure a defect free coating. Bode modulus and phase angle plots for all the M series coatings are shown. Considering that coatings are often modeled as a capacitor and resistor in parallel, so assuming a negligible solution resistance, the impedance of a coating can be written as $|Z| = \dfrac{1}{\frac{1}{R} + j\omega C}$, where $|Z|$ is the impedance, R is the resistance of the coating, C is the capacitance of the coating and $\boldsymbol{\omega}$ is the angular frequency of measurement. At low frequency the impedance is dominated by the resistive component and is a measure of coatings resistance. A coating with $|Z|_{0.01Hz}$ value less than 10^6 Ωcm^2 is believed to have poor barrier performance.[23, 44, 45]

An analysis of the Bode modulus and phase angle plot in Figure 7.8 after 2 hours and after 7 days of immersion reveals interesting results. M2 with no hydrophilic ether groups in it had the maximum $|Z|_{0.01Hz}$ whereas M3 with two (or the most hydrophilic) ether groups displayed the lowest $|Z|_{0.01Hz}$ value. A minor increase in impedance is observed for M5 compared to M4. M4 and M5 have similar polymer system except that the polymer composition in M5 has a lower concentration of hydrophilic ether group compared to system M4 as shown in Table 1. Also a decrease in the $|Z|_{0.01Hz}$ values for all the coating systems was observed at day 7 with superimposition of Bode plots for M4 and M5.

The trend in low frequency impedance, $|Z|_{0.01H}$, behavior of the M series coatings is also observed to correlate with the EEW, although not completely. M2 has the highest EEW and displayed maximum $|Z|_{0.01Hz}$. Low EEW polymers (such as BGC) required higher amount of amine crosslinker and can be expected to generate more of polar tertiary amines and hydroxyl groups in the coatings during crosslinking compared to the coatings obtained

171

from high EEW polymers. Hence lower $|Z|_{0.01Hz}$ values can be expected from low EEW polymers.

Figure 7.8: Bode plot of M series GC polymer based coating after a) 2 hours of constant immersion and b) 7 days of constant immersion.

The trend in low frequency impedance, $|Z|_{0.01H}$, behavior of the M series coatings is also observed to correlate with the EEW, although not completely. M2 has the highest EEW and displayed maximum $|Z|_{0.01Hz}$. Low EEW polymers (such as BGC) required higher amount of amine crosslinker and can be expected to generate more of polar tertiary amines and hydroxyl groups in the coatings during crosslinking compared to the coatings obtained from high EEW polymers. Hence lower $|Z|_{0.01Hz}$ values can be expected from low EEW polymers.
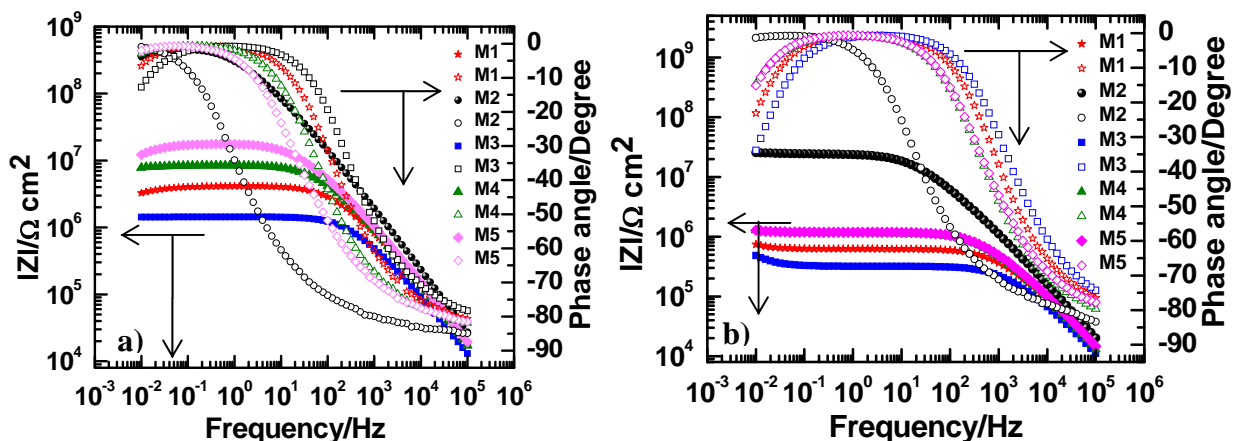
7.3.1.2. Coating stability characterization by single frequency EIS

In an attempt to investigate the utility of SF-EIS in ranking the stability of coating system under wet-dry condition, cyclic SF-EIS was performed on all the five M series coating films. Stability as defined in this work corresponds to when the coating film does not respond to capacitance change under immersion in 5% NaCl and during drying in Ionic liquid. Figure 7.9 displays the cyclic single frequency capacitance plots of M series samples as measured by SF-EIS. Cyclic SF-EIS capacitance measurements consisted of a

wetting cycle under constant immersion condition in 5 wt. % NaCl followed by drying/desorption of the absorbed electrolyte, assisted by ionic liquid. The cycle began by capacitance measurement of the coating by wetting followed by measurement during ionic liquid drying. The drying step was followed again by wetting step and so on.
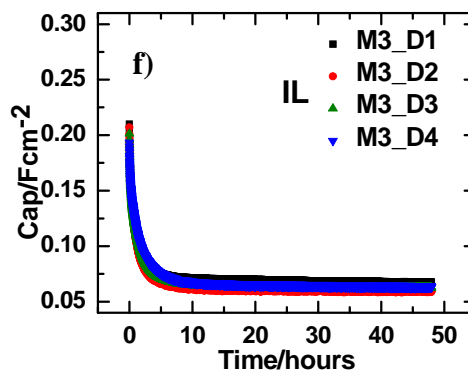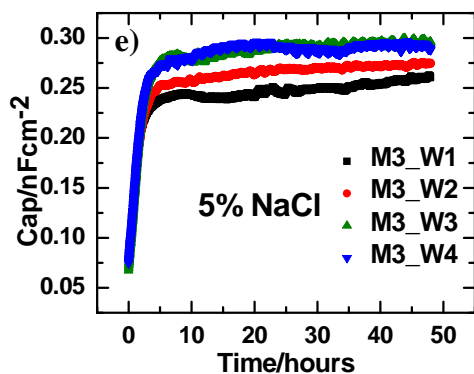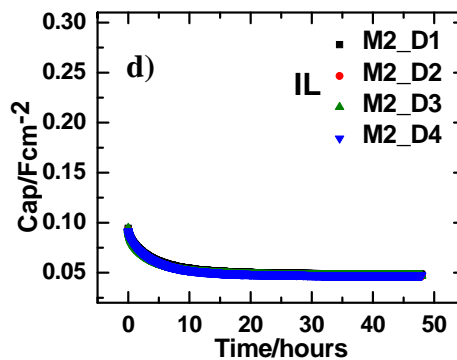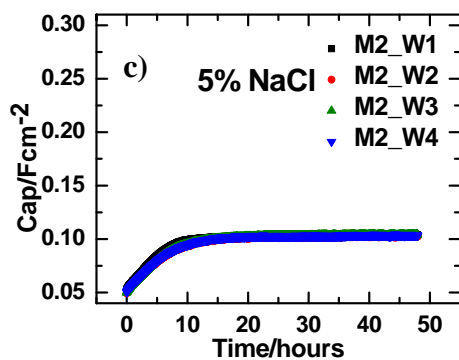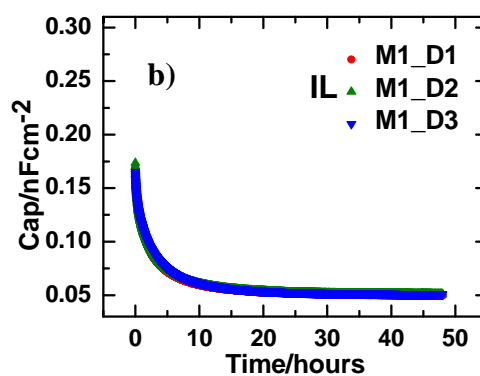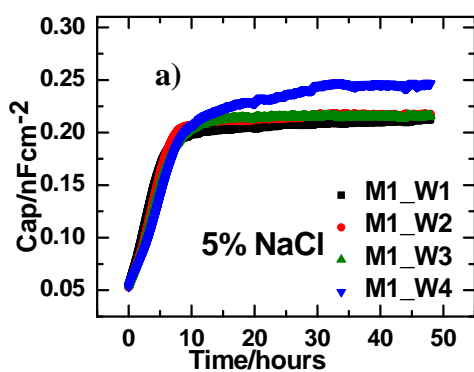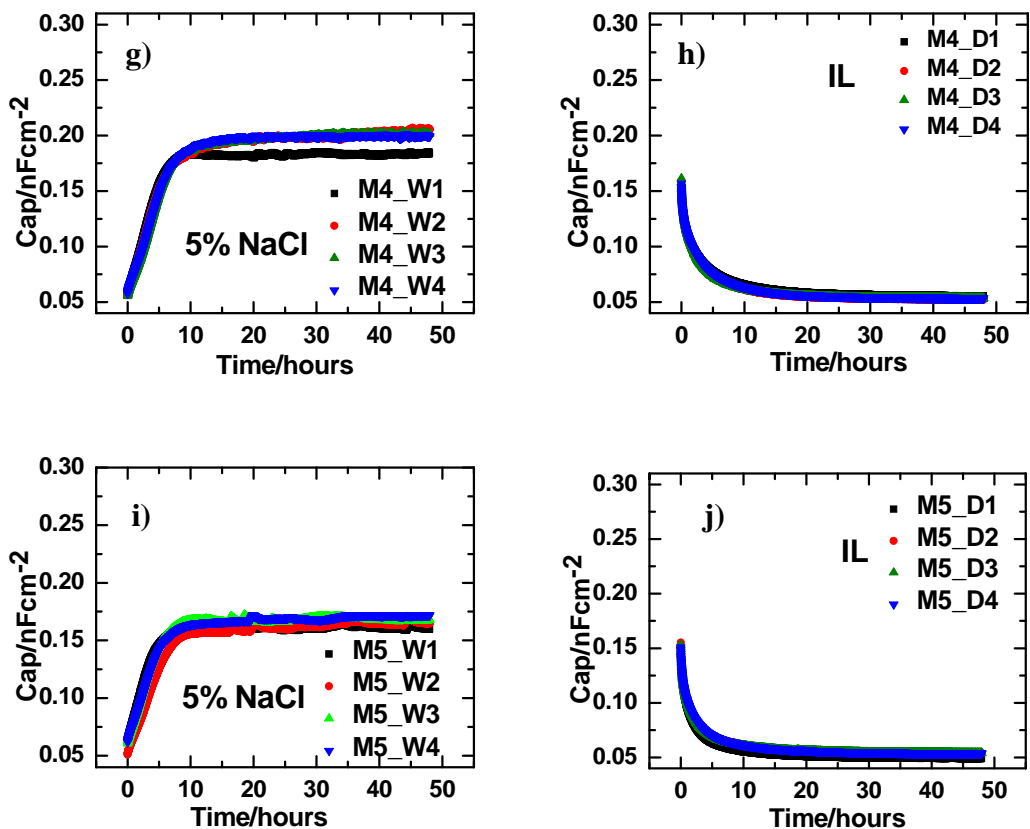
Figure 7.9: Cycles of capacitance as a function of immersion time for coatings a) M1 during wetting b) M1 during drying c) M2 during wetting d) M2 during drying e) M3 during wetting and f) M3 during drying g) M4 during wetting h) M4 during drying i) M5 during wetting and j) M5 during drying.

Four such capacitance wet-dry measurements were done during the wet-dry steps for all the coating samples. The figures on the left (Figure 7.9a, c, e, g and i) corresponds to the wetting cycles whereas the figures on the right (Figure 7.9b, d, f, h and j) correspond to the drying cycle for all the samples. M1_W1 (Figure 7.9a) corresponds to the capacitance of first wetting cycle of coating M1. This was followed by the capacitance measurement of the first drying cycle in ionic liquid M1_D1 (Figure 7.9b). M1_W2 corresponds to the second wetting cycle which was followed by M1_D2 of the drying step, and so on. For sample M1, the sample failed prior to M1_D4 and hence is not plotted.

An examination of the figures reveals interesting information about the stability of the coating. The trend in the capacitance behavior during the drying steps for all the cycles for all the coating samples are similar. During the wetting stages sample M2 and M5 did not display any change in capacitance behavior for all the wetting cycles. However, changes in the capacitance behavior in the wetting stages were observed for samples M1, M3 and M4. Up to cycle 3 coating M1 did not display any change in capacitance. An increase in capacitance was observed during cycle 4. For coating M3 an increase in capacitance was observed during cycle 2 and a further increase was observed during cycle 3. Cycle 4 displayed similar capacitance compared to cycle 3. For coating M4, cycle 2, cycle 3 and cycle 4 displayed similar but increased capacitance behavior compared to cycle 1. Such change in the water uptake behavior for sample M1, M3 and M4 could indicate changes in the structure or molecular orientation in the coating leading to changes in the water uptake behavior.

Coating M3 was formulated without any hydrophilic groups whereas coating M5 was formulated with 15% Ethyleneglycol Propylether. The coating system M3 and M4 had an increased amount of hydrophilic content as observed in Table 1. The higher hydrophilic groups in M3 and M4 might be responsible for causing higher water absorption. This absorption causes plasticization of the coating [16, 46], and can change its structure and orientation. This then results in change in the capacitance behavior observed. M2 and M5 displayed less water uptake compared to M1, M3 and M4 and the coatings were more stable in this wet-dry cycling. The utility of SF-EIS capacitance measurement to ranking the stability of coating is well demonstrated by these data.

175

7.3.2. L series GC coating

7.3.2.1. Electrochemical characterization of L series GC coatings

A comparison of the capacitance measurement during wetting and RTIL assisted drying step can be seen in Figure 7.10. It can be observed that the sample L3 displayed the least capacitance for both the wetting and the drying stages compared to sample L1 and L2. Sample L2 displayed the highest capacitance at saturation during the wetting as well as drying cycle.
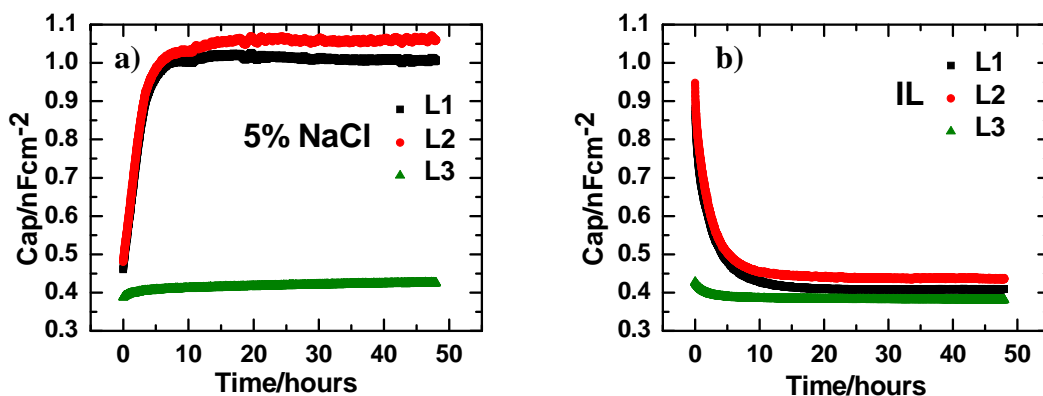
Figure 7.10: Capacitance results for L series GC based coatings as a function of immersion time for samples L1, L2 and L3 at a) 5 wt % NaCl and b) in room temperature ionic liquid.

An influence of polymer structure on the capacitance or the water uptake behavior of the coating is observed. A diffusion coefficient of 6.24×10^{-13} m^2/sec and 6.15×10^{-13} m^2/sec was calculated for L1 and L2 for the wetting stage whereas comparatively low diffusion coefficient of 9.43×10^{-14} m^2/sec was obtained for sample L3 indicating that L3 was more resistant to electrolyte penetration compared to L1 and L2. A plot of diffusion coefficient (D) vs wt. % non-polar hydrocarbon (NPH) content as observed in Figure 7.11 reveals that D, during wetting, decreases with increase in wt. %NPH. Similar diffusion coefficient values of 2.03×10^{-13} m^2/sec and 2.69×10^{-13} m^2/sec and 2.49×10^{-13} m^2/sec were

calculated for sample L1, L2 and L3 during drying step, indicating that the rate of water

release (egress) from the coatings in the presence of RTIL were not much different.
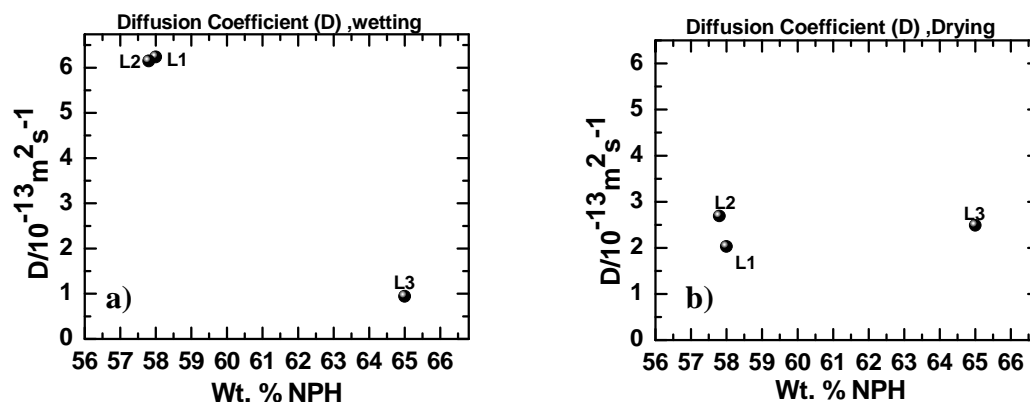
Figure 7.11: Diffusion coefficients as a function of wt. % NPH for L series samples during a) wetting and b) during drying.

The capacitance trend displayed by L series coatings seems to have a direct

correlation with the wt. % non polar hydrocarbon (NPH) content in the coating, calculated

from the coating compositions, as seen in Table 2. The coating L3 with the highest NPH

(65 wt. %) displayed the lowest capacitance compared to the coatings L1 and L2 as

observed in Figure 7.12. Higher non-polar hydrocarbon content in the coating resists the

aqueous electrolyte diffusion and hence low water uptake as shown in the capacitance

plots.
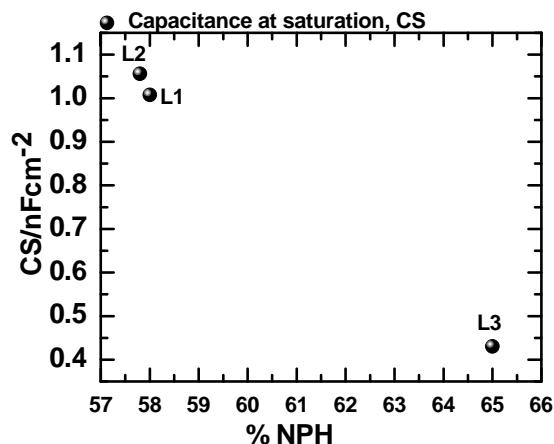
Figure 7.12: Capacitance at saturation as a function of wt. % NPH for L series samples.

Figure 7.13 displays the Bode modulus along with the phase angle plot for the coating system L1, L2 and L3. Coating L3 displays a high $|Z|_{0.01Hz}$ value with purely capacitive $|Z|(\omega)$ behavior after 2 hours with no any change even after 7 days constant immersion in 5 wt% NaCl indicating its excellent barrier performance. Coating L1 and L2 displayed impedance much lower than L3 with $|Z|_{0.01Hz}$ values of around three orders of magnitude less than L3. When compared to L1, L2 displayed a slightly higher $|Z|_{0.01Hz}$ value.
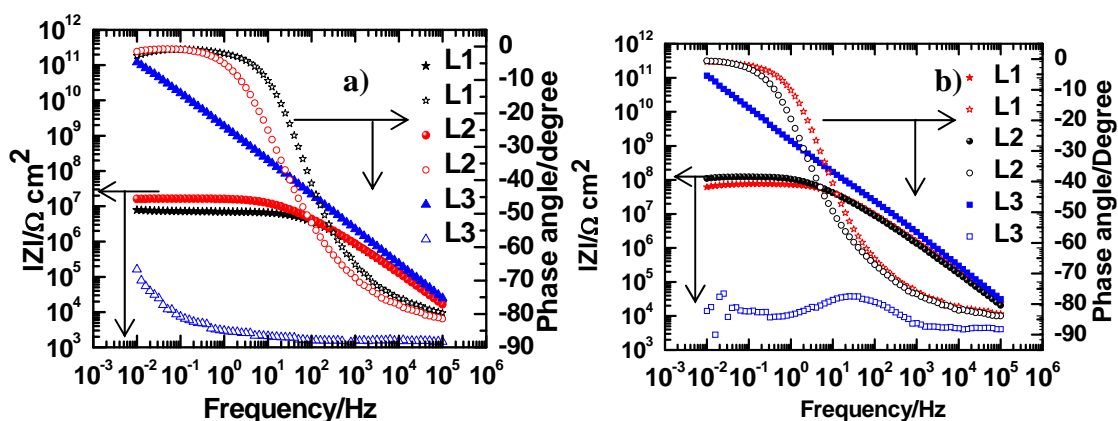
Figure 7.13: EIS Bode plots for coatings L1, L2 and L3 after a) 2 hours and b) 7 days constant immersion in 5 wt. % NaCl.
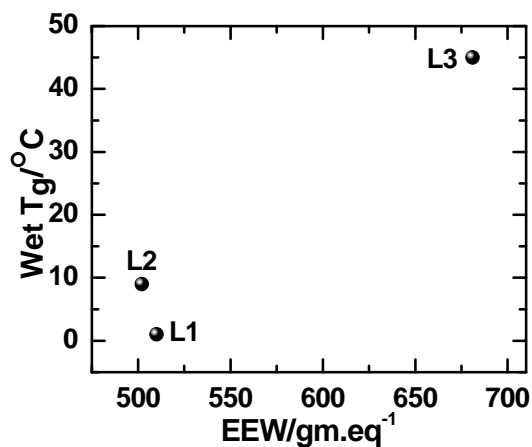
Figure 7.14: Wet T_g as a function of epoxy equivalent weight (EEW) for L series samples.

Table 7.5: Wet and dry T_g of L coatings.

Coatings	Dry T_g (°C)	Wet T_g (°C)
L1	20	1
L2	18	9
L3	57	45

The higher the wet T_g higher is the barrier performance of the coating as observed for the coatings. Wet T_g was determined by wetting the coating film overnight and performing DSC on the wet film. Dry T_g was obtained by performing DSC on the dry sample. A particular composition of *L series GC polymer*, L-C, resulted in the highest NPH, the highest EEW, and the highest T_g (Table 7.3 and Table 7.5 and Figure 7.14) of the L3 coating. The highest EEW of L3 system indicated the lowest amine requirement for crosslinking and lower extent of generation of hydrophilic groups such as hydroxyl and tertiary amine during crosslinking (epoxy-amine reactions). Thus the highest impedance of the L3 coating could be correlated to the highest NPH and the highest EEW of the L-C polymer and the highest T_g of the L3 coating.[25]

7.3.2.2. Coating stability characterization in Wet-Dry cycling by single frequency EIS

In an attempt to investigate the utility of SF-EIS in ranking the stability of coating system, cyclic SF-EIS was also performed on all the three L series coatings. The cyclic SF-EIS consisted of a wetting stage in which capacitance of the coating was monitored under constant immersion condition in 5 wt. % NaCl for 48 hours. This was followed by the drying step in which the absorbed electrolyte during the wetting step was desorbed using

ionic liquid and the capacitance of the coating during desorption was measured. This was

also performed for 48 hours. After the drying step, the wetting step was repeated followed
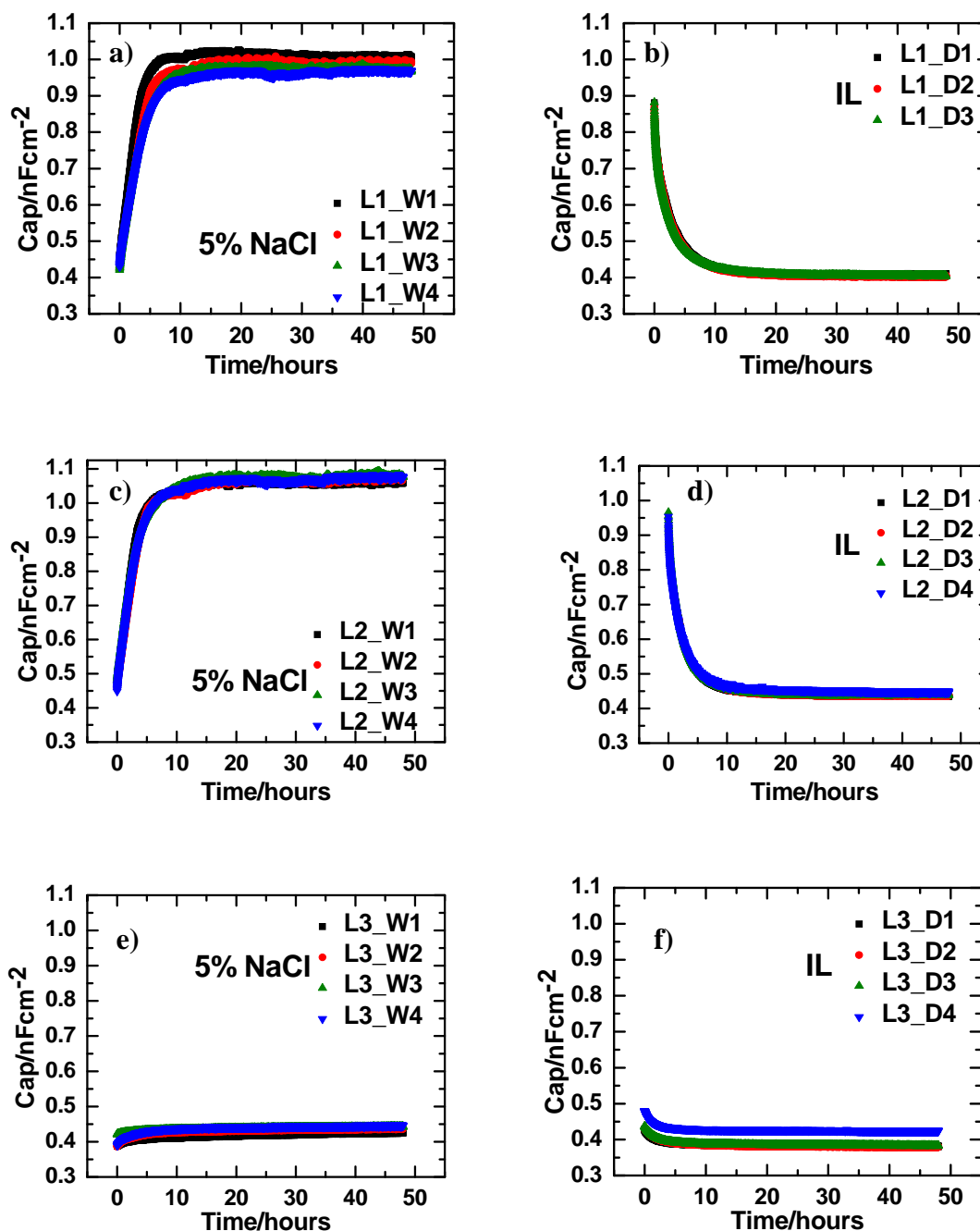
Figure 7.15: Cycles of capacitance as a function of immersion time for coatings a) L1 during wetting b) L1 during drying c) L2 during wetting d) L2 during drying e) L3 during wetting and f) L3 during drying.

by drying and so on. L1_W1 corresponds to the first wetting cycle followed by the drying cycle L1_D1. This was followed by the second wetting cycle L1_W2 and so on. Four such wet-dry cycles were run for all the coatings as seen in the Figure 7.15. The fourth dry cycle for coating L1 could not be measured due to instrumental problems at the time of measurement.

Capacitance behavior as shown in Figure 7.15 reveals important information. In the wetting step coating L2 and L3 displays similar capacitance trend for all the cycles but for coating L1, a slight decrease in the capacitance is observed after every cycle. This might be due to change in the coatings molecular structure or molecular orientation due to coating plasticization by water influencing the water uptake behavior. [46, 47] Coating plasticization can be observed from decrease in T_g measured for wet coating samples as compared to their respective dry samples as seen in Table 7.5. The slight decrease in the capacitance behavior of coating L1 after every cycle compared to coating L2 and L3 indicates that coating L2 and L3 are more stable compared to coating L1.

7.3.3. W series GC system

7.3.3.1. Electrochemical characterization of W series GC coating

The capacitance measurement for the *W series GC polymer* based coating is shown in Figure 7.16. Rust spots were observed on all the samples after the first wetting cycle and hence only the capacitance corresponding to this cycle is shown. W series coatings are based on hydrophilic systems. As observed in Figure 7.16, W4 displays a maximum capacitance whereas W1 and W3 displays almost equal capacitance at saturation. However, the trends in capacitance change with time are different for all the studied samples W1, W3

181

and W4. W2 is a control sample and its formulation details are unknown. Hence a comparison is made among coatings W1, W3 and W4 only.
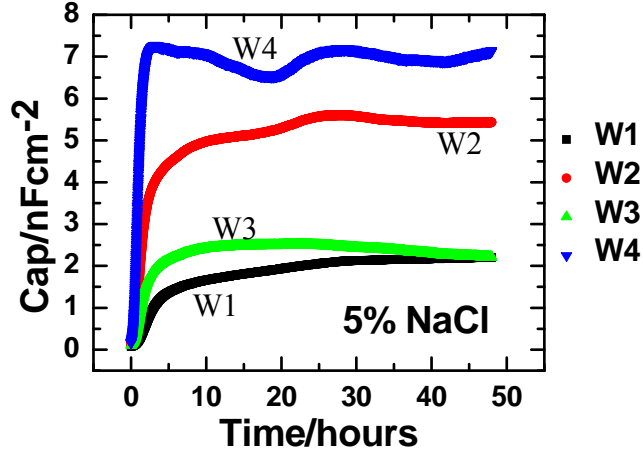
Figure 7.16: Capacitance results for W series GC based coatings as a function of immersion time for samples W1 W2, W3 and W4 in 5 wt. % NaCl.

The different trends in the capacitance evolution indicate that polymer structure and composition influences the water uptake behavior. Coating W4 with the highest amount of hydrophilic mPEG350 in its formulation (10%) displayed maximum water uptake whereas coating W1 with the least amount of mPEG350 (5%) displayed the least water uptake. The reduction in capacitance for W4 after initial rise could be due to swelling since W4 absorbed water the most. Subsequent increase in capacitance can be attributed to corrosion reaction.[48, 49] The diffusion coefficient values also show a similar trend. Maximum diffusion coefficient values of 2.87534×10^{-12} m^2/sec was observed for coating W4 compared to $7.84849 \times 10^{-13} m^2$/sec for coating W1 (Figure 7.17b). Water uptake is fastest for high mPEG contents in the coating compared to low mPEG content. A comparison between coating W1 and W3 also furnishes interesting information. Coating W3 contains higher molecular weight containing mPEG (mPEG550) compared to W1 (mPEG350), at the same mPEG amount (5%), and displays higher capacitance. Higher molecular weight

leads to higher rate of diffusion as is observed from the diffusion coefficient values of 7.848×10^{-13} m^2/sec and 17.283×10^{-13} m^2/sec for coatings W1 and W3 respectively (Figure 7.17b). A direct correlation between hydrophilic content and chain length of polymer with the water uptake behavior of coating has been observed.

The capacitance trend as observed in Figure 7.16 can also be explained on the basis of moles of ether group per mole of GC polymer in the coating as seen in Figure 7.17a. Coating W4 with the maximum value of 0.722 displayed maximum capacitance whereas coating W1 with a value of 0.361 displayed the least. W3 having a value of 0.588 displayed capacitance value comparative to W1. However, only at higher times the capacitance value of W1 and W3 started to merge. Moreover, a direct correlation between the diffusion coefficient values and the moles of ether group per mole of GC polymer was also observed as seen in Figure 7.17b, with higher value of moles of ether group per mole of GC polymer in the coating favoring higher rate of water uptake.
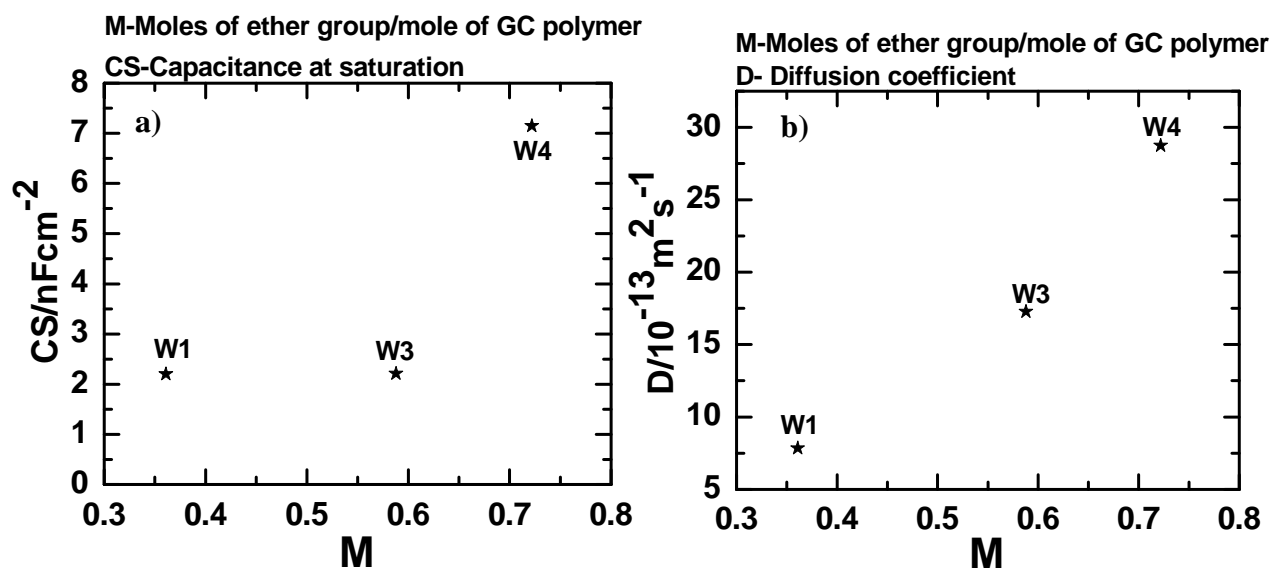
Figure 7.17: Plot of a) Capacitance at saturation as a function of moles of ether group per mole of GC polymer and b) diffusion coefficient as a function of moles of ether group per mole of GC polymer, for W coating samples.

Multi frequency EIS measurement was performed on the W series samples after 2 hours constant immersion. An initial EIS was performed just after immersion to check for defect free sample. Bode modulus and phase angle plots for all the W series coatings are shown in Figure 7.18. As observed from the figures all the four W series coatings displayed poor coating barrier performance with $|Z|_{0.01Hz}$ in the range of 10^5-10^6 ohms cm^2.
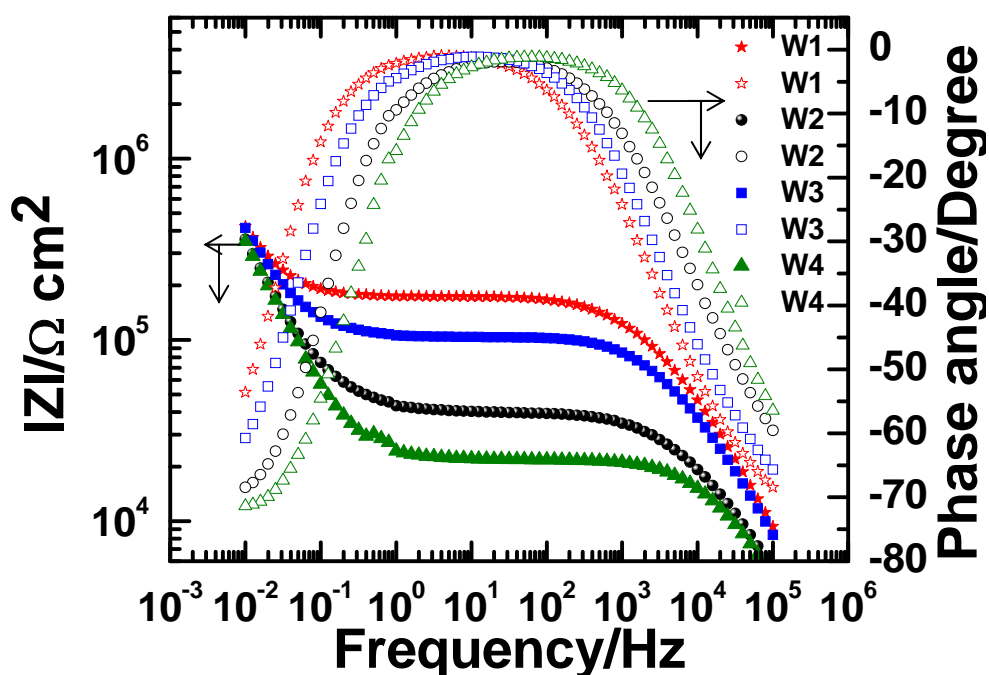
Figure 7.18: Bode plot of W series GC polymer based coating after 2 hours of constant immersion.

Significant change in the low frequency impedance $|Z|_{0.01Hz}$ could not be observed by increasing the EEW of the W series GC polymers (Figure 7.19a). Moreover, the increase in XLD or T_g was not sufficient enough to effect noticeable increase in resistance of the coating as observed from the $|Z|_{0.01Hz}$ values from figure 7.19b and 7.19c.
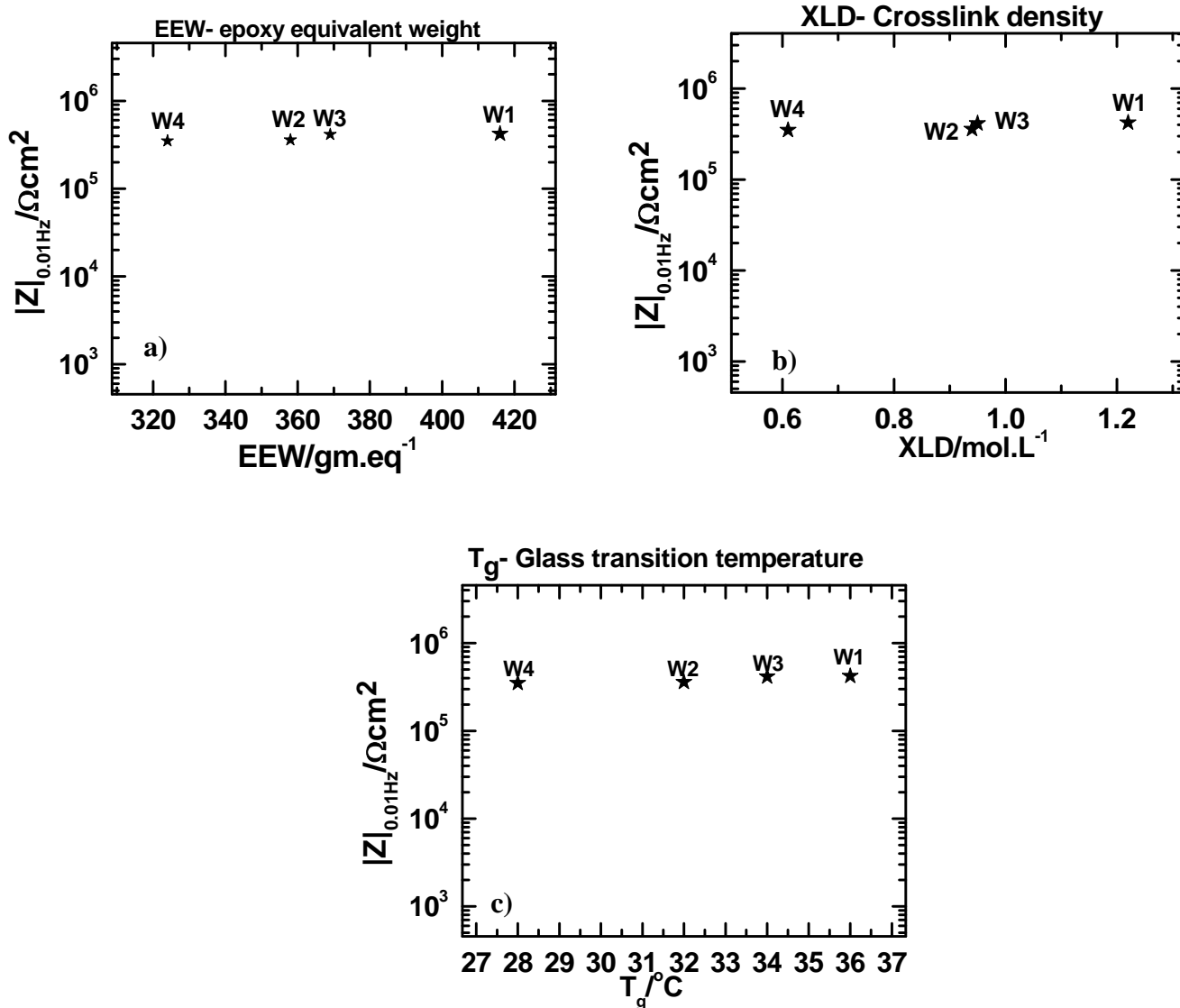
Figure 7.19: Low frequency impedance, $|Z|_{0.01Hz}$, as a function of a) EEW b) XLD and c) T_g of W series coating system.

7.4. Conclusions

The effect of the polymer structure and composition on the EIS response of the coating was studied. It was shown that polymer structure significantly controls the electrochemical properties of the coating films cast from the polymers. The conclusions were as follows:

M series coatings- Coatings possessing the greatest hydrophilic group content in the polymer displayed the highest capacitance whereas those having the greatest hydrophobic group content resisted water absorption. The water diffusion rate also followed a similar trend. Changes in hydrophilic content in the polymer resulted in the change in capacitance behavior, an increase in hydrophilic content increasing the water uptake. The impedance behavior of the coating correlated with the EEW of the polymer, though a linear trend was not observed. SF-EIS can be used to test for coating stability in wet-dry cycling.

L series coatings- An influence of polymer properties on the electrochemical behavior of coatings was observed. Non-polar hydrocarbon (NPH) content and EEW correlated well with the capacitance of the coating as well as with the rate of water uptake under immersion in 5% NaCl. Wet T_g of the coatings correlated with the impedance of the coatings. A small difference in EEW did not correlate completely with $|Z|_{0.01Hz,}$ and did not influence the impedance. SF-EIS can be used to test for coating stability.

**W series coatings**-A direct correlation between the amounts of hydrophilic group in the polymer, the water uptake and diffusion coefficient was observed. Increasing the hydrophilic group in the polymer increased the capacitance as well as the diffusion rate. Increasing the hydrophilic group length at the same hydrophilic group amount also increased the capacitance and diffusion rate. Increasing the EEW, XLD and T_g was not shown to influence the coatings' resistance values as determined from the low frequency impedance of the modulus plots.

The work reported in this paper also has significant implications regarding the methodologies used to design new polymer binder systems for high performance coatings.

Typically, a trial-and-error formulation approach is taken with iterative steps involving the preparation of formulations, testing using conventional methods for corrosion assessment such as salt-spray testing, and reformulation to adjust the performance. However, the preparation of a well-designed series of polymer binders having systematic variations in composition, characterization of the physical and mechanical properties of the binders, coupled with assessment of barrier properties using electrochemical methods as discussed herein, can result in a comprehensive picture of the structure-property relationships in the binder system. Polymer chemists working on the design and synthesis of polymer matrix materials for high performance corrosion protective coatings should remember that one is designing for optimal electrochemical and transport properties in such systems. The barrier properties of such polymers are much more effectively characterized by electrochemical methods under accelerated exposures characteristic of corrosion testing protocols than by only T_g, M_W, and cross-linking measurements. Further, too often, simple water uptake measurements in electrolyte immersion can give excellent supplemental data to other lab tests. This can be done both electrochemically as we have done with SF-EIS measurements or simple gravimetric measurements. Another thing that one should remember is that extensive cross-linking minimizes the amount of free reactive end-groups such as $-OH, -NH_{1-2}$ groups or the corresponding un-reacted epoxy and isocyanate groups (relatively unlikely) which are the very polar groups that in turn give high water transport properties to polymer systems. This information must also be used in interpreting the type of data generated in exposure testing of these polymers in corrosion protective systems. In turn, this information can be used to optimize the polymer composition for the specific

performance properties needed in the application, saving significant time and effort in the research and development stage.

7.5. References

[1] A.V. Rao, D.S. Kanitkar, A.K. Parab, Some speciality coatings from radiation curable poly(acrylic) combinations, Progress in Organic Coatings, 25 (1995) 221-233.

[2] Z.W. Wicks, F.N. Jones, S.P. Pappas, D.A. Wicks, Organic coatings: science and technology, Wiley-Interscience, 2007.

[3] P.A. Edwards, G. Striemer, D.C. Webster, Synthesis, characterization and self-crosslinking of glycidyl carbamate functional resins, Progress in Organic Coatings, 57 (2006) 128-139.

[4] M. Melchiors, M. Sonntag, C. Kobusch, E. Jürgens, Recent developments in aqueous two-component polyurethane (2K-PUR) coatings, Progress in Organic Coatings, 40 (2000) 99-109.

[5] N. Ravindran, D.K. Chattopadhyay, A. Zakula, D. Battocchi, D.C. Webster, G.P. Bierwagen, Thermal stability of magnesium-rich primers based on glycidyl carbamate resins, Polymer Degradation and Stability, 95 1160-1166.

[6] P.A. Edwards, G. Striemer, D.C. Webster, Novel polyurethane coating technology through glycidyl carbamate chemistry, Journal of Coatings Technology and Research, 2 (2005) 517-527.

[7] U. Harkal, A. Muehlberg, J. Li, J. Garrett, D. Webster, The influence of structural modification and composition of glycidyl carbamate resins on their viscosity and coating performance, Journal of Coatings Technology and Research, 7 (2010) 531-546.

[8] H. Deveci, G. Ahmetli, M. Ersoz, R. Kurbanli, Modified polystyrenes: Corrosion, physicomechanical and thermal properties evaluation, Progress in Organic Coatings, 73 (2012) 1-7.

[9] M.T. Rodríguez, J.J. Gracenea, S.J. García, J.J. Saura, J.J. Suay, Testing the influence of the plasticizers addition on the anticorrosive properties of an epoxy primer by means of electrochemical techniques, Progress in Organic Coatings, 50 (2004) 123-131.

[10] J. Li, C.S. Jeffcoate, G.P. Bierwagen, D.J. Mills, D.E. Tallman, Thermal Transition Effects and Electrochemical Properties in Organic Coatings: Part 1 --- Initial Studies on Corrosion Protective Organic Coatings, CORROSION, 54 (1998) 763-771.

[11] J. Kehr, Fusion-bonded Epoxy (FBE): A Foundation for Pipeline Corrosion Protection, NACE International, 2003.

[12] G. Bierwagen, C. Jeffcoate, J. Li, S. Balbyshev, D. Tallman, D. Mills, The use of electrochemical noise methods (ENM) to study thick, high impedance coatings, Progress in Organic Coatings, 29 (1996) 21-29.

[13] G. Bierwagen, L. He, D. Tallman, Time-temperature effects in polymer coatings for corrosion protection as analyzed by EIS, Macromolecular Symposia, 187 (2002) 909-918.

[14] C. Jeffcoate, T. Wocken, G. Bierwagen, Electrochemical assessment of spray-applied thermoplastic coating barrier properties, Journal of Materials Engineering and Performance, 6 (1997) 417-420.

[15] C. Jeffcoate, J. Li, G. Bierwagen, Problems Encountered in Electrochemical Corrosion Testing of Flame Sprayed Powder Coatings, Electrochemical Soc. Symposium Proceedings 95-16, S.R.Taylor, H. Isaacs, & E. Brooman, eds. (1995) p.1960.

[16] G. Bierwagen, The physical chemistry of organic coatings revisited—viewing coatings as a materials scientist, Journal of Coatings Technology and Research, 5 (2008) 133-155.

[17] F. Mansfeld, L.T. Han, C.C. Lee, G. Zhang, Evaluation of corrosion protection by polymer coatings using electrochemical impedance spectroscopy and noise analysis, Electrochimica Acta, 43 (1998) 2933-2945.

[18] P. Kern, A. Baner, J. Lange, Electrochemical impedance spectroscopy as a tool for investigating the quality and performance of coated food cans, Journal of Coatings Technology, 71 (1999) 67-74.

[19] C.G. Oliveira, M.G.S. Ferreira, Ranking high-quality paint systems using EIS. Part I: intact coatings, Corrosion Science, 45 (2003) 123-138.

[20] R.L. De Rosa, D.A. Earl, G.P. Bierwagen, Statistical evaluation of EIS and ENM data collected for monitoring corrosion barrier properties of organic coatings on Al-2024-T3, Corrosion Science, 44 (2002) 1607-1620.

[21] F. Mansfeld, Use of electrochemical impedance spectroscopy for the study of corrosion protection by polymer coatings, Journal of Applied Electrochemistry, 25 (1995) 187-202.

[22] F. Gui, R. Kelly, Performance Assessment and Prediction of Corrosion Prevention Compounds with Electrochemical Impedance Spectroscopy, CORROSION, 61 (2005) 119-129.

[23] B.R. Hinderliter, S.G. Croll, D.E. Tallman, Q. Su, G.P. Bierwagen, Interpretation of EIS data from accelerated exposure of coated metals based on modeling of coating physical properties, Electrochimica Acta, 51 (2006) 4505-4515.

[24] K.N. Allahar, D. Battocchi, M.E. Orazem, G.P. Bierwagen, D.E. Tallman, Modeling of Electrochemical Impedance Data of a Magnesium-Rich Primer, Journal of The Electrochemical Society, 155 (2008) E143-E149.

[25] U. Harkal, Low VOC coating systems from novel glycidyl carbamate resins, PhD Thesis, North Dakota State University, (2010).

[26] U.D. Harkal, A.J. Muehlberg, P.A. Edwards, D.C. Webster, Novel Waterborne Glycidyl Carbamate Coatings, Proceedings of American Coatings Conference'2010, (2010).

[27] G.P. Bierwagen, D.E. Tallman, Choice and measurement of crucial aircraft coatings system properties, Progress in Organic Coatings, 41 (2001) 201-216.

[28] K.N. Allahar, G.P. Bierwagen, V.J. Gelling, Understanding ac-dc-ac accelerated test results, Corrosion Science, 52 (2010) 1106-1114.

[29] K.N. Allahar, B.R. Hinderliter, G.P. Bierwagen, D.E. Tallman, S.G. Croll, Cyclic wet drying of an epoxy coating using an ionic liquid, Progress in Organic Coatings, 62 (2008) 87-95.

[30] G. Bierwagen, K. Allahar, B. Hinderliter, A.M.P. Simões, D. Tallman, S. Croll, Ionic liquid enhanced electrochemical characterization of organic coatings, Progress in Organic Coatings, 63 (2008) 250-259.

[31] A.M. Simoes, D.E. Tallman, G.P. Bierwagen, Use of Ionic Liquids for the Electrochemical Characterization of Water Transport in Organic Coatings, Electrochemical and Solid-State Letters, 8 (2005) B60-B63.

[32] B.R. Hinderliter, K.N. Allahar, G.P. Bierwagen, D.E. Tallman, S.G. Croll, Thermal Cycling of Epoxy Coatings Using Room Temperature Ionic Liquids, Journal of The Electrochemical Society, 155 (2008) C93-C100.

[33] D.M. Brasher, A.H. Kingsbury, Electrical measurements in the study of immersed paint coatings on metal. I. Comparison between capacitance and gravimetric methods of estimating water uptake, Journal of Applied Chemistry, 4 (1954) 62-72.

[34] Q. Su, K.N. Allahar, G.P. Bierwagen, Application of embedded sensors in the thermal cycling of organic coatings, Corrosion Science, 50 (2008) 2381-2389.

[35] G. Grundmeier, W. Schmidt, M. Stratmann, Corrosion protection by organic coatings: electrochemical mechanism and novel methods of investigation, Electrochimica Acta, 45 (2000) 2515-2533.

[36] K.N. Allahar, B.R. Hinderliter, A.M. Simoes, D.E. Tallman, G.P. Bierwagen, S.G. Croll, Simulation of Wet-Dry Cycling of Organic Coatings Using Ionic Liquids, Journal of The Electrochemical Society, 154 (2007) F177-F185.

[37] M.M. Wind, H.J.W. Lenderink, A capacitance study of pseudo-fickian diffusion in glassy polymer coatings, Progress in Organic Coatings, 28 (1996) 239-250.

[38] S. Lindqvist, Theory of dielectric-properties of heterogeneous substances applied to water in a paint film, Corrosion 41 (1985) 69–75.

[39] F. Bellucci, L. Nicodemo, Water Transport in Organic Coatings, Corrosion, 49 (1993) 235-247.

[40] E.P.M. van Westing, G.M. Ferrari, J.H.W. de Wit, The determination of coating performance with impedance measurements--II. Water uptake of coatings, Corrosion Science, 36 (1994) 957-977.

[41] V.B. Mikovi-Stankovi, M.D. Maksimovi, Z. Kaarevi-Popovi, J.B. Zotovi, The sorption characteristics and thermal stability of epoxy coatings electrodeposited on steel and steel electrochemically modified by Fe-P alloys, Progress in Organic Coatings, 33 (1998) 68-75.

[42] V.B. Miskovic-Stankovic, D.M. Drazic, Z. Kacarevic-Popovic, The sorption characteristics of epoxy coatings electrodeposited on steel during exposure to different corrosive agents, Corrosion Science, 38 (1996) 1513-1523.

[43] C. Perez, A. Collazo, M. Izquierdo, P. Merino, X.R. Novoa, Characterisation of the barrier properties of different paint systems: Part I. Experimental set-up and ideal Fickian diffusion, Progress in Organic Coatings, 36 (1999) 102-108.

[44] G.P. Bierwagen, L. He, J. Li, L. Ellingson, D.E. Tallman, Studies of a new accelerated evaluation method for coating corrosion resistance -- thermal cycling testing, Progress in Organic Coatings, 39 (2000) 67-78.

[45] M. Bethencourt, F.J. Botana, M.J. Cano, R.M. Osuna, M. Marcos, Lifetime prediction of waterborne acrylic paints with the AC-DC-AC method, Progress in Organic Coatings, 49 (2004) 275-281.

[46] G. Bierwagen, D. Tallman, J. Li, L. He, C. Jeffcoate, EIS studies of coated metals in accelerated exposure, Progress in Organic Coatings, 46 (2003) 149-158.

[47] Y.P. Chang, P.B. Cheah, C.C. Seow, Plasticizing—Antiplasticizing Effects of Water on Physical Properties of Tapioca Starch Films in the Glassy State, Journal of Food Science, 65 (2000) 445-451.

[48] C. Corfias, N. Pebere, C. Lacabanne, Characterization of a thin protective coating on galvanized steel by electrochemical impedance spectroscopy and a thermostimulated current method, Corrosion Science, 41 (1999) 1539-1555.

[49] F. Deflorian, L. Fedrizzi, S. Rossi, P.L. Bonora, Organic coating capacitance measurement by EIS: ideal and actual trends, Electrochimica Acta, 44 (1999) 4243-4249.

CHAPTER 8. SUMMARY AND CONCLUSIONS

Electrochemical techniques such as electrochemical impedance spectroscopy (EIS) and electrochemical noise methods (ENM) as tools to study and extract information about coating system were the focus of this thesis work. EIS and ENM were used to understand the behavior of coating system, to expedite coating characterization and to study polymer structure-coating property relationships. These techniques in conjunction with embedded sensors were also used to study the in-situ behavior of coating system. The value of using such electrochemical techniques was shown in our studies of the polymer structure-coating property relationships using EIS technique. Research on AC-DC-AC technique and embedded sensors in coatings were performed that extended previous studies further and showed the value of advanced electrochemical techniques.

Three areas of research were the focus of this thesis work. The first area was to extract more information from the AC-DC-AC technique. AC-DC-AC is an accelerated technique that can rank coating performance quite rapidly. This technique has been used to rank coatings, to understand its behavior qualitatively using relaxation signature after DC polarization as well as obtaining quantitative information by modeling the relaxation behavior. Two variables in this technique that can impact the coating performance are the length and magnitude of DC voltage application. At constant application time, higher DC voltage will induce faster coating failure whereas at a constant DC application, a longer time of exposure will induce higher failure. To explore deeper and to obtain more information from this technique chapter 3 of the thesis focused on examining whether the total charge passing through the coating during the DC step determines when a coating fails. Or in other words, it was investigated if the coating fails only at a certain value of charge at the metal coating interface, independent of the applied DC. To verify this, three

sets of experiments were performed. In all the three sets, a constant total amount of charge induced to the coating before it failed was observed that was independent of the applied DC polarization.

The second area of research was to investigate if embedded sensors are sensitive to the changing environmental conditions. Information on the ability of sensor to track humidity change, to locate defect in coatings and their response to B117 exposure condition is not yet available. Chapter 4 of this thesis sought to investigate the response of the embedded sensors to the changing humidity conditions. It was observed that the OCP can reveal sacrificial protection offered by Mg rich pigments. For the measurements made using sensor-substrate configuration, both the low frequency impedance and the high frequency capacitance was influenced by varying humidity condition indicating sensors sensitivity to this condition. Similar results were obtained by measurements made using sensor-sensor configuration. It was also observed that the noise resistance measurement made using reverse sensor configurations could detect changes in humidity. To further explore works with embedded sensors an attempt was made in chapter 5 to investigate if embedded sensors could locate defects in coatings. It was observed that the impedance measured using sensor-sensor configuration displayed difference in EIS measurements made across the defect region compared to measurement made across the intact region, indicating that sensors could be used to locate defects in coatings. A further investigation on the ability of topcoat to influence the EIS measurement using embedded sensors revealed that topcoat could influence the EIS measurement. Differences were observed in the measurements made with low gloss topcoat (chapter 5) as compared to high gloss

topcoat (chapter 6) indicating that the choice of topcoat could be very important in the successful use of embedded sensors.

The third area of research was examining, systematically, polymer structure-coating property relationships using electrochemical impedance spectroscopy. Novel thermosetting glycidyl carbamate (GC) functional polymers were designed with structural (branching) as well as compositional (monomer and concentration) variations. The designed polymers were mixed with amine and coated on steel substrate and cured. EIS measurements were performed on the coating formulations and the influence of polymer structural and compositional variation on the EIS response was investigated. The effect of such changes on the absorption and desorption behavior of water was also investigated. It was observed that polymer modification could alter the electrochemical properties of the coating. Moreover, during this research work a novel method to rank coating stability was developed. It was observed that by cyclic wet-dry capacitance measurement using aqueous electrolyte and ionic liquid, ranking of the performance of organic polymer films can be performed.

CHAPTER 9. RECOMMENDATIONS FOR FUTURE WORKS

The work in this thesis suggests many possible extensions. The AC-DC-AC technique has been successfully used to rank coatings and to obtain relationship between total induced charge and coating failure. The effect of substrates and polymers on the total charge-coating failure relationship can be further explored. Moreover, for coatings that are too robust to be affected by the high DC polarization, using thermal methods jointly with AC-DC-AC may yield better ways to rank such coatings. [1, 2] An increase in temperature can reduce the barrier property of the coating film whereas DC polarization of the substrate would facilitate increased rate of electrolyte diffusion towards the metal-coating interface favoring cathodic reaction and resulting in film delamination and adhesion loss, thereby causing film deterioration.[1, 3]

Embedded sensors provide a unique and convenient feature and facilitate remote in-situ measurements. Results from embedded sensors have proved that such sensors can be very useful in providing information about the health of coated structures that are at remote and inaccessible locations. The fusion of the sensors with EIS/ENM may not only furnish the in-situ state of the coated system but also provide information about the localized corrosion, if any, happening at the substrate underneath. However, further verification of the use of embedded sensors in their actual service environments has to be carried out to verify this technique before their widespread application in the industry. Moreover the wired connections could be inconvenient when embedded sensors are used to monitor large buried coated pipelines or aircrafts. Attempts have to be made to develop wireless technology in embedded sensors too. Other unexplored area in this research is the distance effect.[4] If non-substrate EIS/ENM measurements are to be made where sensors are used for measurements, then the effective distance up to which the sensors responds to

EIS/ENM measurement has to be further verified. Other area in this research is to investigate the optimal size of embedded sensors.[5] Larger sensors might sense larger activity but may disturb the coating performance. Hence an optimum sensor size has to be verified before field usage.

Works on the polymer structure-coating property relationship reported in this thesis has significant implications regarding the methodologies used to design new polymer binder systems for high performance coatings. The preparation of a well-designed series of polymer binders having systematic variations in composition, characterization of the physical and mechanical properties of the binders, coupled with assessment of barrier properties using electrochemical methods as discussed in this thesis, can result in a comprehensive picture of the structure-property relationships in the binder system. Polymer chemists working on the design and synthesis of polymer matrix materials for high performance corrosion protective coatings should consider that one is designing for optimal electrochemical and transport properties in such systems. The barrier properties of such polymers are much more effectively characterized by electrochemical methods under accelerated exposures characteristic of corrosion testing protocols than by only T_g, M_W, and cross-linking measurements. Further, very often, simple water uptake measurements in electrolyte immersion can give excellent supplemental data to other lab tests. This can be done both electrochemically as has been done here with SF-EIS measurements or by simple gravimetric measurements. Another point that has to be considered is that extensive cross-linking minimizes the amount of free reactive end-groups such as $-OH, -NH_{1-2}$ groups or the corresponding un-reacted epoxy and isocyanate groups (relatively unlikely) which are the very polar groups that in turn give high water transport properties to polymer

systems. These informations can also be used in interpreting the type of data generated in exposure testing of these polymers in corrosion protective systems and to optimize the polymer composition for the specific performance properties required in the application, saving significant time and effort in the research and development stage.

9.1. References

[1] G.P. Bierwagen, L. He, J. Li, L. Ellingson, D.E. Tallman, Studies of a new accelerated evaluation method for coating corrosion resistance -- thermal cycling testing, Progress in Organic Coatings, 39 (2000) 67-78.

[2] K.N. Allahar, G.P. Bierwagen, V.J. Gelling, Understanding ac-dc-ac accelerated test results, Corrosion Science, 52 (2010) 1106-1114.

[3] L. Fedrizzi, A. Bergo, F. Deflorian, L. Valentinelli, Assessment of protective properties of organic coatings by thermal cycling, Progress in Organic Coatings, 48 (2003) 271-280.

[4] H.S. Lee, S.W. Shin, J.M. Ahn, Y.C. Kim, Y.T. Kho, Development of corrosion sensors for monitoring steel-corroding agents in reinforced concrete structures, Materials and Corrosion, 54 (2003) 229-234.

[5] N. Saeidi, A. Demosthenous, N. Donaldson, J. Alderman, Design and fabrication of corrosion and humidity sensors for performance evaluation of chip scale hermetic packages for biomedical implantable devices, in: Microelectronics and Packaging Conference, 2009. EMPC 2009. European, 2009, pp. 1-4.